Chapter 6: Simulation of the Formation and Evolution of the Leonid Meteoroid Stream

6.1. Introduction

The Leonid meteor shower has been visible on Earth for over one thousand years. The earliest records of the shower are replete with descriptions emphasizing the awe and horror with which the earliest of the Leonid meteor storms were received (cf. Hasegawa, 1993). More recently, observations from the 1833 Leonid storm in North America became the catalyst for the modern development of the subject of meteor astronomy.

Detailed observational histories of the shower have been published in many references (cf. Brown, 1999; Littman, 1998; Mason, 1995; Yeomans, 1981). As rich as the history of the observation of the stream has been, the history of the attempts to understand its origin, evolution and ultimately to make predictions about its possible future activity is equally rich. Proof of the complexity of the Leonid meteoroid stream lies in the fact that at the close of the 20th century, when yet another cycle of enhanced Leonid activity is at its peak, predictions regarding its activity are little more precise than a century ago.

Olmsted (1834) was the first to analyze the stream in detail. After witnessing the 1833 storm firsthand, he set about trying to understand the shower and was among the first to note that the stream appeared to radiate from one point in the sky, thus establishing the celestial nature of the meteors involved. He also estimated the orbit for the stream and made an attempt to determine its periodicity. Olmsted's work was expanded upon by Olbers (1837) who was the first to estimate correctly the stream's period at 34 years and to predict that a return might be expected in 1867. Herrick (1841) was the first to analyze ancient Leonid returns and he arrived at a similar conclusion/estimate.

From the dates of the occurrence of the shower in older records, Newton (1863) suggested that the shower could have several possible periods. He was unable to distinguish between these on the basis of the ancient observations alone but suggested that computation of the rate of advance of the nodes for different orbits could be used in comparison with the nodal advance computed from the historical accounts to arrive at a solution. This was done by Adams (1867) and proved conclusively that the Leonids had an average 33.25 year period. This was the longest of the possible periods arrived at by Newton in his analysis and was identical to the period for the Leonids assumed by Le Verrier (1867) and Schiaparelli (1867) in their computations of the stream's orbit. Shortly after the determination of the Leonid meteor stream's orbit, it was recognized by several authors to be almost identical to that of 1866I thus leading to the second association between a comet and a meteor stream (the first having been the Perseids and comet Swift-Tuttle the year before).

The predictions made shortly after the 1833 shower were confirmed by major showers/storms in 1866 and 1867 as well as strong returns in 1865 and 1868, all heralding the major advances made in the understanding of the stream during the same years.

With the parent comet now known and the periodicity of the stream firmly established, confident predictions were made of a strong meteor shower in 1899. In the years immediately before the 1899 return, the shower did not produce particularly strong returns although there exists some evidence of increased activity in 1898. The first calculation of the perturbations by the outer planets on the segment of the stream encountered by the Earth in 1866 was made by Berberich (1898), who found that the Leonids had passed close to both Saturn and Jupiter in the few years before 1899 and as a result the meteoroids encountered in 1899 would be perturbed far inside the Earth's orbit. Similar calculations performed by Stoney and Downing (1899) indicated that the storm producing segment of the stream (which they termed the "ortho-Leonids") would be perturbed inwards by more than 0.01 A.U. These large nodal perturbations were cautiously interpreted as being significant enough to perhaps lessen the display in 1899 but the authors of both works were hopeful that the stream was still wide enough to allow some member meteoroids to encounter Earth.

Murakami (1959, 1961a and 1961b) published a series of articles analyzing visual observations made in Japan from the 1930s through the late 1950s and showed that some enhanced activity was present in at least 1931 and 1932, though weak in comparison to the years around the 1833 and 1866 storms. He also investigated the formation of the stream from these observations and concluded that ejection velocities of order 10 m/s could account for the 1000 year lifetime of the observed shower.

Kazimirchak-Polonskaya *et al.* (1967) were the first to make use of computers to investigate perturbations on a collection of hypothetical Leonids starting in 1866 and integrated to the present epoch. They established that the orbit of the Leonids was stable over intervals of centuries and that Jupiter and Saturn were the primary planetary perturbers of the stream.

McIntosh (1973) used an analytical approach to study the effects of the cometary ejection process on the stream and was the first to recognize the importance of radiation pressure on Leonid meteoroids. His model suggested that the major showers occurring in different years close to the time of the comet's passage are from ejections at different perihelion passages. Comparison of the model's results with actual observations suggested that the observations could be best reproduced through dust emission at discrete points along the cometary orbit as opposed to near continuous emission.

A more detailed analytical model was proposed by Sekanina (1974). He included the effects of ejection velocities and radiation forces on individual meteoroids and accounted for planetary perturbations through the measurement of subsequent deviations of forward integrations of initial orbits differing slightly from Tempel-Tuttle. Using historical accounts of the stream in conjunction with this model, he suggested the past activity of the shower was the result of intermittent activity of Tempel-Tuttle, most notably ejections in 868, 1499 and 1767. He found that ejection velocities of order 10 - 100 m/s were needed to explain the observed storms.

The study of the relationship between Tempel-Tuttle and the Leonids was continued by Yeomans (1981). Using past observations of Tempel-Tuttle, he was able to construct an historical ephemeris for the comet by solving for its non-gravitational parameters as well as numerically integrating the comet's equations of motion. Using this cometary ephemeris in conjunction with ancient Leonid observations, he developed an empirical model of the dust distribution around the comet. He found that most Leonid meteoroids lagged spatially outside and temporally behind the comet, in contrast to what would be expected based on the direction of the non-gravitational forces, which would tend to move meteoroids inside and ahead of the comet. Most notably, all past Leonid storms had occurred within 2500 days before or after the comet's perihelion passage and then only if the comet passed 0.025 A.U. inside or 0.01 A.U. outside the Earth's orbit. Based on these results, he concluded that both radiation forces and planetary perturbations were key evolutionary determinants while ejection velocities (which he suggested to be of the order 5-20 m/s) were less important to the development of the stream.

Kondrat'eva and Rezinikov (1985) independently developed an orbital ephemeris for Tempel-Tuttle. They studied the stream using the orbital elements of the comet near perihelion in conjunction with a numerical model where particles were ejected isotropically from the comet and acted upon by planetary perturbations. Through iterative adjustment of the initial orbit upon ejection, they determined the ejection velocities needed at each perihelion passage of the comet to produce the smallest encounter distance with the Earth at the time of the 1833, 1966 and 1999 Leonid returns. Their results suggested that the component of the ejection velocity perpendicular to the comet-sun direction is important in stream evolution, the ejection velocities needed were in the range 10-20 m/s and the ejection point along the cometary orbit is not significant to future development of the stream.

Williams *et al.* (1986) analytically constrain the ejection velocities by using the fact that some Leonid storms occur in two consecutive years and that the change in energy of the ejected particle is purely kinetic. They found that ejection at perihelion must be less than 1 m/s to account for storms occurring in two consecutive years and greater velocities were required for ejection further from perihelion.

A modern numerical model of the stream was presented by Wu and Williams

(1991). They used the ephemeris of Yeomans (1981) and a model of meteoroid ejection from Tempel-Tuttle which was confined to the plane of the cometary orbit with steps of 30° in the direction of ejection and derived the resulting ejection speeds from the model of Whipple (1951). By following the evolution of test particles ejected in this way under the influence of planetary perturbations and radiation pressure effects, they were able to confirm directly that the test meteoroids evolved to positions spatially outside and temporally behind the parent comet in support of Yeomans' (1981) empirical study.

Using a similar approach, Brown and Jones (1993) followed the evolution of several thousand test particles following Whipple's (1951) expression for the ejection velocities. They noted the possible importance of the 1:3 mean motion resonance with Jupiter on the stream's development and concluded that the stream's evolution is driven by planetary perturbations and modified by radiation pressure.

Kresak (1993) investigated the relationship between the IRAS dust-trails and meteor storms, which he viewed as the same phenomenon but observed from different perspectives. He explicitly noted the appearance of Leonid storms was controlled by close encounters of the stream with Jupiter which served to disperse the dense dust "trail" behind the comet and thus limit the stream's ability to produce meteor storms on Earth. He further suggested that the dispersion process responsible for meteor storms within a trail proceeded primarily through differences in radiation pressure between particles and to a lesser extent the initial ejection velocities of the particles involved. The correspondence between the IRAS dust trails and meteor storms suggested on the basis of observations of both, that the ejection velocities responsible for the formation of the trails were of order 5 m/s and the dominant particle population in the trails had $\beta=10^{-3}$.

Wu and Williams (1996) investigated the past evolutionary histories of ten photographically determined Leonid orbits and concluded that the semi-major axes and eccentricities of the observed Leonids were determined primarily by initial ejection velocities. Combining this fact with backward integrations of the observed Leonid meteoroids, they suggest that Leonids are ejected from Tempel-Tuttle with velocities of order 0.6 km/s. To simulate the formation of the stream, they utilized a mean ejection velocity at perihelion for 90 test particles from cometary passages in 1866, 1899 and 1932 which produce periods such that the meteoroids approach the Earth in 1966 (but were ejected with velocities less than 0.6 km/s) and then repeat this procedure for 1998-1999. They examined the number of meteoroids making close approaches to the Earth and concluded that only modest to weak showers may be expected in 1998-1999.

Williams (1997) suggested that the lack of strong Leonid displays when the parent comet is far from perihelion might result from perturbations by Uranus. He noted that Tempel-Tuttle is close to a 5:2 mean motion resonance with Uranus and that the planet might be responsible for "sweeping" clean Leonid meteoroids from that portion of the orbital arc far from the parent comet, accounting for the lack of Leonid displays away from the comet's perihelion passage.

Asher (1999) investigated the likely ages of Leonid displays over the last 160 years. He showed that for short periods (up to a few orbital revolutions), most meteoroids released at perihelion on orbits sufficiently similar to Tempel-Tuttle experience deterministic evolution which can be used to map the specific perturbations from a given ejection epoch which producing Leonid meteors intersecting Earth's orbit at the time of witnessed showers/storms. Noting that differential planetary perturbations between daughter Leonids and Tempel-Tuttle is the dominant factor in the delivery of Leonids to Earth, he was able to estimate the separation distance at nodal crossing between previous ejections and the Earth's orbit at specific Leonid returns. On this basis he concluded that the storms of 1966 and 1833 were caused by ejections from Tempel-Tuttle in 1899 and 1799 respectively.

In this work, we attempt to simulate the formation of the Leonid stream using existing physical models, which describe the cometary-meteoroid ejection process. Using Monte Carlo techniques to produce a suite of initial meteoroid orbits, we then follow these test particles by applying numerical integration to epochs of documented Leonid activity over the last 160 years and compare the results to observations. We have previously applied a similar model to study of the Perseid stream (Brown and Jones, 1998).

In particular, we wish to compare the results of our integrations with observations to attempt to verify the general veracity of the initial conditions used and to determine what constraints can be placed on the initial conditions of the formation of the stream.

Notably we hope to address the following questions through simulation:

- What is the age and origin of the ejecta, which constitute documented Leonid storms/showers, particularly those of 1966/69, 1901/03, 1866/67 and 1832/33?
- What do the activity profiles from past Leonid storms, when compared to modelling results imply about initial ejection velocities from Tempel-Tuttle?
- What is the relationship between the orbital geometry of Earth and Tempel-Tuttle in the past relative to the delivery of Leonids at the present time?
- What is the dependence on initial velocities/conditions/densities/masses of meteoroids for delivery at Earth at the present epoch?
- What is the mean spread of the stream over time due to planetary perturbations (i.e. how does the relative density of the stream change over time)?
- What effect does each of the major planets have on the evolution of the stream?
- What are the dominant evolutionary processes affecting the structure of the stream (ejection velocities, radiation pressure or planetary perturbations) and over what time scales do they dominate the evolution of the stream?
- What is the best model representation of the ejection process?
- What causes the abrupt decrease in observed activity of the stream in years just before and after the return of Tempel-Tuttle?

6.2 Model for the Formation of the Leonids and Observational Considerations.

6.2.1 Overview of Model

To simulate the formation of the Leonid stream we proceed as previously for the Perseids (Brown and Jones, 1998). Briefly, the basic procedure consists of generating a suite of test particles close to each perihelion passage of Tempel-Tuttle and following each of these through to the epoch of interest. The "daughter" Leonids are created through random ejection on the sunward hemisphere of Tempel-Tuttle and are distributed at random in true anomaly inside 4 A.U. The osculating elements for Tempel-Tuttle are taken from Yeomans *et al.* (1996). A total of 10 000 test meteoroids are ejected in each decadal mass interval from 10 g - 10^{-5} g, for a total per perihelion passage of 70 000 test particles. This procedure is repeated for each of the last 15 perihelion passages of the comet so that each complete "run" consists of just over 1 million test particles.

After the initial conditions are specified in this way, each test particle is numerically integrated forward from ejection to the epoch of interest and followed until it reaches its descending node (the only point along its orbit at which it might possibly be observable from the Earth) and its Keplerian elements at the time of nodal passage are stored. The integration includes the direct and indirect perturbations of all planets from Venus to Neptune, radiation pressure and the Poynting-Robertson effect. The integrator used is a 4th order variable step-size Runge-Kutta (Jones, 1985).

This basic procedure is repeated for four different physical models of ejection and three different values of meteoroid bulk density for a total of 12 different runs. The four physical models are derived from the work of Crifo (1995) on distributed gas production within the cometary coma and the Jones (1995) model with variations in the heliocentric dependence on ejection velocity and a parabolic distribution in ejection probabilities. For each of these models we adopt bulk meteoroid densities of 0.1, 0.8 and 4.0 g/cm^{-3} in turn, due to uncertainties in the actual meteoroid bulk density and to investigate the role of differing assumed densities on the evolution of the stream. These densities, along with the range in initial particle masses, translate into a range of β's from ~10^{-5} - 10^{-2}. Table 6.1 and its description provide more details for each of these physical model choices. Fig. 6.1 shows a typical range of ejection velocities from Tempel-Tuttle for these model choices. Note that we have used a mean radius of 2 km for 55P/Tempel-Tuttle of throughout in accordance with recent observations (Hainaut *et al.* 1998).

Our approach at this stage is to generate initial conditions which are "reasonable" within the constraints of our imperfect understanding of the cometary coma dust environment rather than to suggest any particular model as most appropriate. In particular, we recognize that there are large uncertainties in many of the physical quantities (i.e. density of meteoroids, relationship between meteoroid mass and luminosity etc.) and choose to instead explore the effects of widely different (but still "reasonable") ejection conditions (velocities, points of ejection and ejection directions) and meteoroid densities over a wide range of masses in this Monte Carlo fashion. This same approach has been used previously to study the formation and evolution of the Perseid stream (Brown and Jones, 1998) and more extensive details and discussion can be found in that work.

6.3 Observational Considerations

Leonid meteors are observable from the Earth only when their nodal distance from the sun is equal to the Earth's orbital distance and when the Earth is at the node at the same time. This automatically implies that only a very small percentage of all the meteoroids in the stream can actually be observed at Earth in any given year. However, this constraint is far too strict for the interpretation of modelling results; even with a total of 10^7 test particles only a handful would meet these conditions. As a result it becomes necessary to adopt some form of temporal and spatial sieving to make sensible, statistically meaningful results. The important consideration is what choice of temporal and spatial binning is still physically representative of the initial conditions without being so strict affords too few particles in the end to analyze. If our bins are too large we will "see" features in the final modelling which do not intersect the Earth; if too small we may miss features which now have too few particles representing them.

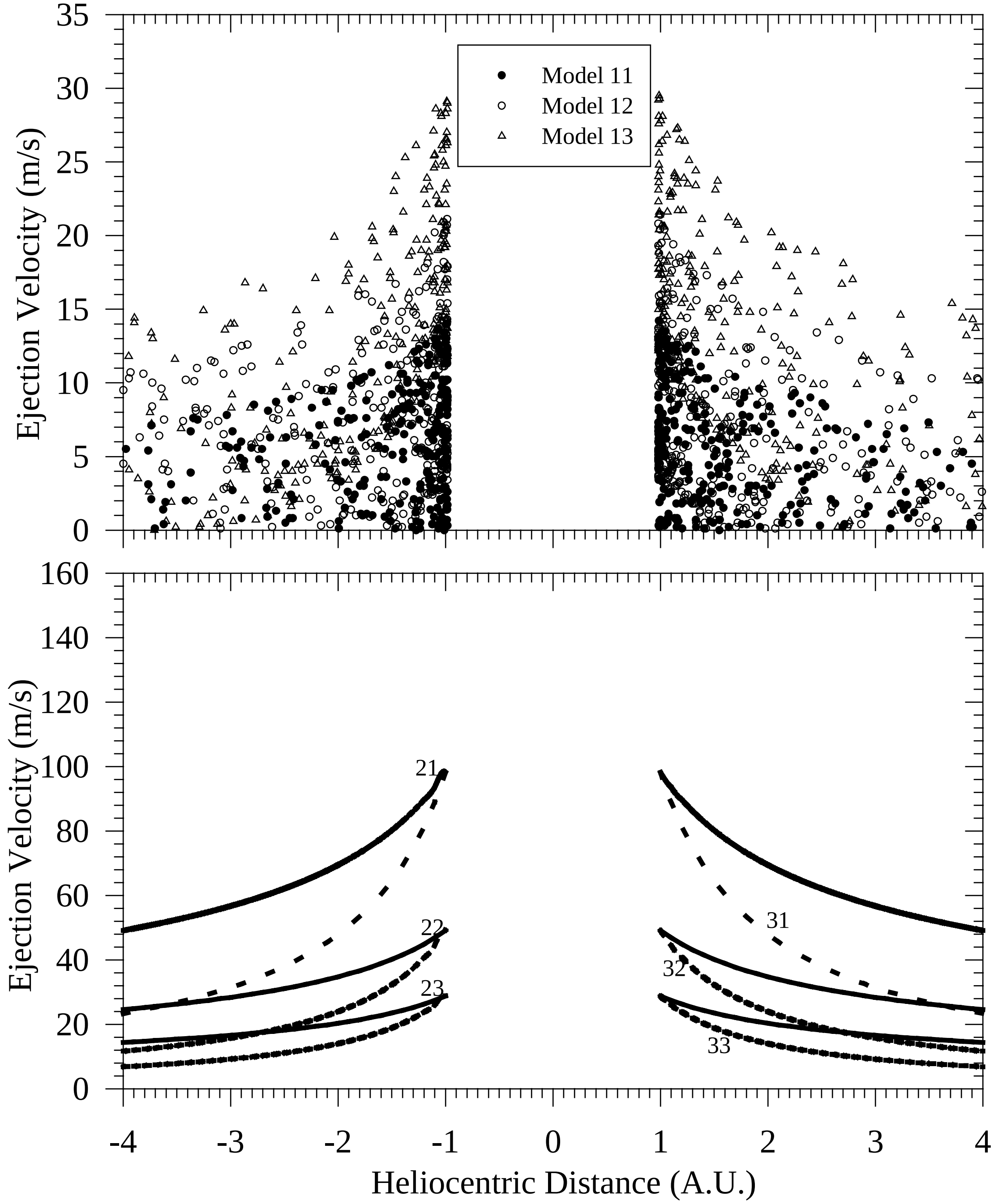

Fig 6.1: Ejection velocities for meteoroids of mass 10^{-3} g for Leonids for models 11,12 and 13 (top) and for 21-33 (bottom). Negative values in the abscissa are pre-perihelion.

Table 6.1: The model numbers, literature references for original material and ejection formulae used to simulate the formation of the Leonid meteoroid stream. Note that in addition to each model number a second number is also used to refer to the density as 1 (100 kg m^{-3}), 2 (800 kg m^{-3}) and 3 (4000 kg m^{-3}). Thus model 12 uses the Crifo distributed production model ejection velocity formula and assigns all meteoroids a bulk density of 800 kg m^{-3}.

Model #	Name	Ejection Formula
1	Crifo Distributed Production Crifo (1995)	$Log_{10}(V_{eject}) = -2.143 - 0.605 Log_{10}(radius) - 0.5 Log_{10} r$ $P(V - Veject) = \frac{1}{e^{3.7}} \exp\left[\frac{3.7 - 10.26(V - Veject) + 4.12(V - Veject)^2}{1 - 1.03(V - Veject) + 0.296(V - Veject)^2}\right]$
2	Jones Ejection Distribution with Modified Heliocentric Velocity Dependence Jones (1995)	$V_{eject} = 10.2\, r^{-0.5} \rho^{-\frac{1}{3}} R_c^{\frac{1}{2}} m^{-\frac{1}{6}}$ P(V-Veject) = 1 for V=Veject and 0 otherwise
3	Jones Ejection Distribution Jones (1995)	$V_{eject} = 10.2\, r^{-1.038} \rho^{-\frac{1}{3}} R_c^{\frac{1}{2}} m^{-\frac{1}{6}}$ P(V-Veject) = 1 for V=Veject and 0 otherwise
4	Jones ejection distribution with parabolic probability distribution Jones (1995)	$V_{eject} = 10.2\, r^{-1.038} \rho^{-\frac{1}{3}} R_c^{\frac{1}{2}} m^{-\frac{1}{6}}$ $P(V - Veject) = 1 - (\frac{V}{Veject} - 1)^2$ for 0<V<2Veject and 0 outside this range

One approach is to use the inherent numerical limitations of the integrator in concert with the normal process of chaotic divergence of initially similar orbits. Together these produce a lower limit to the meaningful size of the spatial and temporal binning chosen over the time-scales of interest.

To investigate this, we use the initial osculating elements for Tempel-Tuttle in 1499 and integrate these forward to 1998, using the same numerical parameters used for particle integrations. By comparing these final results with those from the Yeomans *et al.* (1996) ephemeris we are able to define an effective lower limit for the useful binning intervals. In particular, since our integrations do not take into account the effects of non-gravitational forces for Tempel-Tuttle (which the Yeomans *et al.* (1996) results do) we expect that our results will be larger than the actual results; hence any choice for the binning intervals will be similarly conservative.

We have examined the differences between the osculating elements for Tempel-Tuttle from our integrations and those given from Yeomans *et al.* (1996) at the epoch of the comet's 1998 perihelion passage. On this basis, we have found that the difference in the times of perihelion passage and nodal distance after 500 years are, respectively, 0.025 years (roughly one week) and 7×10^{-4} A.U. (about 7 Earth diameters). This leads us to adopt a bin size of 0.02 years and 0.001 A.U. in nodal distance for the simulations. In a representative examination of both temporally and spatially larger bin sizes we noted that our final results became significantly different once bin sizes ~ 3 times larger than the above were used. The nodal distance was particularly sensitive to this.

As our purpose is (in part) to investigate the densest portions of the Leonid stream (these being associated with the "trails" from Tempel-Tuttle), we note that the above choice of bin sizes is compatible with the spatial size of IRAS dust trails, which are slightly smaller than 10^{-3} A.U. in width at 1 A.U (Kresak, 1993). Asher (1999) has also independently estimated the cross-section of the storm-producing portions of the Leonid stream as 10^{-3} A.U. in general accord with the foregoing.

An alternate approach is to adjust the bin sizing until the activity profiles for a particular year match those observed. Unfortunately, this requires some conversion between the number of accepted test particles and flux, which is not possible at this stage (see next section). An approximate idea of usable bins can be generated, however, by examining the bin sizes at which "features" begin to appear that were (or were not) actually recorded. This technique was applied to the 1998 and 1966 shower/storm and confirmed our overall choice of bin widths in qualitative terms.

6.4 Simulation Results - Recent Epochs (1833-1965)

In what follows we describe in some detail the results of the simulations for different epochs and compare these to observations. Several important factors should be kept in mind. First, the simulations extend back only 500 years (except for the single long-term simulation referenced to the current (1998) epoch discussed in Sect. 6.5). Results showing a predominant population of meteoroids from this age may simply reflect the greater diffusion of older populations, leading to the acceptance of a small number of meteoroids under any conditions, and not the true population (which may be older still).

Secondly, the test particles accepted are counted and summed in each mass bin with no additional weighting. In reality, some initial mass distribution exists within the cometary coma and there should be many more small meteoroids than larger ones. However, the value for the mass distribution is very uncertain; there has only been one direct measurement of the mass distribution inside a cometary coma (McDonnell *et al.*, 1987) yielding a value of s=1.7 (from Halley's comet) and then only at masses smaller than those used here and made over a short interval of time. Ground-based observational attempts to determine this mass distribution exponent (cf. Fulle, 1996) have consistently suggested large changes in the exponent as a function of time as well as large inter-comet variations and pre/post perihelion asymmetries in the value of this exponent. Since the determination of a final "activity" here at Earth is heavily dependent on this power-law exponent, it becomes almost impossible a priori to make accurate flux estimates from model results without knowing the initial mass distribution exponent (if a single value even exists over the seven orders of magnitude mass investigated here). Limited experimentation with the present results using the Halley-determined value of the initial mass exponent (s=1.7) suggested that relative activities are somewhat unchanged (as compared to a simple unweighted summation of all test particles), but this conclusion does not hold when significantly steep distributions (s=2 or higher) are used and where the presence of only 1-2 test particles of small mass can utterly distort the entire distribution.

As a result of this limitation, we are examining effectively the transfer efficiencies as a function of mass and are summing these values over discrete mass ranges in an attempt to cover a physically meaningful range in β. Fortunately, it is likely that for true Leonid meteoroids a range in bulk densities and shapes affords a modest range in β for any given mass making this approach a reasonable first approximation.

Variations in the accepted cone angle will likely modify the results, which follow. In an earlier study of the Perseid shower (Brown and Jones, 1998), we found only modest changes resulting from moderate shifts in the accepted cone angle and have chosen not to investigate this aspect further although it certainly warrants some attention. Given our very limited observation history of Tempel-Tuttle (cf. Yeomans *et al.*, 1996), it is unlikely we would be able to constrain cone angle solely on the basis of past observations. Re-examining all the results with cone angles as another variable is beyond the scope of this work.

6.4.1 The 1965 Epoch

Fig 6.2 shows a typical nodal footprint from the simulations using visual-class particles (mass>0.001 g) for the entire 1965 epoch for models 22 and 23 at three mass categories with 10 000 particles in each category ejected. Note the strongest concentration is just inside the Earth's orbit near the nodal point of Tempel-Tuttle. As expected, the spread in size of the nodal region increases as mass decreases. Fig 6.3a shows a similar distribution, with nodal distances plotted as a function of time for the ejection primarily responsible for the 1966 storm (1899). Note the monotonic increase in nodal distance as a function of nodal passage time for the densest region. This structure crosses the Earth's orbit at almost precisely the location of the 1966 Leonid storm and is almost certainly responsible for it. This pattern is the result of differential planetary perturbations on the material, primarily from Jupiter. Note that the removal of direct perturbations from Jupiter leaves this material entirely inside the Earth's orbit (Fig 6.3b).

Using our adopted temporal and spatial sieving sizes, we have isolated the simulated activity from visual-sized Leonids for each year from 1961-1969. With these distributions, we have computed the locations of predicted maxima (defined in the simulations as simply the largest number of test particles in a particular bin) as a function of solar longitude for each of these years through weighting the results from each model by the number of test particles in the maximum bin. The locations of observed maximum from visual activity are from Chapter 5 and are given in Fig 6.4 along with the theoretical locations for the 1965 and previous epochs. Of note is the close correspondence between the observed locations of maximum and the weighted theoretical locations in 1966 and 1969. These years have the most complete observations and most certain times of maximum. The years before 1965 are poorly covered observationally and have few test particles.

In Table 6.2 we also list the ejection years which produce the largest number of test particles per model within our sieving constraints for each year. It is apparent that the displays in different years are from quite different sources. The outburst in 1961, for example, is due almost entirely to material ejected in 1499 or earlier, whilst the stronger outburst in 1969 is from ejecta released in 1932. Particularly interesting are the most probable sources of the displays from 1965 and 1966; the former is composed primarily of large meteoroids (see Fig 6.5) with ages >500 years, while the storm of 1966 is due to material ejected in 1899. These results lead to immediate explanations of why the 1965 display was long-lived and made up of many large meteoroids and why the 1969 display was so narrow and yet so far from the location of the 1966 display: the populations in the two years were of entirely different ages and hence had different perturbation histories.

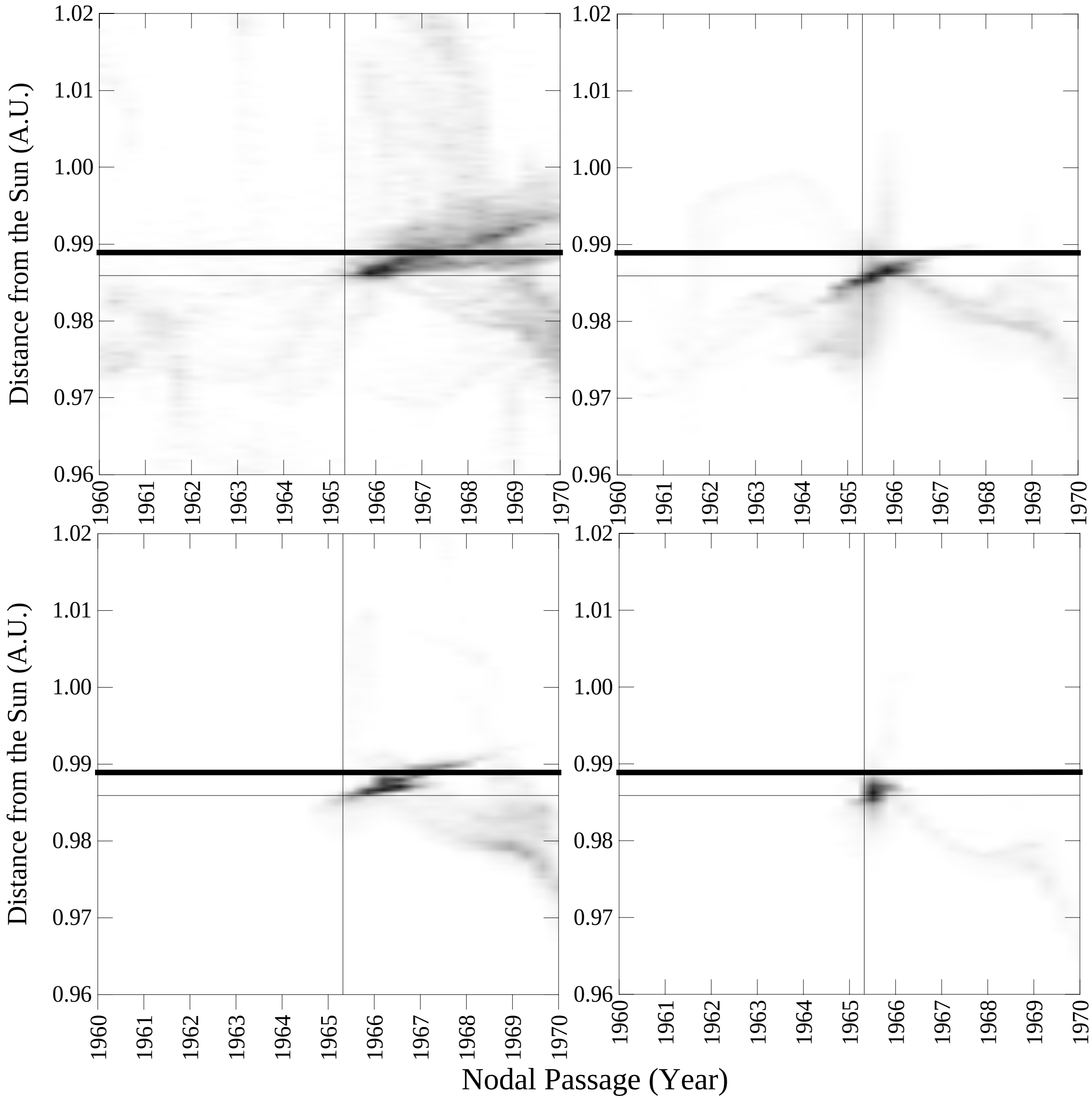

Fig 6.2: Test particle nodal distributions at the April 1965 epoch for model 31 meteoroids of mass 10^{-3} g (β=4×10^{-3}) (top left), 10 g (β=2×10^{-4})(top right) and for model 12 meteoroids of mass 10^{-3} g (β=10^{-3}) (bottom left) and 10 g (β=5×10^{-5}) (bottom right). The bold line is the distance of the Earth from the Sun on Nov 17 each year and the intersection of the thin lines marks the nodal crossing time and distance for 55P/Tempel-Tuttle during the 1965 epoch. The distributions represent the summation of all ejections from 1466 – 1932 A.D. for these particular mass categories.

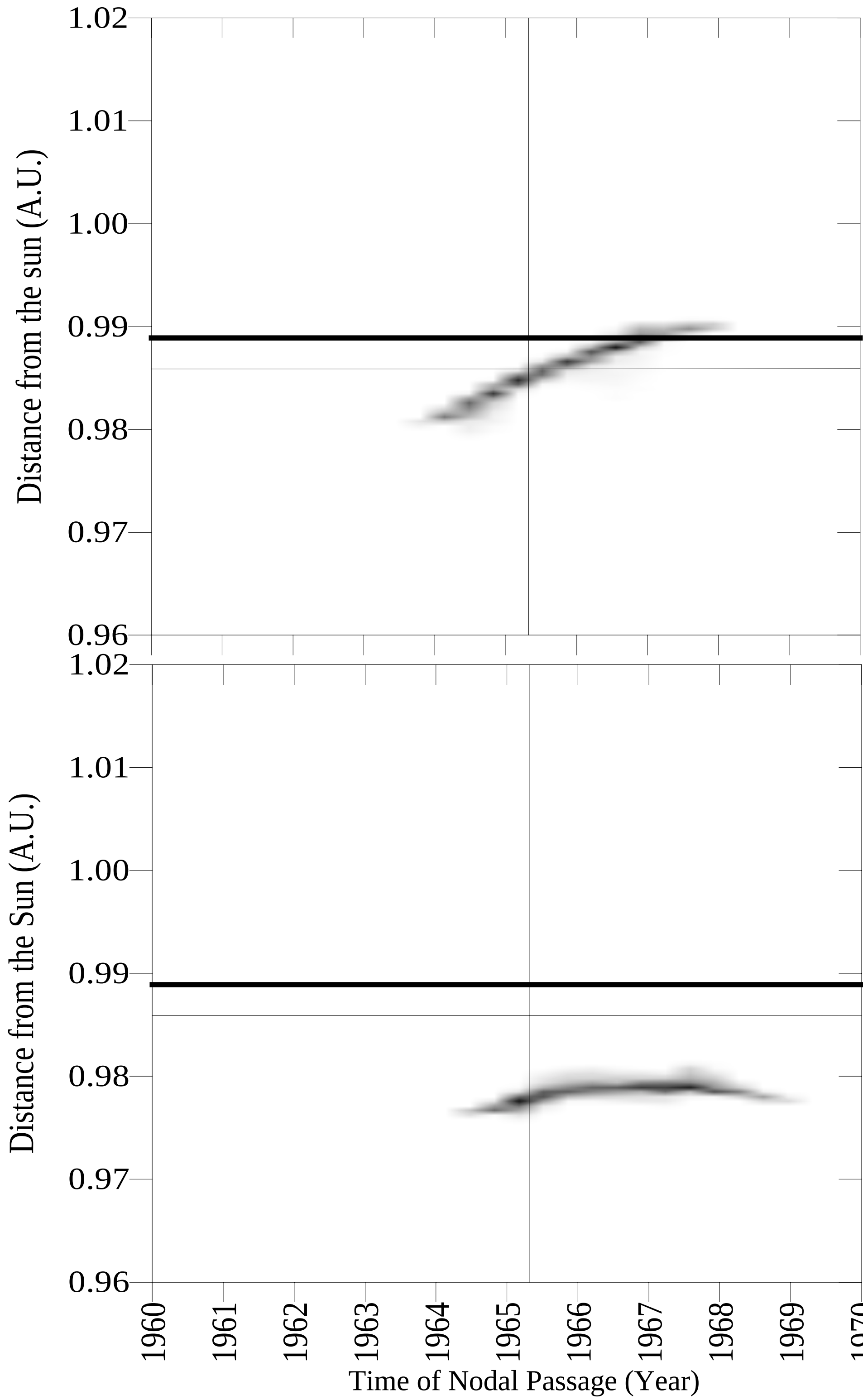

Fig 6.3: Nodal distribution for meteoroids ejected in 1899 of mass 0.1 g using model 42 at the 1965 epoch with all planetary perturbations (a) – (top) and without Jupiter (b) - (bottom).

Table 6.2. Age of Leonid showers for each given year as a function of the model. The first number in each box is the total number of test particles with nodal radaii within 0.001 A.U. of Earth and nodal passage within 1 week of the Earth's passage. Successive numbers give the primary ejection year contributing to activity from the model (in brackets) and the fraction of all particles in a particular year from the ejection.

Model/Year	1961	1964	1965	1966	1967	1968	1969
11	12 **1499(1.0)**	40 **1766(.93)** 1499(.05)	147 **1666(.41)** 1699(.22)	411 **1899(.70)** 1932(.27)	26 **1932(.88)** 1699(.12)	58 **1932(.97)** 1599(.03)	102 **1932(1.0)**
12	6 **1499(1.0)**	52 **1766(.81)** 1566(.08)	147 **1666(.35)** 1499(.20)	265 **1899(.94)** 1866(.03)	1 **1899(1.0)**	19 **1599(.47)** 1566(.32)	0
13	17 **1499(.94)** 1599(.06)	90 **1766(.51)** 1499(.17)	173 **1499(.42)** 1766(.19)	73 **1899(1.0)**	0	54 **1566(.61)** 1599(.39)	0
21	39 **1499(.79)** 1599(.08)	42 **1499(.24)** 1466(.19)	221 **1866(.21)** 1833(.15)	251 **1899(.74)** 1932(.20)	62 **1932(.53)** 1899(.47)	40 **1932(.58)** 1566(.15	34 **1932(1.0)**
22	44 **1499(.84)** 1599(.11)	74 **1766(.41)** 1499(.24)	207 **1466(.19)** 1499(.13)	219 **1899(.74)** 1932(.20)	16 **1932(.56)** 1899(.38)	30 **1599(.50)** 1566(.37)	0
23	33 **1499(.76)** 1599(.11)	124 **1766(.42)** 1499(.23)	210 **1466(.22)** 1499(.18)	123 **1899(.98)** 1932(.02)	0	46 **1566(.52)** 1599(.39)	0
31	18 **1499(1.0)**	38 **1766(.29)** 1499(.29)	198 **1666(.18)** 1866(.16)	313 **1899(.74)** 1932(.21)	57 **1932(.54)** 1899(.42)	42 **1932(.67)** 1599(.17)	37 **1932(1.0)**
32	32 **1499(.91)** 1599(.09)	101 **1766(.61)** 1499(.15)	225 **1466(.23)** 1499(.22)	221 **1899(.77)** 1932(.19)	17 **1899(.53)** 1932(.41)	36 **1599(.53)** 1566(.36)	0
33	28 **1499(.82)** 1599(.14)	129 **1766(.47)** 1499(.24)	209 **1499(.34)** 1466(.19)	97 **1899(.97)** 1866(.03)	0	55 **1566(.67)** 1599(.33)	0
41	24 **1499(.88)** 1599(.04)	39 **1766(.38)** 1466(.21)	168 **1666(.21)** 1699(.17)	248 **1899(.70)** 1932(.23)	53 **1932(.62)** 1899(.34)	41 **1932(.68)** 1599(.20)	34 **1932(1.0)**
42	22 **1499(.86)** 1566(.09)	79 **1766(.59)** 1499(.16)	201 **1499(.28)** 1699(.15)	238 **1899(.81)** 1932(.14)	16 **1932(.50)** 1899(.50)	32 **1599(.41)** 1566(.28)	4 **1932(1.0)**
43	25 **1499(.80)** 1599(.20)	104 **1766(.49)** 1499(.22)	181 **1499(.42)** 1466(.19)	122 **1899(.93)** 1866(.04)	2 **1899(1.0)**	43 **1566(.65)** 1599(.28)	0

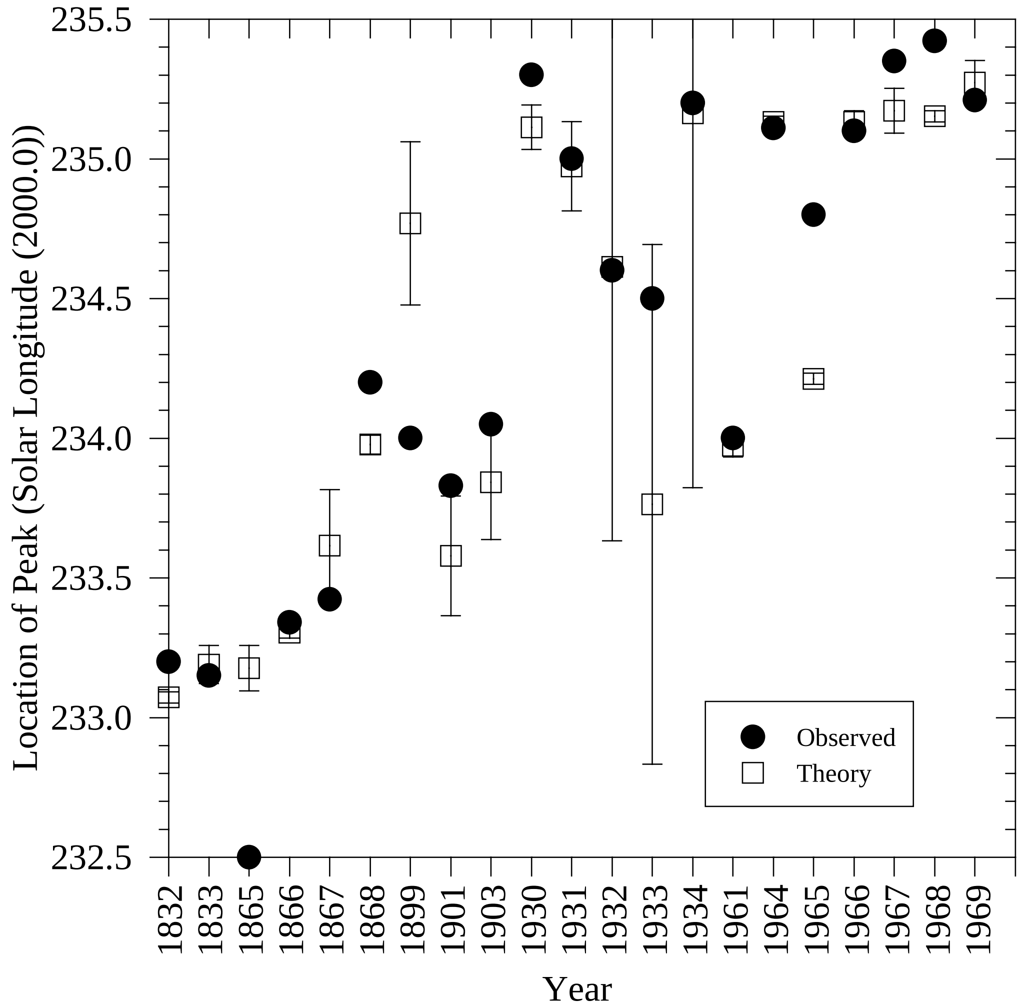

Fig 6.4: The observed locations for maxima (solid circles) for the Leonids from 1832 – 1969 (from Chapter 5) compared to the average weighted location from the modelling (open squares). The weighted location for each year is found by summing the peak locations found from each of the models (using a sieve of 0.001 A.U. and 1 week nodal passage time) and weighting by the number of test meteoroids in the solar longitude bin of the peak.

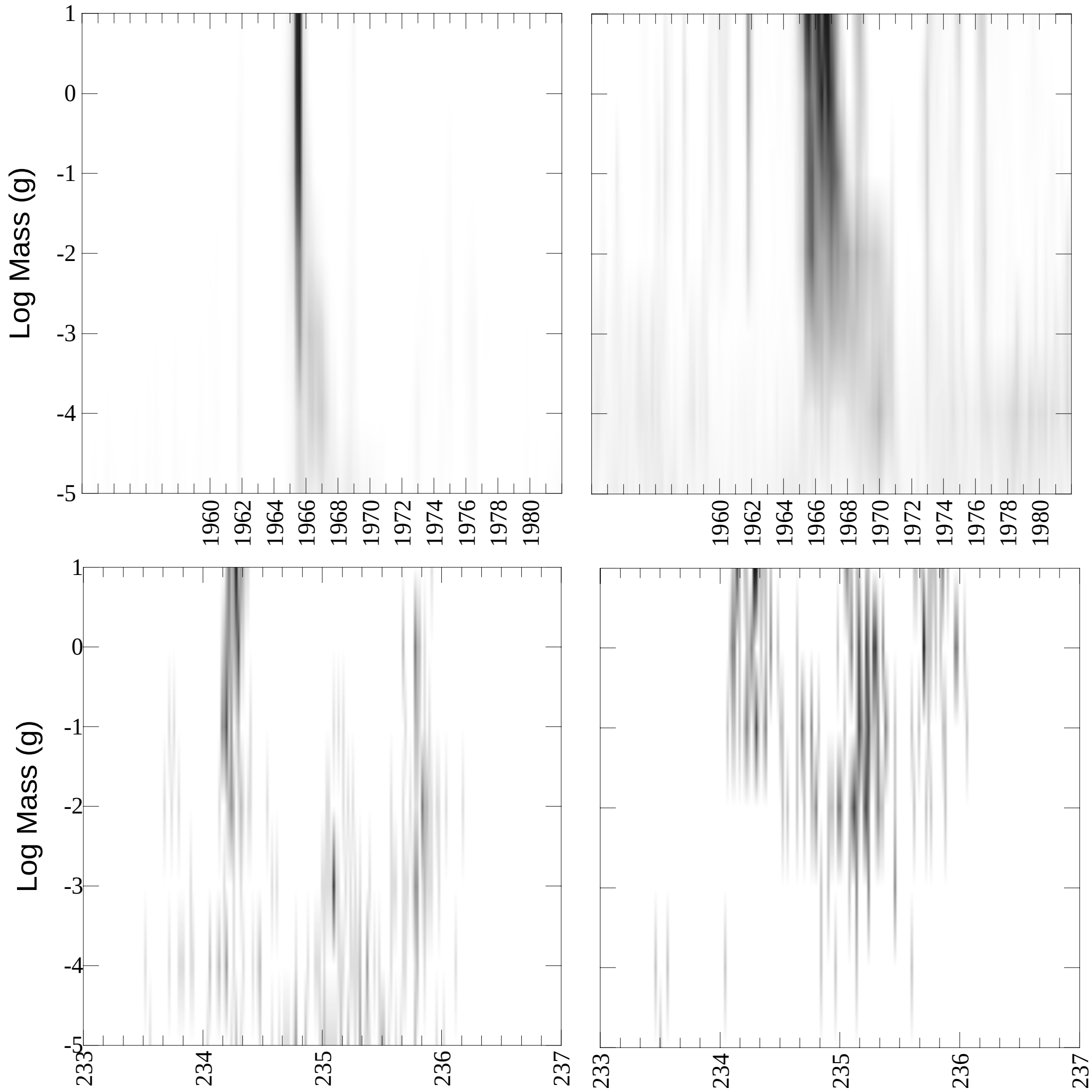

Fig 6.5: The distribution of Earth-intersecting meteoroids for model 13 (top left) and model 21 (top right) as a function of mass and time of nodal passage. The bottom plots show the distribution in solar longitude of Earth-intersecting Leonids during the 1965 Leonid shower for model 13 (lower left) and model 21 (lower right).

Of the displays in this epoch, the 1966 storm is the strongest and among the best documented. Fig 6.6a shows the distance between each of the "trails" ejected from Tempel-Tuttle from 1633-1932 at the time of the November, 1966 storm. Each point represents the average for a given model, the error margins representing the standard deviation of the individual points. It is clear that the 1899 trail passed extremely close to Earth in November, 1966 (independent of the ejection model or range of β used) while the trail from 1932 was several times more distant from Earth (and had wider spreads depending on the range of β and ejection model used). However the latter may still have contributed to activity.

Since it is only two revolutions old, its cross-sectional size provides a quasi-direct means of estimating initial ejection velocities since such young ejections should be relatively undisturbed by planetary perturbations. Fig 6.7 shows the gaussian width of the activity profile, for the two hours centred around the peak in November, 1966 from 1899 ejecta, for each model as a function of the normal component of the initial ejection velocity. Recalling that the gaussian width of the 1966 storm was of order 0.01°-0.015° (the former based on visual observations and the latter on radar observations (Brown *et al.,* 1997)), this implies normal components of ejection velocity of 2-3 m/s, corresponding (approximately) to total ejection velocities of order ~5 m/s based on our modelling.

To examine this question further, the initial velocities of material ejected in 1899 (which are accepted as within both our chosen binning intervals and the solar longitude interval from 235.1° - 235.2°) at the node in 1966 was investigated. Specifically, the radial, transverse and normal components of the ejection velocities as a function of ejection distance from the sun for each run and mass category were computed. It was found that some material at higher ejection velocities, possibly ejected as far as 4 A.U. from the sun in 1899, was accessible to the Earth at the time of the 1966 storm (though this does not necessarily mean Tempel-Tuttle was active at this distance to supply such material). However, the plots showed certain very narrow ranges in β (near 10^{-3}) at low ejection velocities that have an order of magnitude greater transfer efficiency than neighboring regions. Certainly the ejection models produce fewer high velocities (which also have larger degrees of freedom) but the sharpness of these transfer peaks cannot be explained in this manner (and we can eliminate very high ejection velocities as incompatible with the observed cross-section of the storm from Fig 6.7). Examination of the masses involved and their ejection velocities suggests that, in the case of the 1966 storm, material with very low ejection velocities (3-5 m/s total) had much higher dynamical transfer efficiencies from 1899. In addition, these regions were confined to very small ranges in true anomaly as well as β. The implication is that the 1966 storm may have represented very specific as opposed to representative material ejected from Tempel-Tuttle in 1899, with other true anomalies not accessible to Earth.

Fig 6.6b shows these same trail distances for 1969 and demonstrates conclusively that the material in that year must have been from ejections in 1932 as no other trail was close to Earth. More interestingly, the 1969 display is notable only in those trails with an abundance of low density meteoroids and is confined to a very narrow range of possible beta's (β~0.005-0.01). This can be qualitatively understood as the dual requirements of having to increase the period of 1969-observable Leonids to allow them to trail the comet by some 4 years combined with the narrow profile implying a recent origin; only young, high-β particles meet both requirements. Fig 6.8 shows the relationship between the gaussian width of 1932 ejecta in 1969 versus the normal component of the initial ejection velocity for material within 2 hours of the measured peak. From the visually observed width of 0.02°, we arrive at normal components of the ejection velocity of order 5-7 m/s, implying total ejection velocities ~10 m/s.

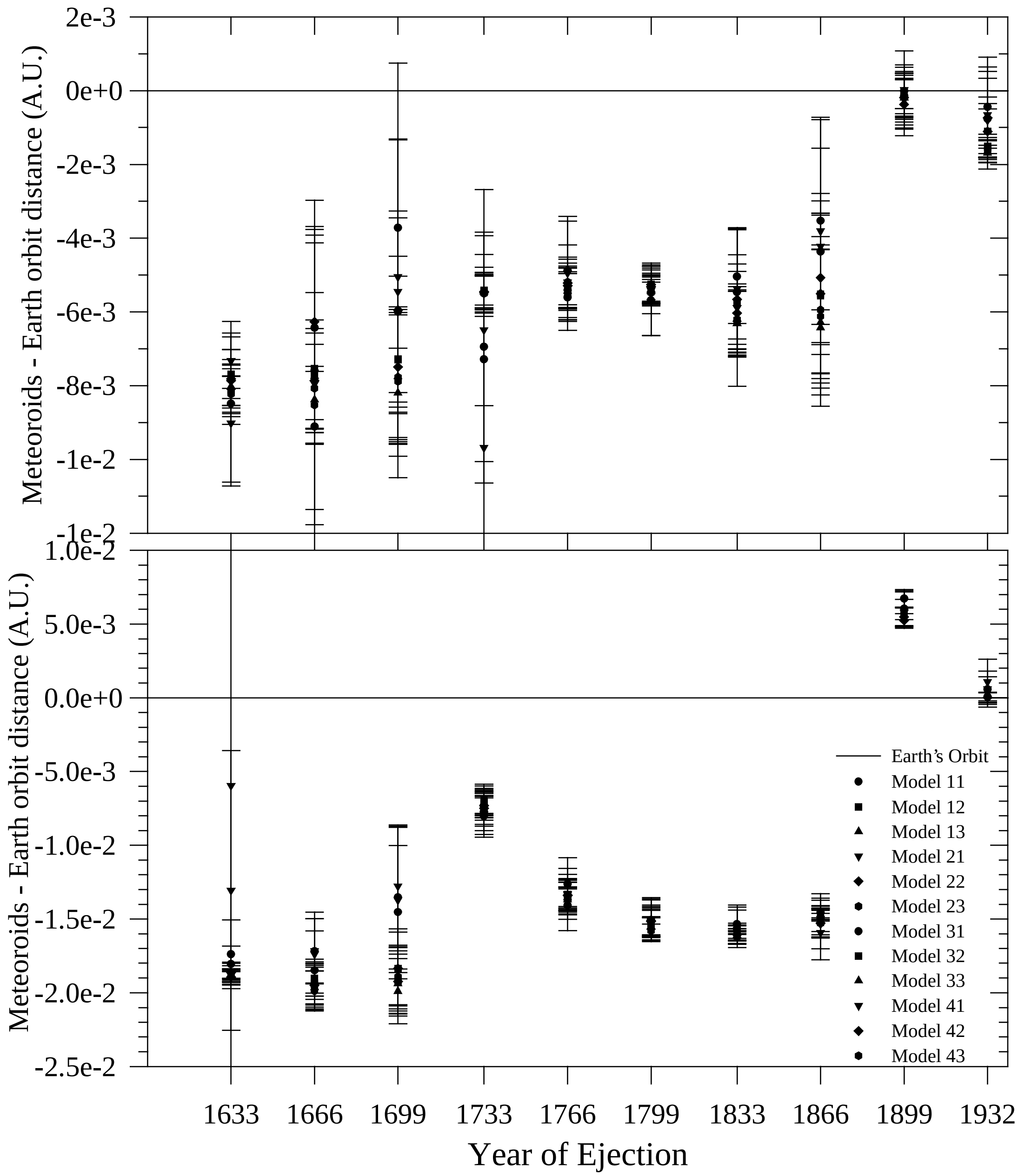

Fig 6.6: Average distance between ejected meteoroids in different years (abscissa) and the Earth at the time of the Leonid storm in 1966 (a) - (top) and the 1969 shower (b)-(bottom). Each model is represented by a different symbol – (see legend). Only test particles within 1 week of the peak of the shower in each year are included. The error margins are the standard deviations in the nodal distances from the sun for each model.

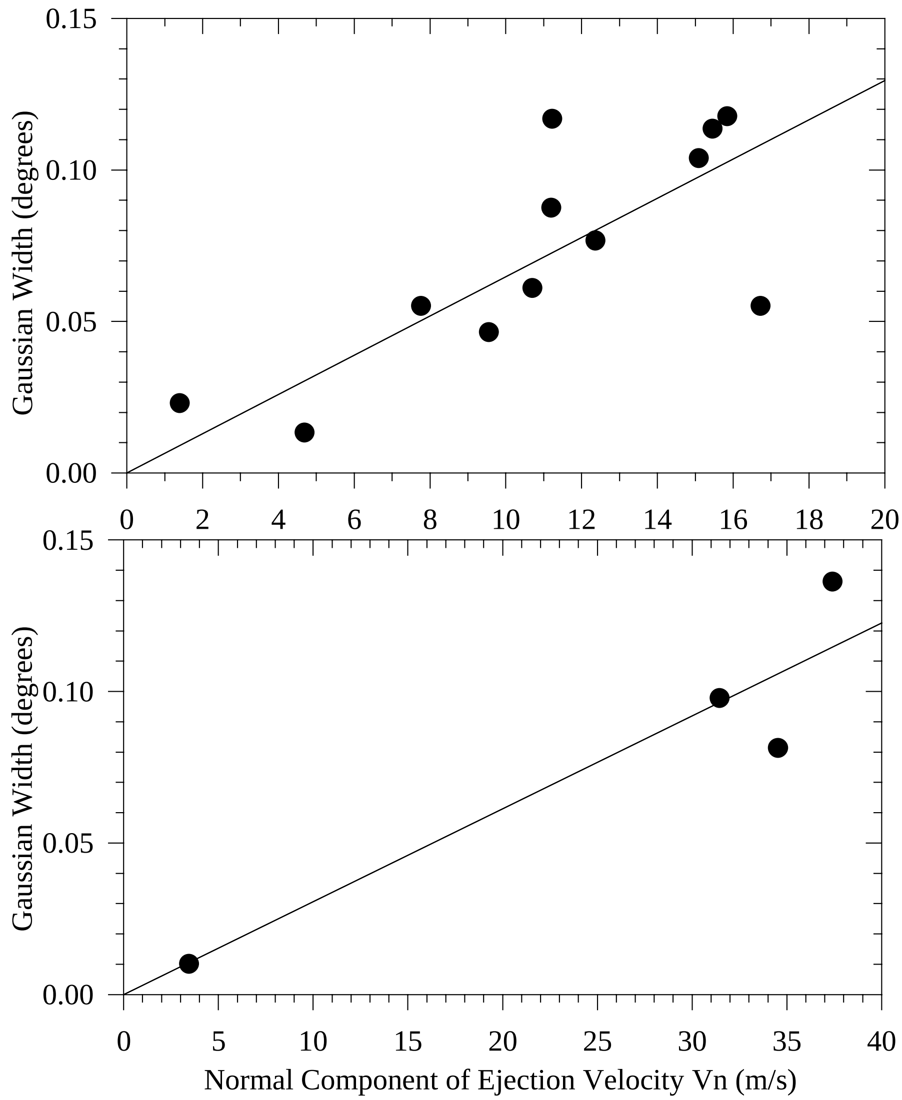

Fig 6.7 (top): The measured gaussian width from all models of the distribution of visual-sized Earth-intersecting meteoroids ejected in 1899 and encountered in 1966 between solar longitude 235.1°-235.2° as a function of the normal component V_n of the initial ejection velocity. Each model is represented by a single solid circle.

Fig 6.8 (bottom): The measured gaussian width from all models of the distribution of visual-sized Earth-intersecting meteoroids ejected in 1932 and encountered in 1969 between solar longitude 235.23°-235.33° as a function of the normal component V_n of the initial ejection velocity.

6.4.2 The 1932 Epoch

Fig 6.9 shows the cumulative number of test particles for models 11-21 as a function of nodal passage time during all Leonid returns from 1833-1998. The figure provides insight into the numbers of Leonid meteoroids passing through the node near the Earth as a function of time; of course the Earth samples only the stream once per year. The numbers of Earth-accessible test particles are significantly lower during the 1932 epoch than in 1965, a direct consequence of the larger comet-Earth orbital distance.

On many of the model outputs, a sharp increase in the number of test particles near the Earth occurs in 1932, near the time of the comet's passage. As well, in all models, this feature is short-lived, lasting only a few months and subsiding before the time of the 1932 shower. As a result, the lack of a major shower/storm during this cycle is unsurprising.

Indeed, from Table 6.3 it is apparent that all shower returns during this interval were dominated by old ejecta - typically 200-300 years in age and certainly not candidates for storms.

The locations of the observed shower maxima in Fig 6.4 for the 1932 epoch show good agreement between observed and theoretical values, particularly considering that the locations of the maxima result from ejections several centuries in age. The largest discrepancies (i.e. 1933) may well be the result of limited observational sampling, there being no observations available between 233.5°-234.5°.

The older activity throughout the 1930's is largely consistent with that expected from the simulations on the basis of the locations and magnitude of the maximum number of accepted test particles as compared to the observed peak ZHRs.

Table 6.3: Age of Leonid showers for a given year as a function of model. The first number in each box is the total number of test particles with nodal radaii within 0.001 A.U. of Earth and nodal passage within 1 week of the Earth's passage. Successive numbers give the primary ejection year contributing to the activity from the model and (in brackets) the fraction of all particles in a particular test year from this ejection.

Model/Year	1930	1931	1932	1933	1934
11	0	1 **1499(1.0)**	11 **1633(.45)** 1566(.27)	1 **1533(1.0)**	5 **1533(.60)** 1899(.40)
12	0	20 **1499(.50)** 1599(.20)	11 **1533(.36)** 1466(.27)	9 **1533(.67)** 1599(.33)	0
13	17 **1699(.94)** 1833(.06)	110 **1499(.35)** 1599(.12)	20 **1533(.40)** 1433(.30)	0	0
21	75 **1699(.49)** 1833(.31)	54 **1499(.28)** 1466(.22)	33 **1699(.33)** 1433(.12)	23 **1533(.57)**	18 **1899(.67)** 1433(.22)
22	74 **1699(.70)** 1833(.22)	122 **1499(.32)** 1466(.20)	26 **1699(.38)** 1433(.19)	11 **1533(.91)** 1599(.09)	1 **1599(1.0)**
23	69 **1699(.87)** 1833(.12)	194 **1499(.30)** 1466(.27)	29 **1433(.38)** 1533(.34)	12 **1533(1.0)**	0
31	31 **1699(.84)**	56 **1499(.27)** 1466(.21)	26 **1533(.54)** 1599(.12)	21 **1533(.81)** 1899(.19)	20 **1899(.75)** 1433(.25)
32	58 **1699(1.0)**	113 **1499(.27)** 1466(.23)	27 **1533(.67)** 1699(.15)	12 **1533(.92)** 1599(.08)	0
33	73 **1699(.99)** 1599(.01)	179 **1499(.39)** 1466(.16)	24 **1533(.71)** 1466(.25)	12 **1533(1.0)**	0
41	44 **1699(.50)** 1633(.20)	64 **1499(.39)** 1466(.16)	16 **1533(.50)** 1433(.19)	22 **1533(.73)** 1599(.05)	17 **1899(.76)** 1433(.18)
42	50 **1699(.80)** 1833(.14)	92 **1499(.35)** 1466(.25)	23 **1533(.57)** 1466(.17)	11 **1533(1.0)**	0
43	60 **1699(.90)** 1833(.07)	168 **1499(.26)** 1466(.24)	18 **1533(.72)** 1466(.17)	5 **1533(1.0)**	0

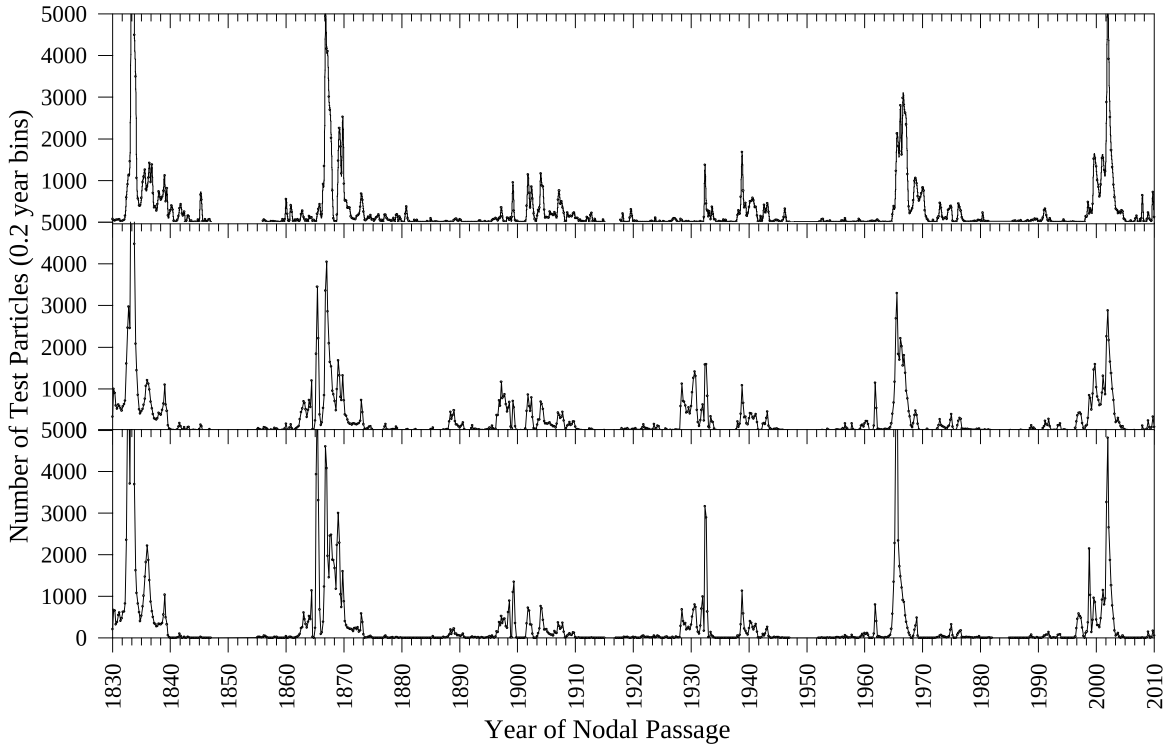

Fig 6.9: Total number of visual-sized test particles per 0.2 years for models 11 (top), 22 (middle) and 43 (bottom) that are within 0.001 A.U. of Earth's orbit.

6.4.3 The 1899 Epoch

As with the 1933 epoch, the 1899 epoch is most notable for its relatively weak activity and lack of any strong storms. However, the late occurrence of two modest showers in 1901 and 1903 did make the interval more active than in the 1930s. For the three years that had some observational determination of the location of peak activity (from Brown, 1999) and some test particles present, we plot these in Fig 6.5. Note that the 1898 display while observed to be relatively strong, had no test particles from any models "accepted" from the last 15 perihelion passages; it is probable that this return is older than 500 years.

The location of the peak in 1899 is uncertain for both the models (due to the small number of test particles involved) and also the observations due to the broad, flat level of observed activity. The exact locations of the 1901 and 1903 shower peaks are somewhat uncertain observationally as a result of poor longitude coverage, but the agreement with the models is satisfactory.

Activity throughout this epoch is dominated by relatively strong perturbations from both Jupiter and Saturn in 1898 and 1895 respectively, an effect noted at the time (cf. Stoney and Downing, 1899). The net result of these two combined perturbations is to move most of the material nearest the nodal passage of the comet well inside the Earth's orbit. Fig 6.10 shows the distribution of nodal distances as a function of nodal passage times for meteoroids from models 11 and 32. This effect also shows up in the distribution of the total number of Earth-accessible meteoroids as a function of time of nodal passage as given in Fig 6.4. Note the gap from 1900-1901 and a smaller gap in early 1899 as well as the relatively small number of test particles involved compared to the 1966 and 1932 epochs.

Table 6.4 shows the breakdown of material and ages for each of these returns. None of the years had any significant contribution from recent passages; indeed, the 1901 display is likely the result of material ejected either in 1733 or 1566 while the 1903 display is most probably from material ejected in 1499-1533. For both these years, the material being of order 5-10 revolutions in age suggests lower fluxes (relative to storm years) and very modest activity at best (see section 4 for more details). Fig 6.11 shows the distance from Earth to past trails in 1901 and for the 1903 shower in Fig 6.12. Note that the location of the maximum in solar longitude is the only discriminant for the age of the ejection responsible for the 1901 display, with the 1566 ejection peaking some 0.2° later than both the observed peak and the peak associated with 1733 meteoroids. This highlights the uncertainty of using close approach distances between past ejections and current activity alone to judge the age of a given return.

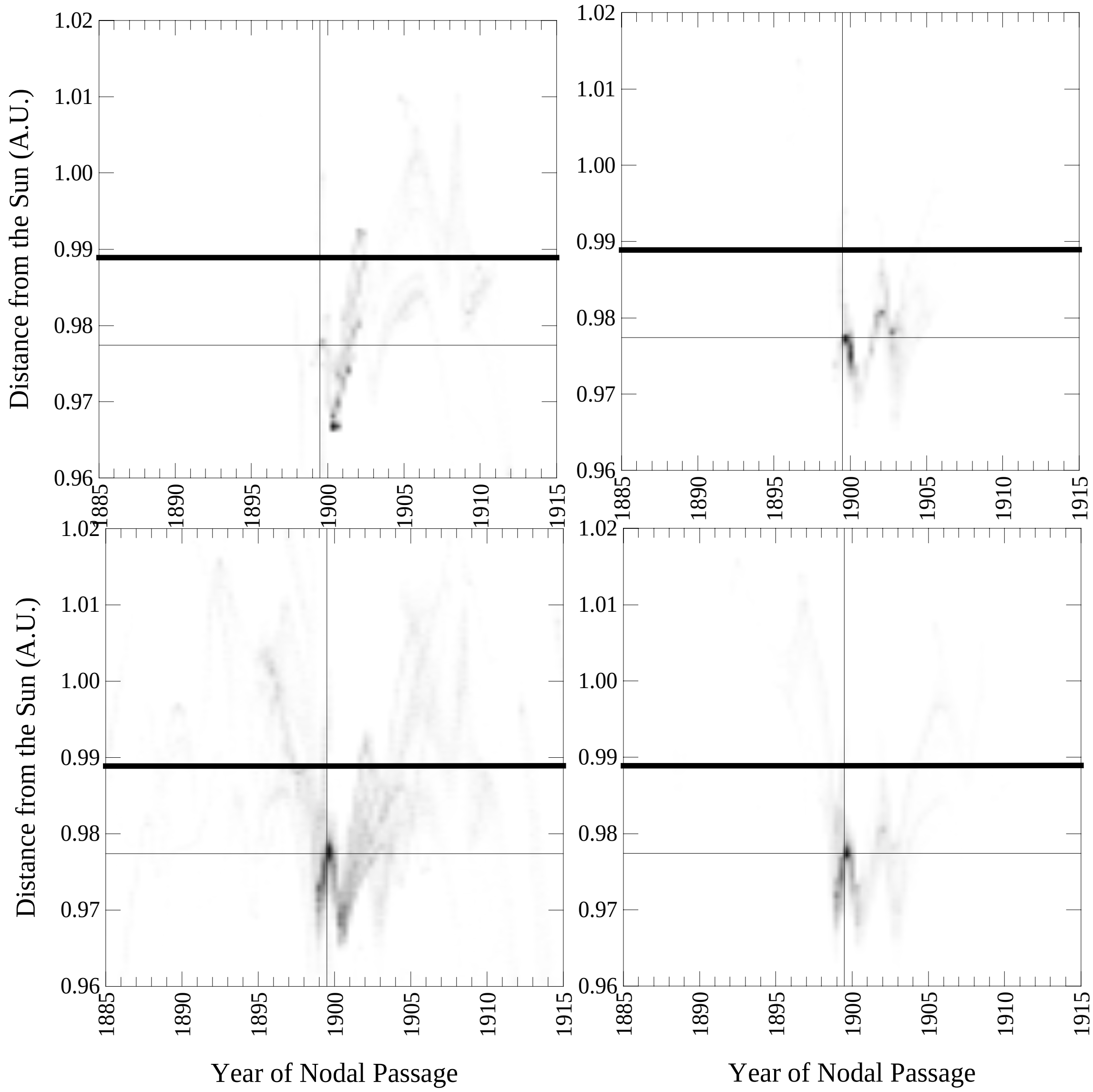

Fig 6.10: Test particle nodal distributions at the 1899 epoch for model 11 meteoroids of mass 10^{-1} g (β=10^{-3}) (top left), 10 g (β=2×10^{-4}) (top right) and for model 32 meteoroids of mass 10^{-3} g (β=10^{-3}) (bottom left) and 10 g (β=5×10^{-5}) (bottom right). The bold line is the distance of the Earth from the Sun on Nov 17 each year and the intersection of the thin lines marks the nodal crossing time and distance for 55P/Tempel-Tuttle during the 1899 epoch. The distributions represent the summation of all ejections from 1399 – 1866 A.D. for these particular mass categories.

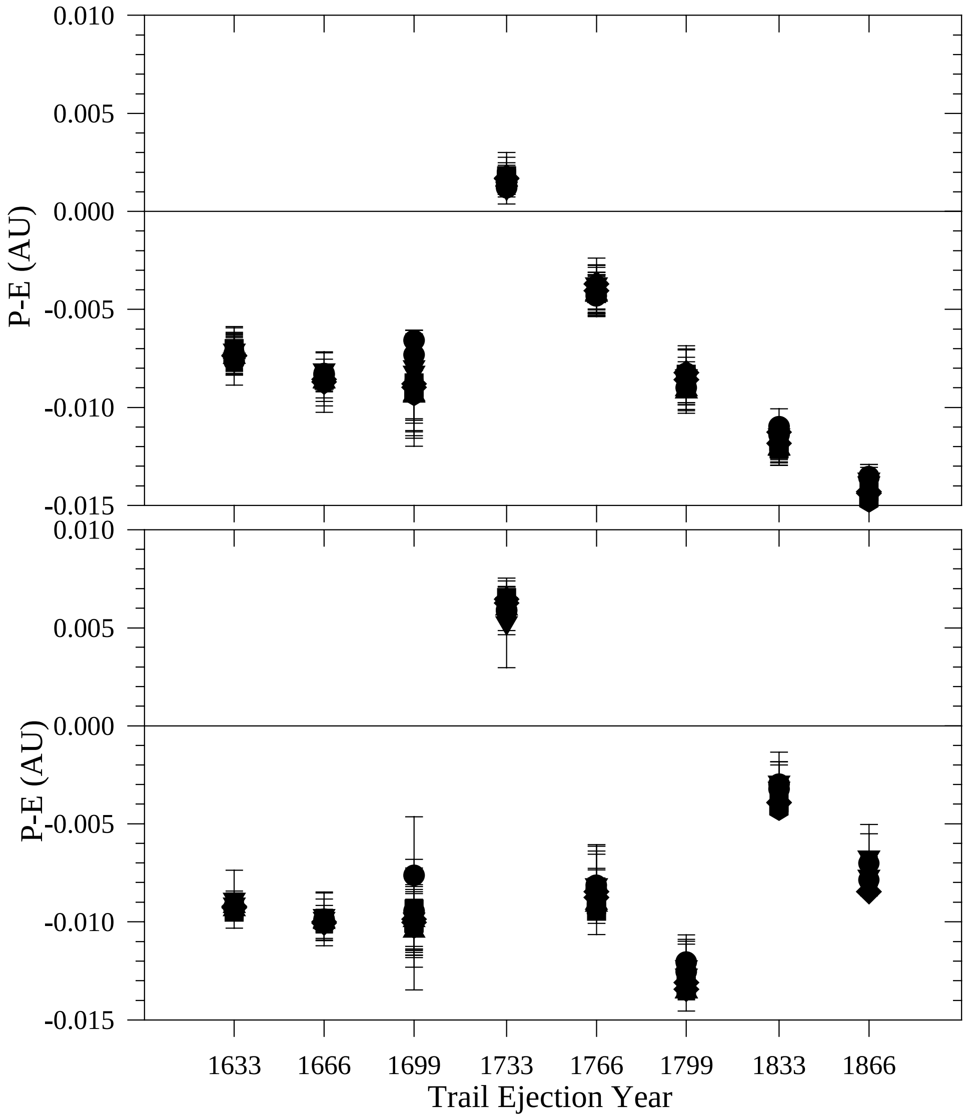

Fig 6.11 (top): Average distance between meteoroids ejected in different years (abscissa) and the Earth at the time of the Leonid shower in 1901. The model-symbol correspondence is the same as Fig 6.6. The error margins represent the standard deviations in the nodal distances from the sun for each model.

Fig 6.12 (bottom): Average distance between meteoroids ejected in different years (abscissa) and the Earth at the time of the Leonid shower in 1903. The model-symbol correspondence is the same as in Fig 6.6. The error margins represent the standard deviations in the nodal distances from the sun for each model.

Table 6.4: Age of Leonid showers for a given year as a function of model. The first number in each box is the total number of test particles with nodal radaii within 0.001 A.U. of Earth and nodal passage within 1 week of the Earth's passage. Successive numbers give the primary ejection year contributing to the activity from the model and (in brackets) the fraction of all particles in the year from this ejection.

Model/Year	1899	1901	1903
11	3 **1399(.67)** 1566(.33)	109 **1733(.39)** 1399(.17)	87 **1499(.23)** 1533(.22)
12	0	104 **1566(.55)** 1399(.17)	103 **1533(.50)** 1499(.17)
13	0	86 **1566(.55)** 1399(.24)	47 **1533(.49)** 1566(.19)
21	2 **1399(.50)**	58 **1733(.38)** 1766(.16)	49 **1533(.39)** 1499(.16)
22	0	68 **1399(.26)** 1566(.21)	65 **1533(.49)** 1499(.17)
23	2 **1566(.50)**	56 **1566(.36)** 1399(.32)	55 **1533(.56)** 1499(.11)
31	1 **1599(1.0)**	73 **1733(.40)** 1766(.16)	58 **1533(.45)** 1466(.14)
32	1 **1599(1.0)**	67 **1566(.36)** 1399(.22)	67 **1533(.63)** 1566(.12)
33	0	76 **1566(.50)** 1399(.22)	49 **1533(.47)** 1566(.24)
41	3 **1599(.33)** 1566(.33)	64 **1733(.38)** 1399(.19)	64 **1533(.31)** 1499(.22)
42	0	76 **1566(.32)** 1599(.20)	73 **1533(.55)** 1566(.14)
43	0	88 **1566(.61)** 1399(.17)	58 **1533(.50)** 1399(.17)

6.4.4 The 1866 Epoch

The 1866 epoch produced two Leonid meteor storms (1866, 1867) and at least one strong shower (1868). It also marked the first occasion when sufficient visual data were collected and recorded to produce activity profiles. Fig 6.13 plots the nodal radius as a function of nodal passage time for models 33 and 41 meteoroids with $10^{-5} < \beta < 4\times10^{-3}$. The densest portions are similar in shape to the previous epochs, namely a slight increase in nodal radius with time visible in all models and at all masses due to differential perturbations from Jupiter (principally) as well as Saturn. To demonstrate the significance of these perturbations on the observability of the stream at the 1866 epoch, Fig 6.14 a,b,c shows the nodal radius-time plot for material ejected in 1733 for model 22 meteoroids of mass 10^{-3}g (β=10^{-3}). The top plot is the actual distribution, the middle plot removes direct perturbations from Jupiter and the final plot eliminates both Jupiter and Saturn's influence. The accessibility of meteoroids from this ejection is entirely due to distant perturbations from Jupiter and Saturn, which moved nodes outward during the four revolutions since ejection, as was found for the 1966 storm. Other models and different β show very similar behaviour.

Table 6.5 shows the makeup of test particles as accepted from each model for the years 1865-1868. From Fig 6.4, only 1866 and 1867 have well-determined peak locations in agreement with the theoretical values; 1865 had very poor observer coverage (and was weak in the modelled activity) and 1868 shows a very broad maximum with poor longitude coverage, making its position uncertain by at least several hours.

The weak 1865 shower is likely caused by ejections in the time period 1533-1599 with no recent material evidently accessible in that year.

The storm of 1866 is almost certainly due to meteoroids ejected in any or all of 1733/1766/1799, with 1733 predominating when all solar longitudes are summed. A breakdown of the summation of the modelled meteoroids in a narrow window of three hours, centred on the measured position of the 1866 storm, shows a more even split among the three ejection years. It is probable that the 1866 storm was the result of1 material from at least two and possibly three ejections. Significantly, for the three hour window nearest the peak, the sum of material from 1733-1766-1799 represented 95% or more of the total sum for all test particles from the last 500 years for all models.

The peak locations of the model activity profiles and the observed 1866 storm differ by approximately one hour (the model predictions being earlier near the node), more than the time difference found for the 1966 storm. This might be a significant effect, though it is close to the level of binning used.

The width of the storm profiles is assumed to be primarily the result of ejection velocities (cf. Kresak, 1992). In Fig 6.15 we show the final gaussian width of each modelled profile in 1866 for each particular ejection and the average normal component of the ejection velocity for the associated material in 1866. This is shown for each of the ejection epochs 1733, 1766 and 1799. It is clear that very low normal velocities are associated with very narrow peaks (as expected), but the spread at slightly larger widths for the 1733 ejection is more surprising. It is clear that the 1799 and 1766 ejections have small widths and exhibit the behaviour expected, with small increases in the average normal velocity component associated with similarly small increases in the final measured activity widths. For 1733 this pattern completely breaks down, with all models showing much larger widths at a given velocity than either of 1799 or 1766 and no correlation remaining between the initial ejection velocities and the nodal dispersions. Heuristically we expect some small increase in the width of the distribution over time due to planetary perturbations (though this is the opposite of what happens between the 1766 and 1799 ejections) but clearly this is an order of magnitude larger change than would be expected based on the observed differences between 1766 and 1799. In fact, planetary perturbations from Saturn and Jupiter acting solely on the 1733 ejecta near Tempel-Tuttle's 1733 and 1766 perihelion passages are entirely responsible for the rapid "dispersal" of this material normal to the stream's orbital plane. This is a prime example of a "trail" disconnection or dispersal caused by planetary perturbations (see Sect. 6.5) and underscores the possible pitfalls in using wider (weaker) Leonid showers to measure initial ejection velocities.

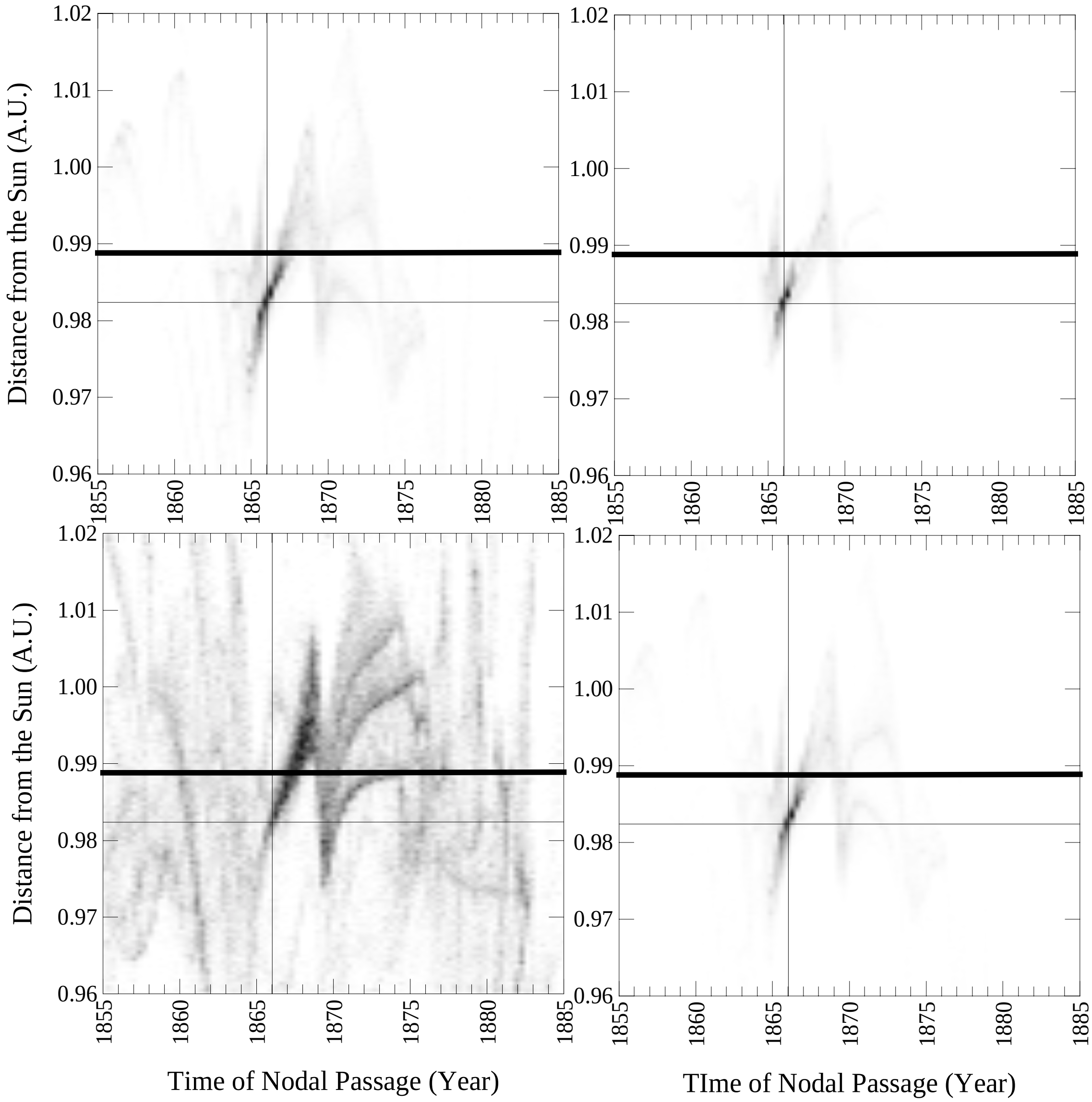

Fig 6.13: Test particle nodal distributions at the 1866 epoch for model 33 meteoroids of mass 10^{-3} g (β=3×10^{-4}) (top left), 10 g (β=2×10^{-5}) (top right) and for model 41 meteoroids of mass 10^{-3} g (β=10^{-3}) (bottom left) and 10 g (β=2×10^{-4}) (bottom right). The bold line is the distance of the Earth from the Sun on Nov 17 each year and the intersection of the thin lines marks the nodal crossing time and distance for 55P/Tempel-Tuttle during the 1866 epoch. The distributions represent the summation of all ejections from 1366 – 1832 A.D. for these particular mass categories.

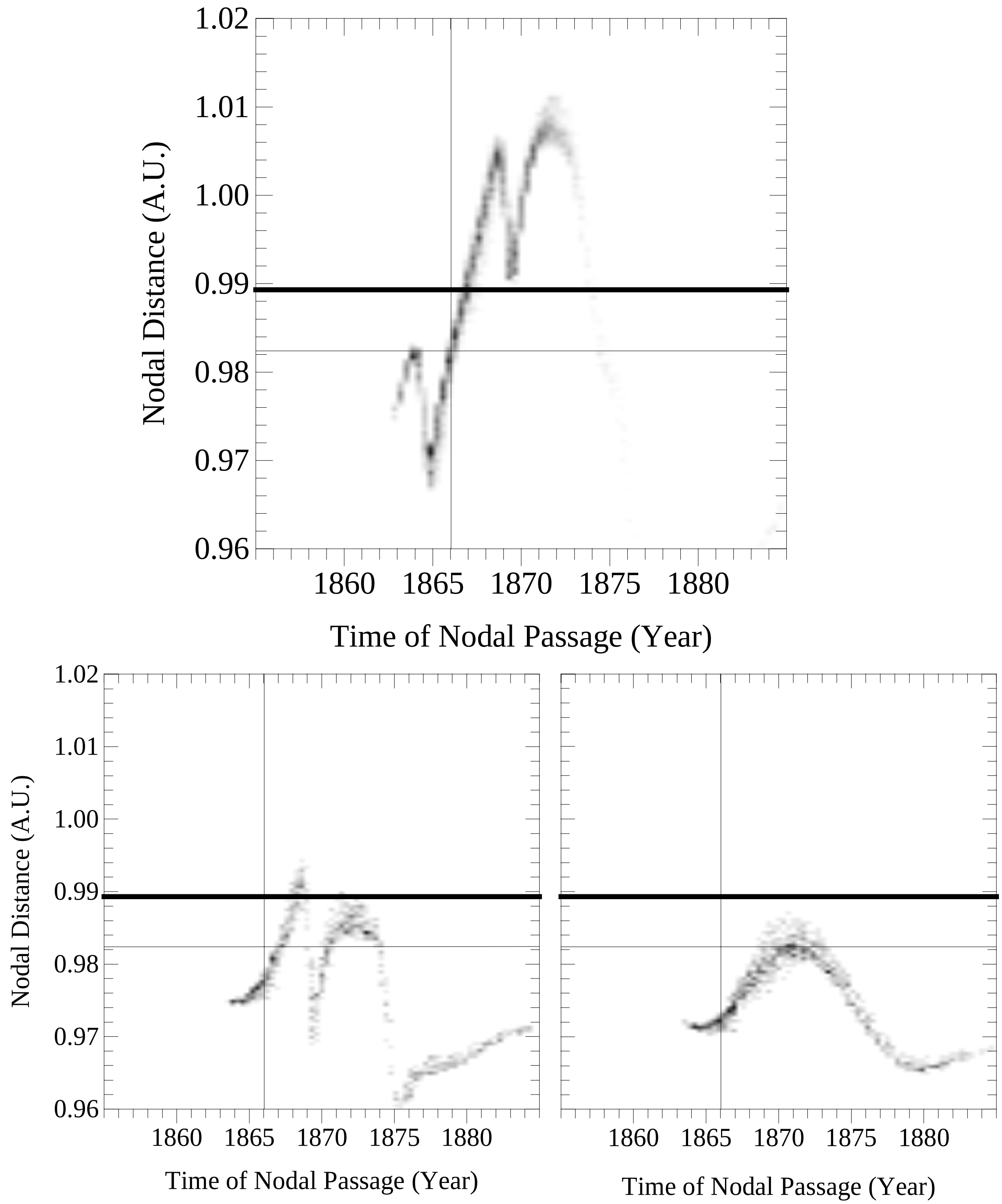

Fig 6.14: Nodal distribution for meteoroids ejected in 1733 using model 22 with a mass of 10^{-3} g at the 1866 epoch with all planetary perturbations (top), without Jupiter (bottom - left) and without Jupiter or Saturn (bottom – right).

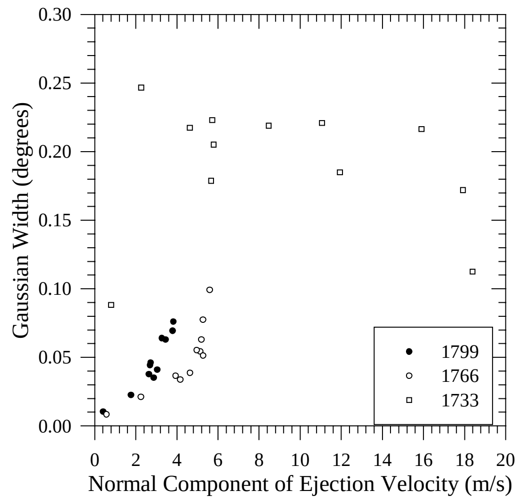

Fig 6.15 (top): The measured gaussian width, for all models of the distribution of visual-sized Earth-intersecting meteoroids ejected in 1733-1799 and encountered in 1866 between solar longitude 233.2°-233.4° as a function of the normal component V_n of the initial ejection velocity.

Fig 6.16 (below): The measured gaussian width, from all models of the distribution of visual-sized Earth-intersecting meteoroids ejected in 1832 and encountered in 1867 between solar longitude 233.3°-233.5° as a function of Vn.

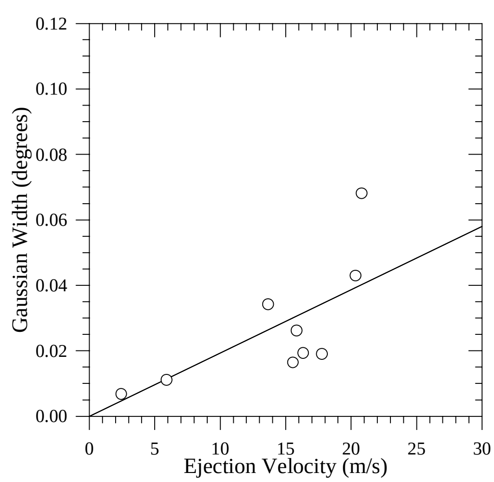

Table 6.5: Age of Leonid showers for a given year as a function of model. The first number in each box is the total number of test particles with nodal radaii within 0.001 A.U. of Earth and times of nodal passage within 1 week of the Earth's passage through the stream. The following numbers give the primary year contributing to the activity from the model and (in brackets) the fraction of all particles in a particular test year from this ejection.

Model/Year	1865	1866	1867	1868
11	63 **1599(.52)** 1566(.24)	816 **1733(.54)** 1766(.25)	268 **1833(.57)** 1699(.16)	68 **1833(.50)** 1566(.18)
12	59 **1599(.32)** 1566(.20)	1065 **1733(.64)** 1799(.16)	481 **1666(.38)** 1699(.25)	1095 **1466(.21)** 1499(.20)
13	39 **1599(.41)** 1533(.23)	854 **1733(.67)** 1766(.16)	533 **1666(.40)** 1699(.28)	997 **1533(.21)** 1599(.17)
21	23 **1599(.17)** 1533(.17)	407 **1733(.48)** 1766(.22)	252 **1833(.64)** 1666(.10)	180 **1833(.33)** 1533(.12)
22	22 **1566(.27)** 1533(.14)	780 **1733(.47)** 1766(.25)	269 **1833(.35)** 1666(.17)	255 **1833(.12)** 1533(.15)
23	31 **1566(.23)** 1533(.19)	1081 **1733(.61)** 1799(.19)	292 **1666(.30)** 1699(.25)	401 **1599(.15)** 1566(.15)
31	18 **1533(.33)** 1366(.28)	605 **1733(.41)** 1799(.32)	230 **1833(.55)** 1699(.10)	173 **1833(.36)** 1499(.12)
32	29 **1566(.24)** 1366(.17)	895 **1733(.53)** 1799(.22)	288 **1833(.29)** 1666(.23)	292 **1533(.17)** 1599(.14)
33	26 **1599(.27)** 1366(.23)	1055 **1733(.65)** 1799(.16)	384 **1666(.39)** 1699(.24)	448 **1533(.17)** 1599(.15)
41	24 **1599(.29)** 1566(.29)	564 **1733(.43)** 1799(.26)	228 **1833(.60)** 1666(.11)	179 **1833(.32)** 1599(.03)
42	32 **1599(.22)** 1466(.25)	924 **1733(.53)** 1799(.21)	336 **1833(.25)** 1666(.24)	354 **1533(.15)** 1599(.12)
43	27 **1533(.33)** 1599(.26)	953 **1733(.65)** 1766(.17)	457 **1666(.41)** 1699(.23)	579 **1533(.19)** 1599(.16)

Based on these results, the storm of 1866 is most probably due to material from

1766 and/or 1799, the 1733 material being much less concentrated than that of the other two returns. Its predominance in the overall breakdown of the dominant ejection years from 1866 is understandable given that we are integrating its activity over the entire range of solar longitudes in 1866; in the smaller intervals associated with the 1866 storm, 1799 and 1766 ejections prevail.

Assuming the ejections in 1799/1766 caused the 1866 storm, the observed width in 1866 near 0.02° would imply average normal components of ejection velocity of at most 1-3 m/s at most based on our modelling results. This finding is consistent with total average ejection velocities of order 5 m/s, very similar to that found for the 1966 storm.

The range of β from 1799 and 1766, from our initial ejection models which "compose" the 1866 storm are relatively limited, (though the distribution is wider than for the 1966 storm), with a strong peak near 2×10^{-4} and an overall range from $8\times10^{-5} < \beta < 4\times10^{-4}$. Examination of the orbital locations of ejection in these peak β intervals shows no concentration in true anomaly analogous to the 1966 storm ejecta from 1899.

The 1867 storm is interesting as it appears to be from younger material than 1866 (i.e. only one revolution old). As this storm lagged behind the comet by almost two full years, it is unsurprising (and indeed required) that the β are all higher than in 1866, with a peak near 10^{-3} and a range from 4×10^{-4} to 2×10^{-3}.

Fig 6.16 shows the equivalent gaussian widths of the 1833 ejecta in 1867 versus the normal component of the ejection velocity, to be, on average, higher than 1866 for a given solar longitude width (as expected for younger ejecta). The relation between width of the final distribution and ejection velocity is not as precise as for the material making up the 1866 return, in large part due to the smaller number of test particles available (a factor of 2-5 less than in 1866 depending on the model). As well, the sharp peaks for such young ejecta are nearer in width to the bin size used (0.005 degs in solar longitude). The observed width of the 1867 storm (0.022°) corresponds to material which has normal components of ejection of ~10 m/s and total ejection velocities of 15-20 m/s.

The 1868 shower shows no distinct peak or maximum in the observations, though typical model results (Fig 6.17) suggest a broad peak in activity should have occurred. The observed broad maximum for the short sampling time of the observations (~5 hours) does not contradict this result and suggests that this material may have been quite old, though no single ejection era is particularly dominant in 1868 (see Table 6.6).

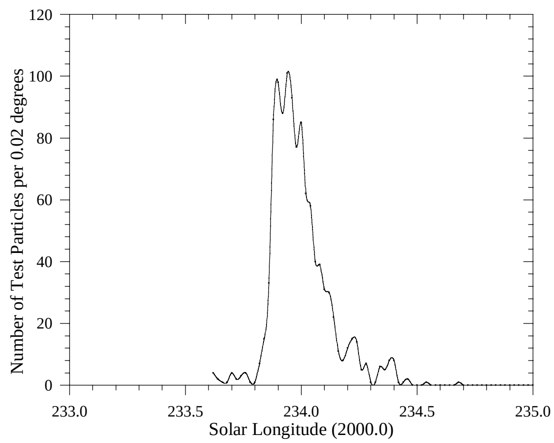

Fig 6.17: Number of visual-sized Earth-intersecting test particles as a function of solar longitude in 1868 for model 12.

6.4.5 The 1833 Epoch

The storms of 1832 and 1833 were not well documented. Other than an approximate time of maximum for both (see Brown, 1999), no clear activity profile is available.

From the computed nodal distribution it is determined that the densest portion of the stream passes very close to Earth's orbit in 1833. The characteristic upward sloping nodal distance (due to distant direct perturbations from Jupiter) is visible as in the previous epochs studied.

From Fig 6.9, it is notable that the maximum numbers reached in this interval for all models is a factor of several above most previous epochs, attesting to the high delivery efficiency in this era. The peak in test particle flux is reached in 1833 between the times of the 1832 and 1833 storms.

The 1832 storm appears to have been long-lived (Brown, 1999) and the particle makeup in this year supports an origin of at least four or five revolutions in age for the shower/storm of 1832. Table 6.6 lists the years contributing to the integrated flux over all solar longitudes in 1832. It is clear that older material (particularly from 1666) dominates the fluence. Fig 6.18a shows the location of the last six ejection "trails" in 1832 relative to the Earth's orbit. The 1699 and 1666 trails are clearly closest to Earth in 1832, explaining the results in Table 6.7. Fig 6.19a shows the stream activity profile for model 12 on November 12/13, 1832. The activity lasts almost twelve hours in general accord with observations. The discrepancy between the relative youth of the trails and the large spread in nodal longitudes is, in part, a consequence of inbound perturbations by Jupiter on the section of these trails in 1732. Note that all models have significant numbers of test particles in 1832 only for values of $\beta<5\times10^{-4}$.

The 1833 storm is most likely the result of the 1799 ejection. Table 6.6 shows clearly the dominance of this population near the Earth on Nov 13, 1833. Fig 6.18b shows the trail locations in 1833 for ejections back to 1633. Note that while 1799 is marginally closer than the previous three trails, the increased diffusion for the older trails lessens their relative contributions compared to 1799. The distribution of test particle masses in 1833 is shown in Fig 6.19b. It is clear from the figure that the majority of the test particles are encountered near 233.17°, less than 0.5 hours from the estimated time of maximum (cf. Brown, 1999). A broader distribution covering all masses is also apparent in this and other models and may explain the reports of heightened activity for several hours on either side of the main maximum.

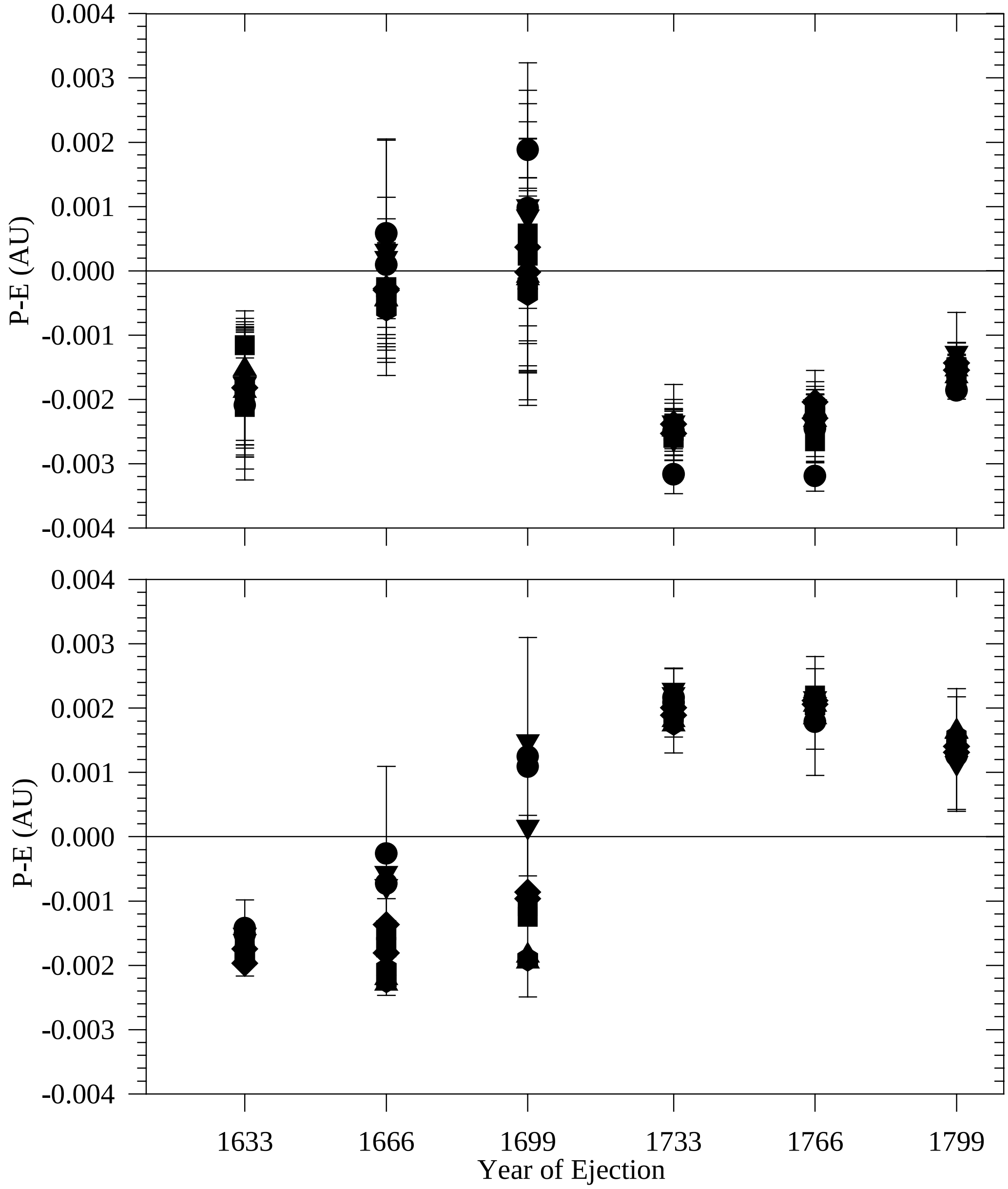

Fig 6.18: Average distance between ejected meteoroids in different years (abscissa) and the Earth at the time of the Leonid storm in 1832 (a) - (top) and the 1833 shower (b)-(bottom). Symbol-model correspondence is the same as in Fig 6.6. Only test particles within 1 week of the peak of the shower in each year are included. The error margins represent the standard deviations in the nodal distances from the sun for each model.

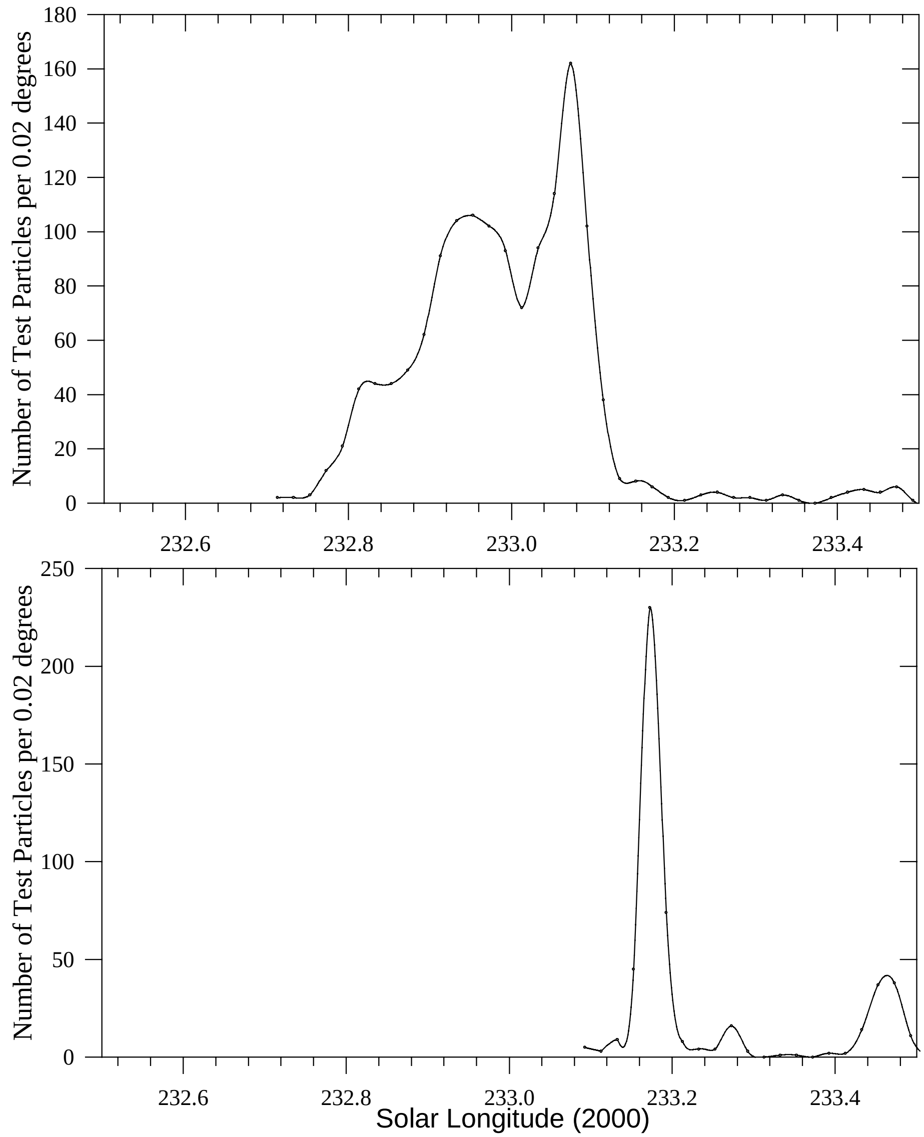

Fig 6.19: Number of Earth-intersecting test particles as a function of solar longitude in 1832 (a – top) and in 1833 (b- bottom) for model 12 meteoroids.

Table 6.6: Age of Leonid showers for a given year as a function of model. The first number in each box is the total number of test particles with nodal radaii within 0.001 A.U. of Earth and times of nodal passage within 1 week of the Earth's passage through the stream. The following numbers give the primary year contributing to the activity from the model and (in brackets) the fraction of all particles in a particular test year from this ejection. Columns for 1832a and 1833a refer to only those meteoroids between 233-233.3°.

Model/Year	1832	1833	1832a	1833a
11	278 **1666(.85)** 1399(.06)	832 **1799(.67)** 1766(.12)	31 **1399(.52)** 1333(.23)	672 **1799(.83)** 1766(.15)
12	1439 **1666(.37)** 1699(.27)	609 **1799(.56)** 1733(.13)	343 **1366(.18)** 1333(.17)	402 **1799(.85)** 1766(.10)
13	1871 **1666(.28)** 1699(.23)	390 **1799(.33)** 1733(.32)	686 **1399(.22)** 1333(.16)	150 **1799(.85)** 1766(.07)
21	417 **1799(.25)** 1666(.21)	572 **1799(.70)** 1766(.12)	168 **1799(.35)** 1333(.14)	394 **1799(.85)** 1766(.12)
22	583 **1666(.32)** 1633(.13)	548 **1799(.64)** 1733(.11)	207 **1799(.20)** 1333(.16)	363 **1799(.87)** 1766(.10)
23	815 **1666(.26)** 1699(.15)	434 **1799(.54)** 1733(.17)	321 **1399(.25)** 1333(.17)	269 **1799(.88)** 1766(.09)
31	397 **1666(.39)** 1799(.15)	519 **1799(.71)** 1766(.08)	141 **1799(.36)** 1399(.12)	349 **1799(.87)** 1766(.09)
32	665 **1666(.35)** 1699(.14)	541 **1799(.65)** 1733(.12)	233 **1799(.15)** 1333(.17)	373 **1799(.90)** 1766(.06)
33	862 **1666(.31)** 1699(.21)	396 **1799(.44)** 1733(.28)	291 **1399(.24)** 1433(.16)	191 **1799(.92)** 1766(.06)
41	460 **1666(.35)** 1699(.16)	499 **1799(.70)** 1766(.09)	154 **1799(.29)** 1399(.15)	344 **1799(.88)** 1766(.10)
42	796 **1666(.34)** 1699(.15)	537 **1799(.59)** 1733(.10)	270 **1399(.19)** 1433(.16)	345 **1799(.88)** 1766(.10)
43	1126 **1666(.31)** 1699(.20)	423 **1799(.42)** 1733(.28)	396 **1399(.22)** 1433(.16)	210 **1799(.84)** 1766(.09)

6.5 Long-term Integrations

In an effort to understand the longer term dynamics of the stream over an interval comparable to the full duration of its observed activity (first recorded in 902 A.D.), we have used the ephemeris of Tempel-Tuttle back to 82 A.D. and generated test particles for each perihelion passage for model 22. This represents a total of 57 perihelion passages of the comet. Each passage had 10 000 particles ejected at each of the seven decadal masses as in all other integrations. The integrations were stopped and information on each test particle stored at the nodal passage closest to the current epoch (1998). We have chosen model 22 as this was found to be the model most successful in reproducing Perseid activity in Brown and Jones (1998), without knowing *a priori* if the model will also be representative of the Leonids.

Fig 6.20 shows the fraction of all Leonids from each past ejection accessible to Earth (i.e. having nodes within 0.001 A.U.) at the present epoch (as a fraction of the total), along with the distance between the Earth's and the comet's orbit.

Two distinct temporal regimes are apparent: ejections since 1100 A.D. and those before. Through a combination of the longer time available for diffusion for old ejecta and (for ejections prior to 850 A.D.) larger distances from Earth's orbit, the older ejecta contribute significantly less on an ejection-by-ejection basis than does more recent material (as would be expected). The very small number of particles accessible prior to ~1100 A.D. suggests that the "annual" activity from the stream is due to material with an effective age of this order (roughly 1 millenium).

Interestingly, for most ejections since 1100 A.D. there is only a weak correlation between the total number of particles visible at the present epoch and the distance between the Earth's and comet's orbit. While the largest numbers are from ejections where the comet's orbit is inside the Earth's, the difference is marginal compared to slightly older ejecta where the comet's orbit is outside the Earth's. Much of the material in the 1100-1500 A.D. range which ends up at Earth, has small β (i.e. large meteoroids).

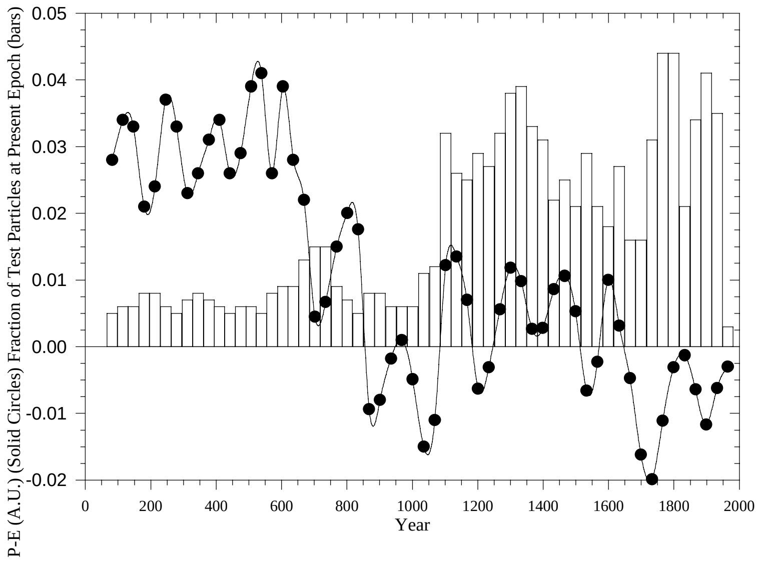

Fig 6.20 (above): The fraction of all visual-sized Leonid meteoroids within 0.001 A.U. of the Earth (at the 1998 epoch) as a function of the epoch of their ejection (bars). The solid line and circle represent the distance between the cometary node and the Earth referenced to the time of perihelion at each epoch.

Fig 6.21 (below): The fraction of visual-sized Leonid meteoroids within 0.001 A.U. of the Earth at the 1998 epoch for three different models over the last 500 years.

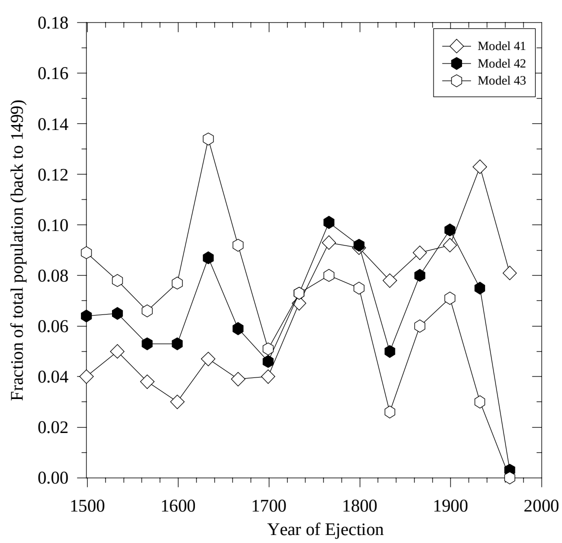

For ejection times from 300-500 years before the present, a distinct trend is visible in all models, such that higher densities (lower β's) are associated with larger numbers of particles currently visible at Earth. For ejections less than 300 years in age, no clear density-dependent sorting is in evidence as shown in Fig 6.21. This may be an effect of faster diffusion for higher β driven by differential planetary perturbations.

Thus, in terms of the total number of particles accessible at present to the Earth presently, the comet-Earth distance is only of secondary importance. This is likely a direct result of the fact that, throughout almost all of this interval, the comet orbit-Earth distance has been very small and so nodal diffusion (due to planetary perturbations), on time-scales from < tens of revolutions dominate the slight changes in comet-Earth distance (except potentially for the oldest ejecta where the distances become large and for the very concentrated young material which Earth can only intersect if it is sufficiently close to the comet's orbit).

It is important to note that the total number of test particles currently "intersecting" the Earth's orbit from a given ejection as we have measured it is not directly correlated with the magnitude of the resulting peak activity, but rather is a crude measure of the integrated flux along the orbit (i.e. integrated in mean anomaly) and across it (i.e. integrated in solar longitude). To determine the probable peak flux and significance of recent ejections, it is necessary to quantify the average decrease in flux at the node for the stream as a whole - that is, measure the dilution along the orbit (due to spreading caused by differing periods), across it (due to diffusion in the nodal longitude) and perpendicular to the stream orbit in a radial direction (spread in nodal distances).

To examine the question of diffusion in more detail, we have computed the average standard deviation, σ, of ascending node, nodal distance from the sun and mean anomaly in the elements for all visual-sized Leonid meteoroids (referenced to their nodal passages). The resulting distributions over the last 2000 years for model 22 are shown in Figs 6.22, 6.23 and 6.24 respectively. These are the standard deviations in the plotted quantities for individual (not cumulative) ejections for the years specified.

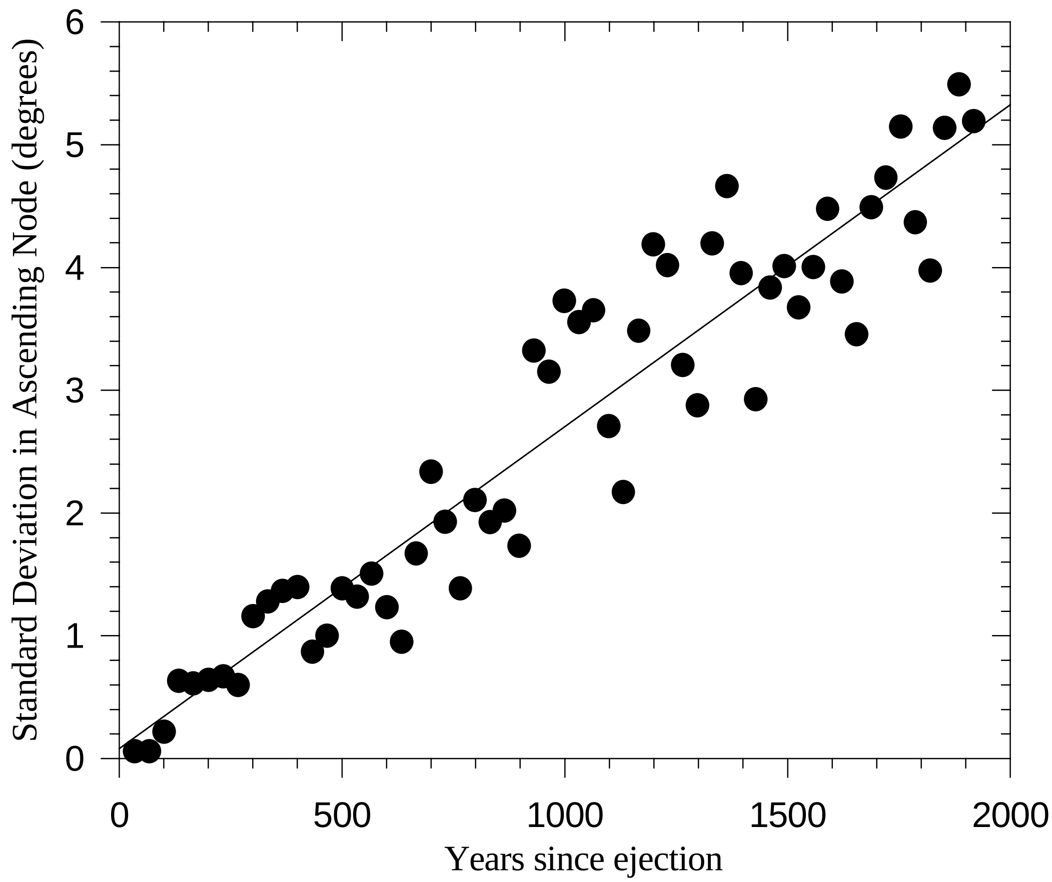

Fig 6.22: The standard deviation in the value of the ascending node for all visual-class meteoroids from model 22 for the last 2000 years. The solid line is the regression fit corresponding to Eq 6.1.

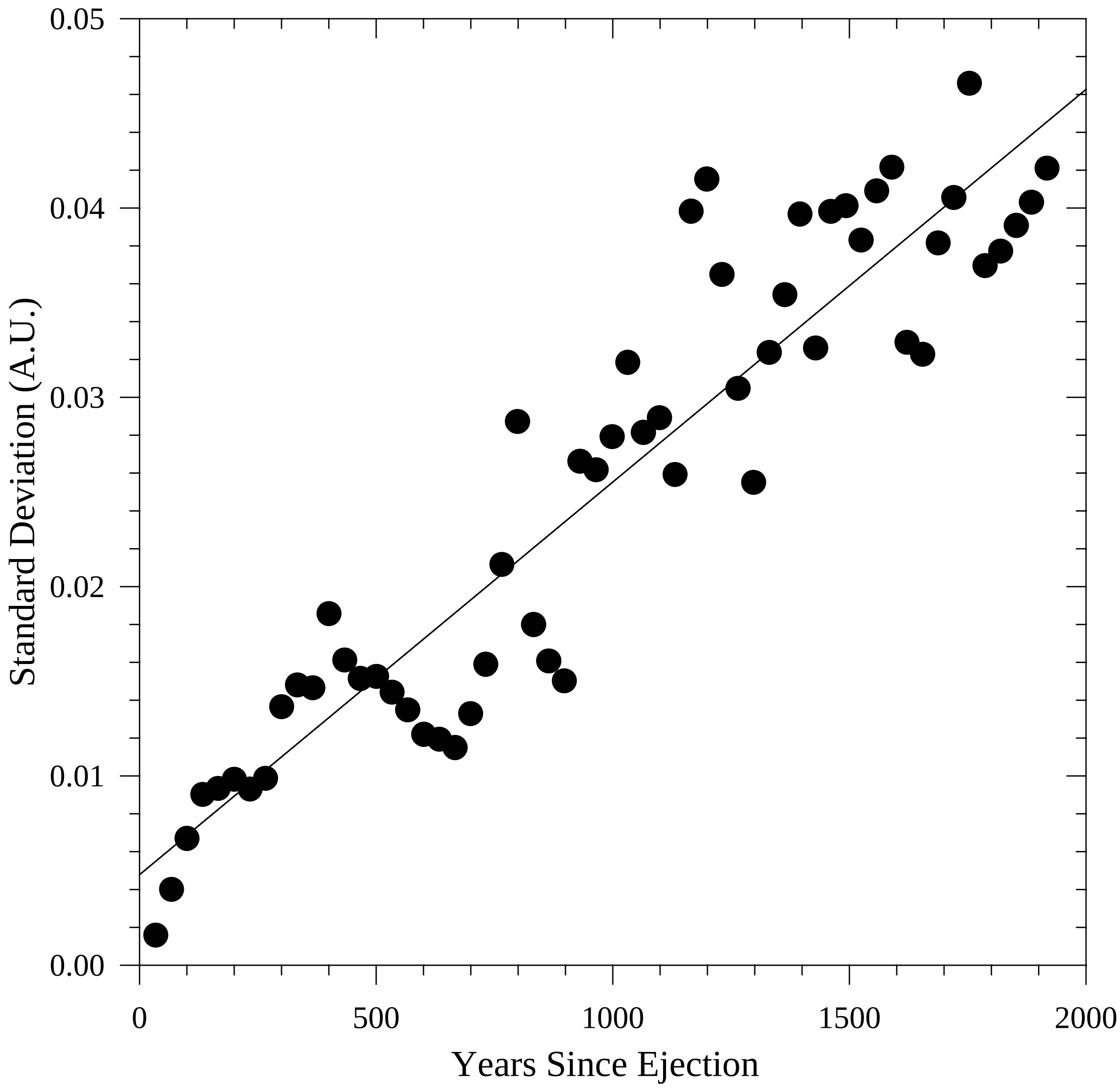

Fig 6.23: The standard deviation in the nodal radius for each ejection from 89 – 1965 using model 22 and visual-sized meteoroids. The solid line represents the regression fit as found in Eq. 6.2.

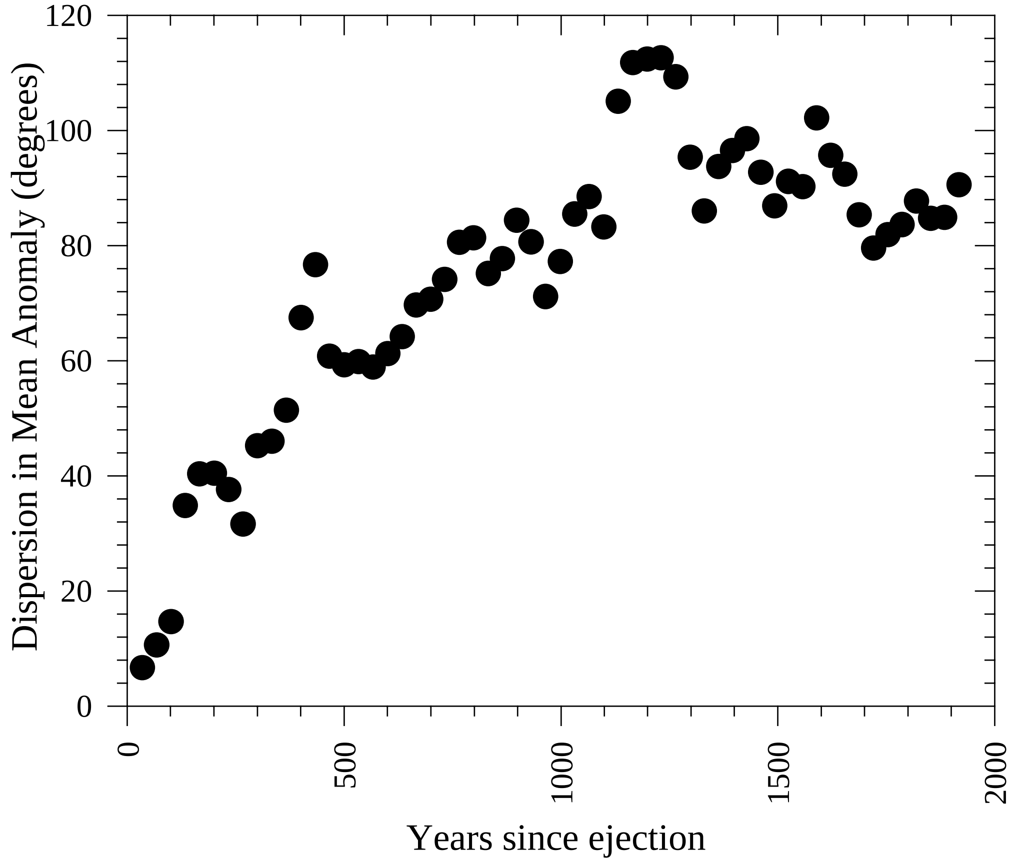

Fig 6.24: The standard deviation in the mean anomaly for all visual-class Leonid meteoroids ejected using model 22 over the last 2000 years.

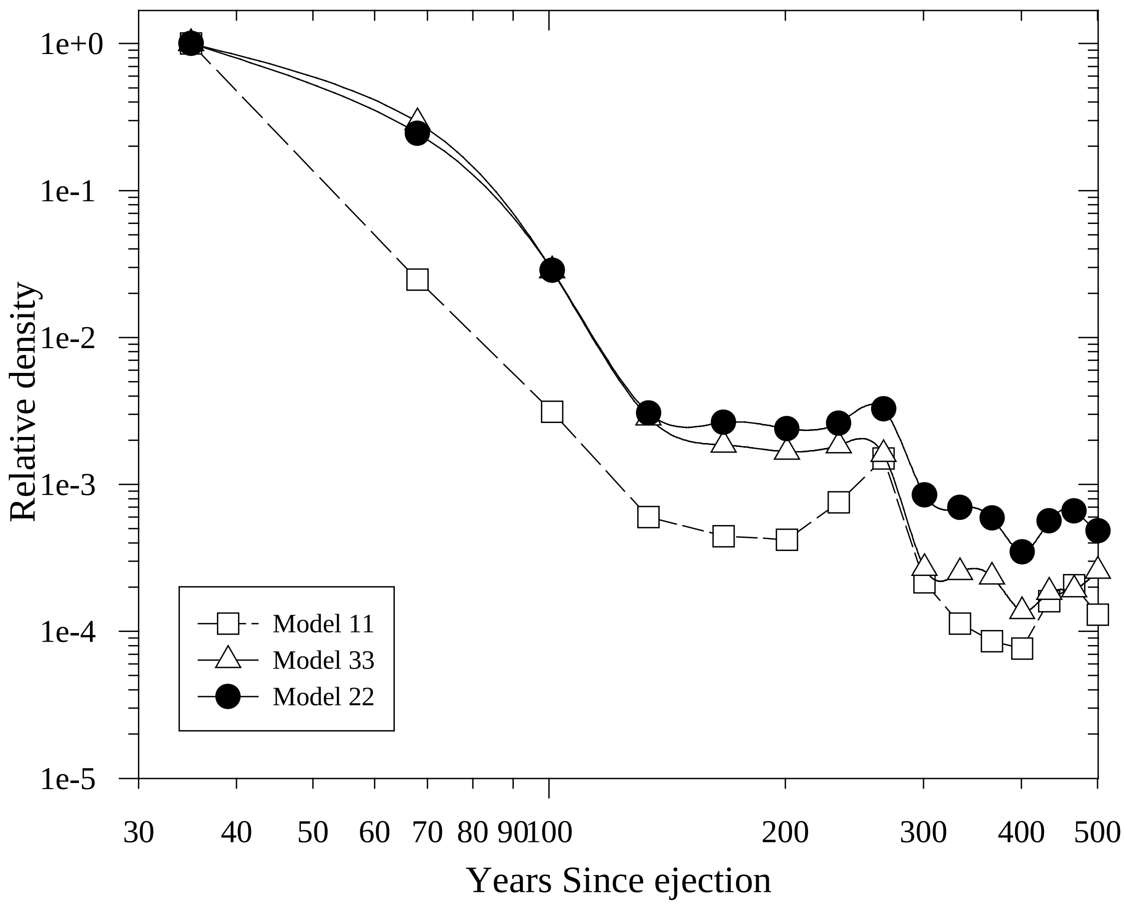

Fig 6.25: The evolution of the average relative particle density for visual-class meteoroids within the Leonid meteoroid stream, measured at the node, for models 11, 22 and 33 (see legend).

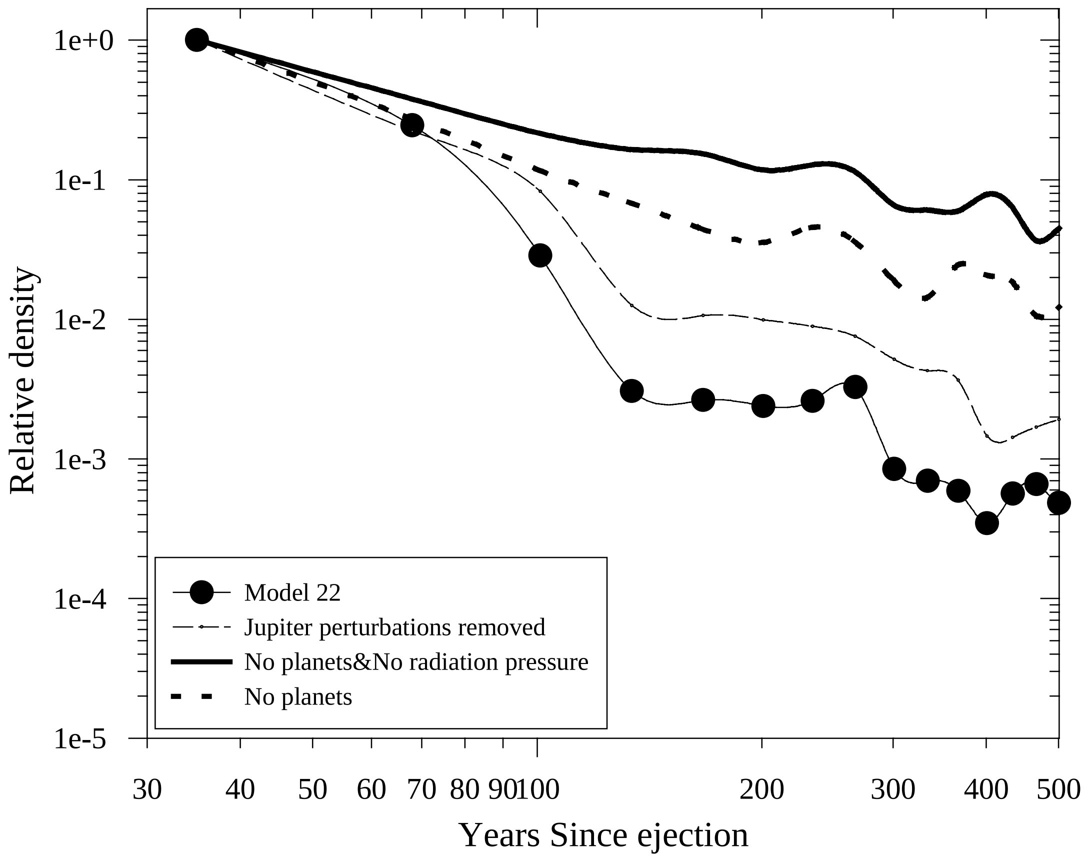

Fig 6.26: Comparison of the evolution of the average relative density change in the Leonid stream as a function of time: using model 22 initial ejection conditions for visual-sized meteoroids with Jupiter removed; all planetary perturbations removed and finally with all planetary perturbations and radiation pressure forces removed (see legend).

It is apparent that significant fluctuations in these values occur as a result of planetary perturbations, mainly from Jupiter (see later). However, the general trend of increasing dispersion with age is present in all distributions.

For model 22 meteoroids, averaged over the visual-sized mass classes (10^{-3} g - 10 g or $5\times10^{-5} < \beta < 10^{-3}$), a linear relationship in the dispersion of the nodal longitude (in degrees, J2000), λ, holds over the full 2000 years and is of the form

$$\sigma_\lambda = (0.08 \pm 0.1) + (2.6 \pm 0.1)\times 10^{-3}\, T \tag{6.1}$$

where T is in years from Jan 1, 2000 A.D. measured positive backwards. Similarly, the dispersion in the nodal radius, r, in A.U. can be represented as

$$\sigma_r = (4.8 \pm 1.2)\times 10^{-3} + (2.1 \pm 0.1)\times 10^{-5} T \tag{6.2}$$

Taken together, these two distributions provide a time-dependent measure of the mean spread in the cross-section of the stream on the ecliptic plane and also demonstrate that the rate of nodal longitude spread is roughly twice that due to the spread in nodal radius for model 22.

The relative rate of spreading along the orbital arc is measured through the dispersion in mean anomaly within the stream. However, after less than ~10 revolutions (depending on the values of β involved), a significant fraction of meteoroids will have made n-1 revolutions relative to the comet and the mean anomaly spread and its average become less meaningful measures.

In particular, for model 22 meteoroids, we have found that some particles begin lapping after ~200 years. For ejections less than 200 years in age, the spread in mean anomaly, M, for model 22 meteoroids can be represented by

$$\sigma_M = (0.7 \pm 5.8) + (0.19 \pm 0.04) T \tag{6.3}$$

Taken together, these three equations can provide an idealized measure for the average relative rate of change of particle density and hence flux within the stream as measured at the node. They also provide an approximate indication of the average length of time dense structures such as the storm-producing portions of the stream can endure.

Using the actual measured dispersions in the ascending nodes, nodal distance and mean anomaly, we can calculate the modelled average relative change in density compared to the density after only one revolution (the youngest material which we can sample at Earth). This is shown graphically in Fig 6.25 for model 22 and for three other models for comparison.

From Fig 6.25, the decrease in density of the stream as measured at the node after formation is such that it falls by ~2-3 orders of magnitude between its first revolution and a century later, almost independent of the starting model and range of β's involved. This offers a potential explanation as to why Leonid showers a significant distance away from the comet's perihelion passage are far less noteworthy in their maxima (due to the large decrease in flux for older material, which lies further from the comet's nodal passage). It also implies that Leonid returns more than 3-4 passages old are likely to result in only modest peak activities; the storm-producing segment of the shower is certainly only a few revolutions old at most based on this result. Note that the behaviour in Fig 6.25 is relative to the average peak concentration measured at the point of the average mean anomaly and so represents the smallest decrease in density expected - locations further from the peak concentration will have even smaller fluxes relative to the initial values; the values in Fig 6.25 are average upper limits. Note that the intermodel differences in the average absolute level of relative density is deceptive as each model obviously has a slightly different "initial" density after one revolution, depending on the range of ejection velocities and β represented.

The steep decrease in density over the first three to four revolutions, followed by a leveling off, suggests that different dispersive mechanisms dominate evolution over differing time-scales.

To examine this question, in Fig 6.26 we have plotted the results of model 22 integrations again. As well, the same integration has been performed removing the direct perturbations from Jupiter (dashed line), all direct planetary perturbations (dotted line) and finally all planetary perturbations as well as radiation pressure effects (solid line).

Here the solid line represents the diffusional effects of initial ejection velocities alone, which for model 22 averages several tens of meters per second near perihelion. At these ejection velocities, the initial dense stream would take nearly ten revolutions to fall to 10% of its first revolution density for the range of ejection velocities adopted. Radiation pressure effects produce nearly another order of magnitude decrease in density over the same time interval and planetary perturbations decrease the density yet another order of magnitude with Jupiter being the primary agent in the decrease after the first ten revolutions.

For the first few revolutions (which are relevant to the question of meteor storms), the effects of radiation pressure and ejection velocity dominate until after approximately the third revolution when the effects of planetary perturbations begin to determine the stream’s subsequent density evolution.

In addition to the large variation in flux, the location in solar longitude of the maximum of the Leonid shower does show a significant variation from year-to-year (cf. Brown, 1999). It is typically assumed that any significant showers/storms will occur at or near the node of the comet (cf. Yeomans, 1981), an entirely reasonable assumption predicated on the youth of the material involved and thus the expected similarity in the orbital evolution of the parent comet and daughter meteoroids. Fig 6.27 shows the solar longitude location of the maximum concentration of meteoroids delivered to the present epoch for each of the last 57 perihelion passages of the comet for model 22 meteoroids. Each point represents the present location of the maximum number of test particles in 0.02° degree bins, with the error margins corresponding to the positions where this number has fallen to one-sigma less than the peak value from ejection during the time of the comet’s passage along the abscissa.

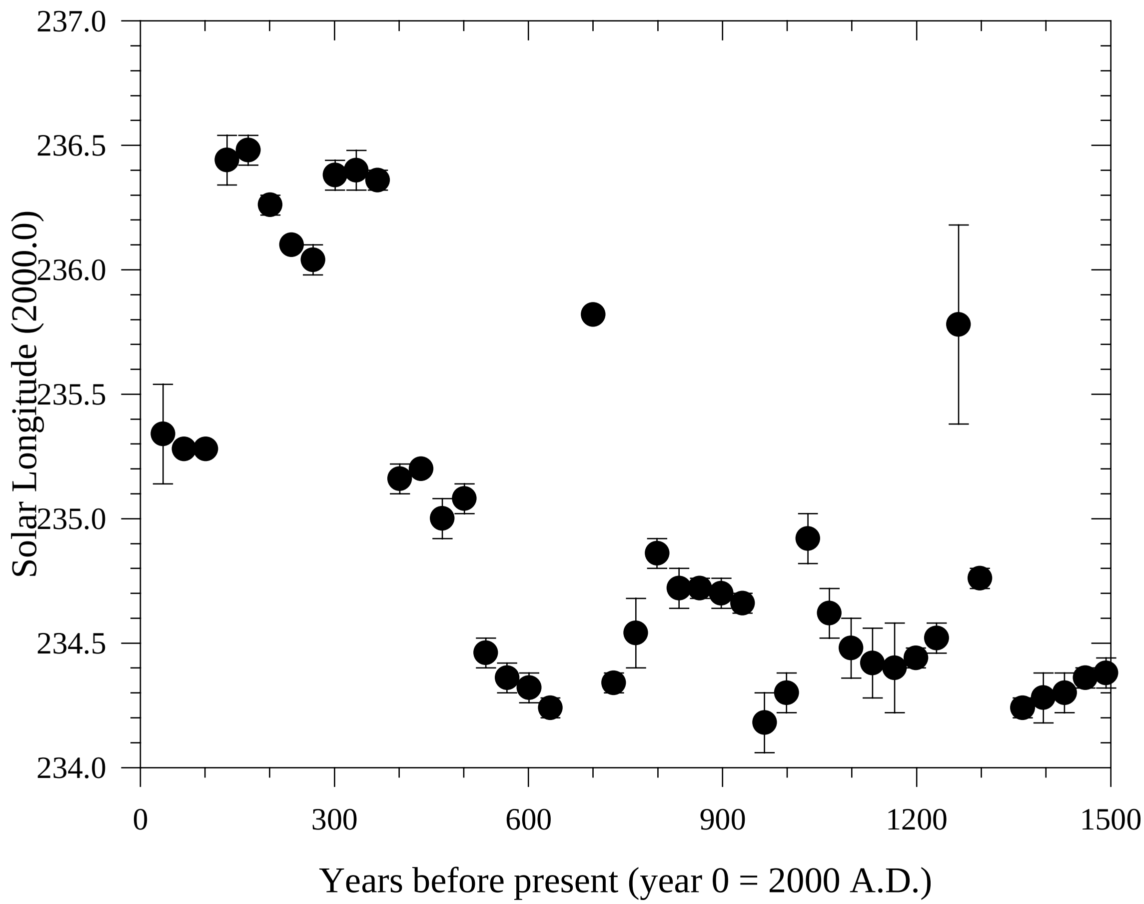

Fig 6.27: The locations of maximum particle concentration as a function of solar longitude for ejections over the last 1500 years referenced to the 1998 epoch. Each dot represents the most populated solar longitude bin at the present epoch for model 22 ejections at the era given in the abscissa of visual-class meteoroids. Only meteoroids within 0.001 A.U. of Earth's orbit are counted.

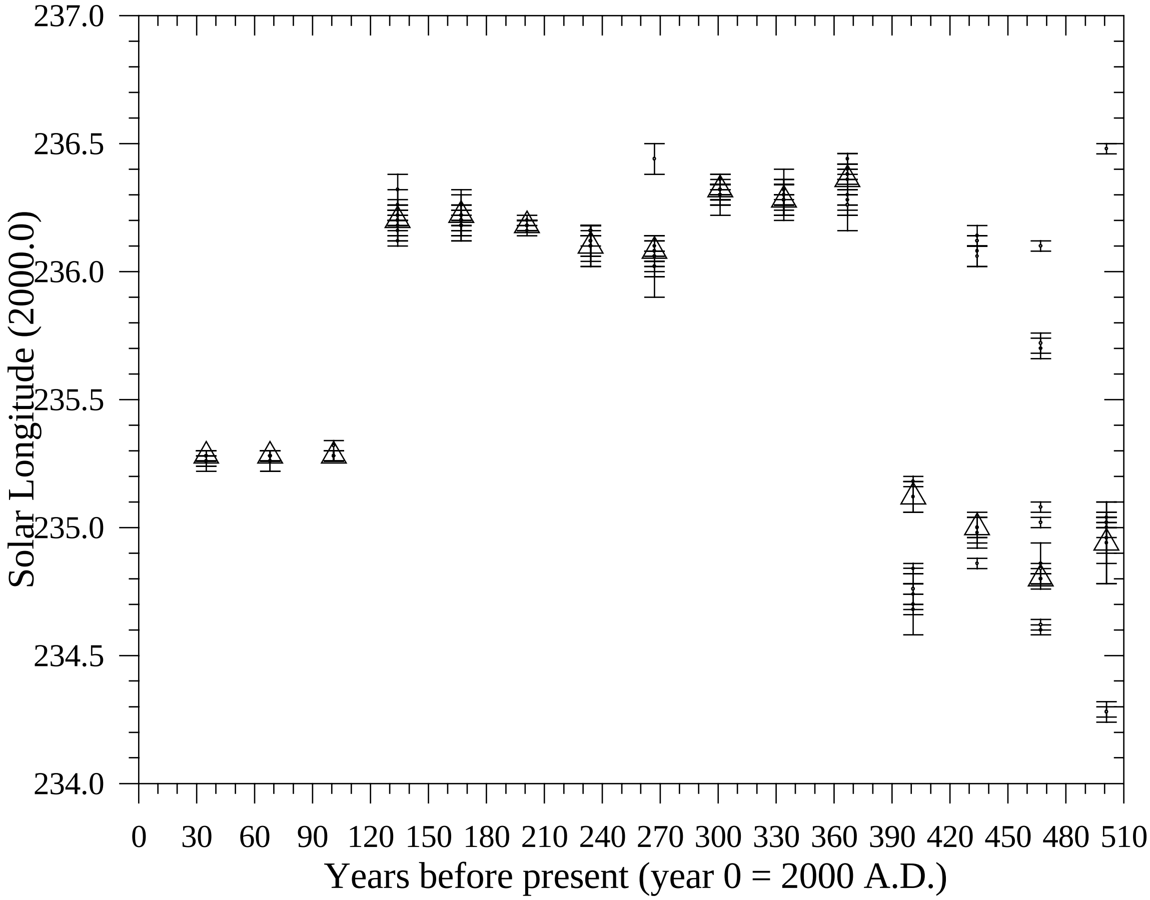

Fig 6.28: The locations of maximum particle concentration as a function of solar longitude for ejections over the last 500 years referenced to the 1998 epoch. Each open triangle represents the most populated solar longitude bin at the present epoch for model 22 ejections of visual-class meteoroids at the era given in the abscissa (same as Fig 6.27). Locations and error ranges for other peaks for all other models are also given as error bars.

It is immediately apparent that the positions of the maximum are correlated with their ejection times; specifically, groups of “maxima” are clustered at or near the same positions for several revolutions and then move some distance. The abrupt changes in peak locations are entirely caused by the perturbing effects of Jupiter, which acts to shift the locations relative to the comet through perturbations perpendicular to the orbital plane of the stream.

That ejecta from different years are so tightly correlated in peak solar longitude implies that the locations of maximum in years showing heightened activity at the present epoch can be used as an approximate measure of the likely age of material involved. That this effect is not strongly model nor density dependent, we show in Fig 6.28, the same plot as in Fig 6.27 but with all models given (the open triangles refer to the same plot as Fig 6.27, namely model 22). It is apparent that over the last 500 years at least, the shifts are fairly model and density independent.

6.6 Discussion

6.6.1 Role of Planetary Perturbations

The Leonids are a high inclination stream and do not pass close to any planet other than Earth. The closest distances between the present orbit of Tempel-Tuttle and each of the three major outer planets are shown in Fig 6.29. Based on this geometry it would seem that all three planets might affect the stream to varying degrees.

As discussed in connection with the Perseids (see Chapter 4), streams of high eccentricity can be significantly affected for Earth-intersection from distant direct perturbations by the Jovian planets. These distant encounters on the stream were shown to produce small perturbations on Perseid meteoroids which lead to intersection with the Earth.

Unlike the relatively straightforward planetary impulse pattern with the Perseids, the Leonids may experience significant perturbations both before and after perihelion from both Saturn and Jupiter. To further complicate the situation, the orbital period of the stream is such that the section of the stream which experiences perturbations from Jupiter pre-perihelion also experiences more distant direct perturbations from Jupiter on the post-perihelion leg, the interval being three years between the encounters. Additionally, since Jupiter makes approximately 2.5 revolutions for each complete revolution of Saturn (and the encounter longitudes between the stream and Jupiter or Saturn are nearly the same), the Jupiter-Saturn pre-perihelion impulses tend to come in pairs (within 1-2 years of each other). From Fig 6.29 it is also apparent that the stream can have close encounters with Uranus near aphelion, an effect that has been suggested to be of pre-eminent importance in the stream's development (Williams, 1997).

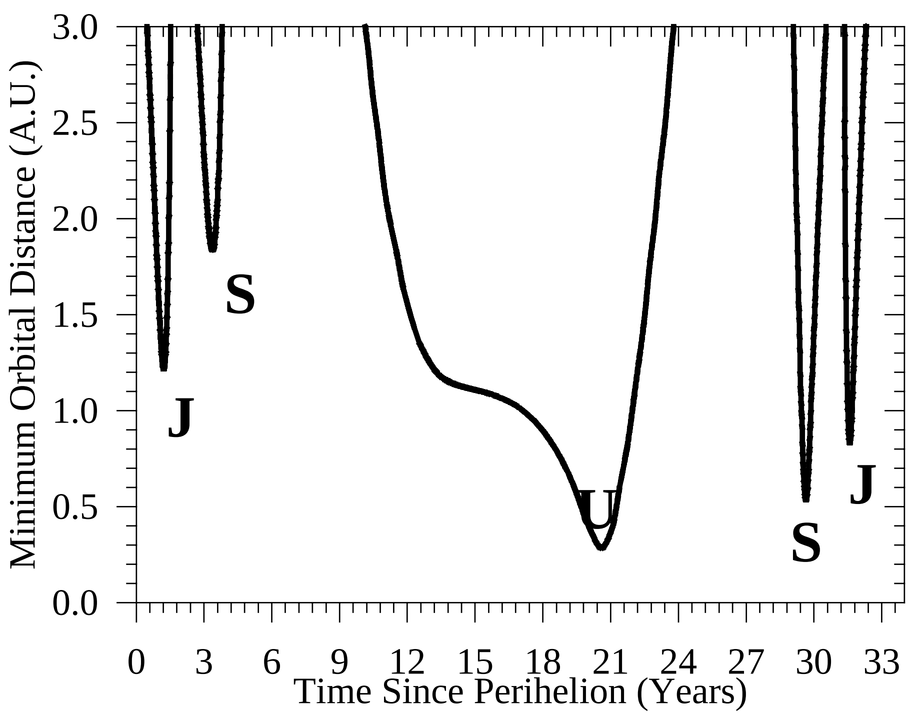

Fig 6.29: The minimum distance of 55P/Tempel-Tuttle's current osculating orbit (referenced to the 1998 epoch of perihelion) from the orbit of each of the major planets as a function of the time since perihelion for hypothetical test particles making the minimal approach distance to each planet's orbit.

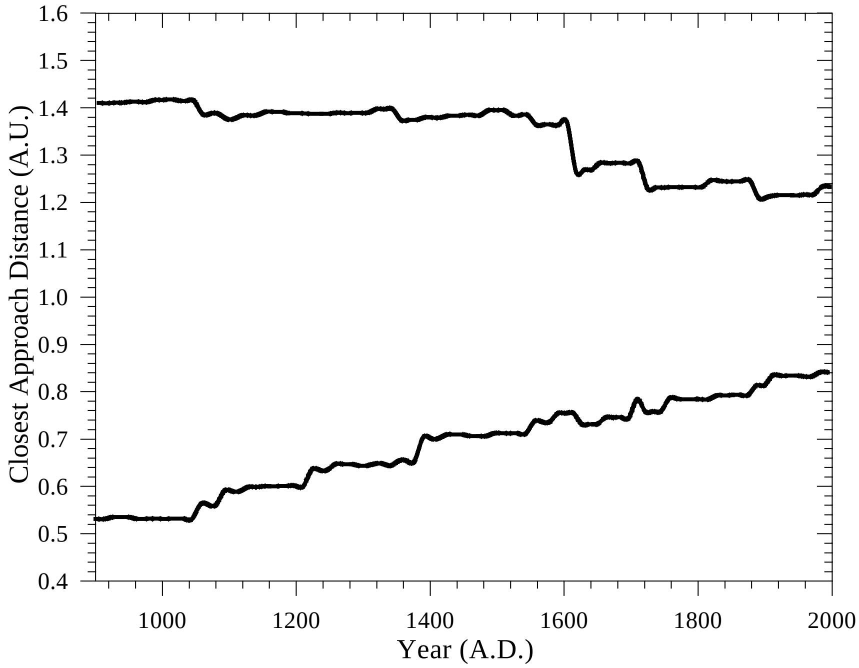

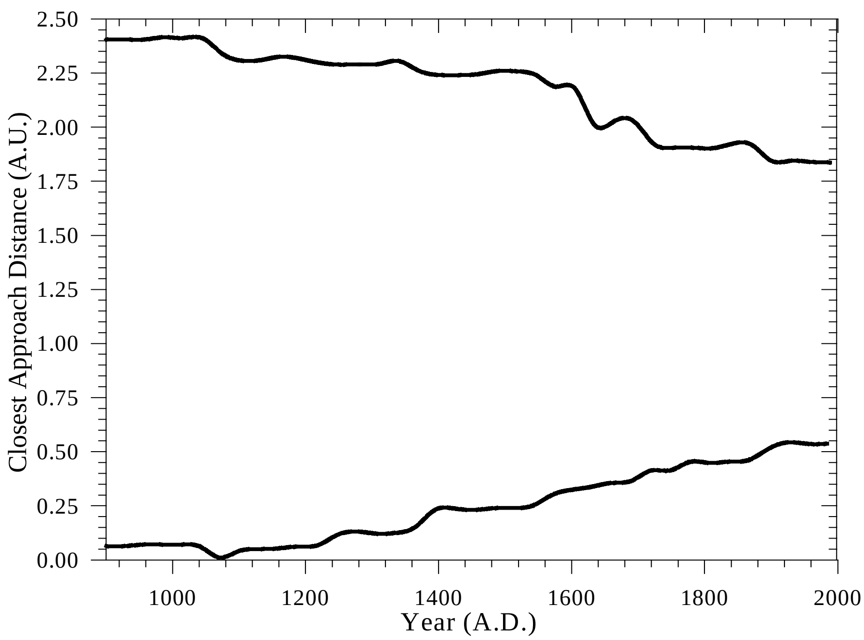

Fig 6.30 (top): Minimal approach distance between 55P/Tempel-Tuttle's osculating orbit at perihelion and Jupiter's orbit. The upper curve is for outbound (post-perihelion) passages and the lower curve is for inbound (pre-perihelion) passages.

Fig 6.31 (bottom): Same as Fig 6.30 but for Saturn's orbit.

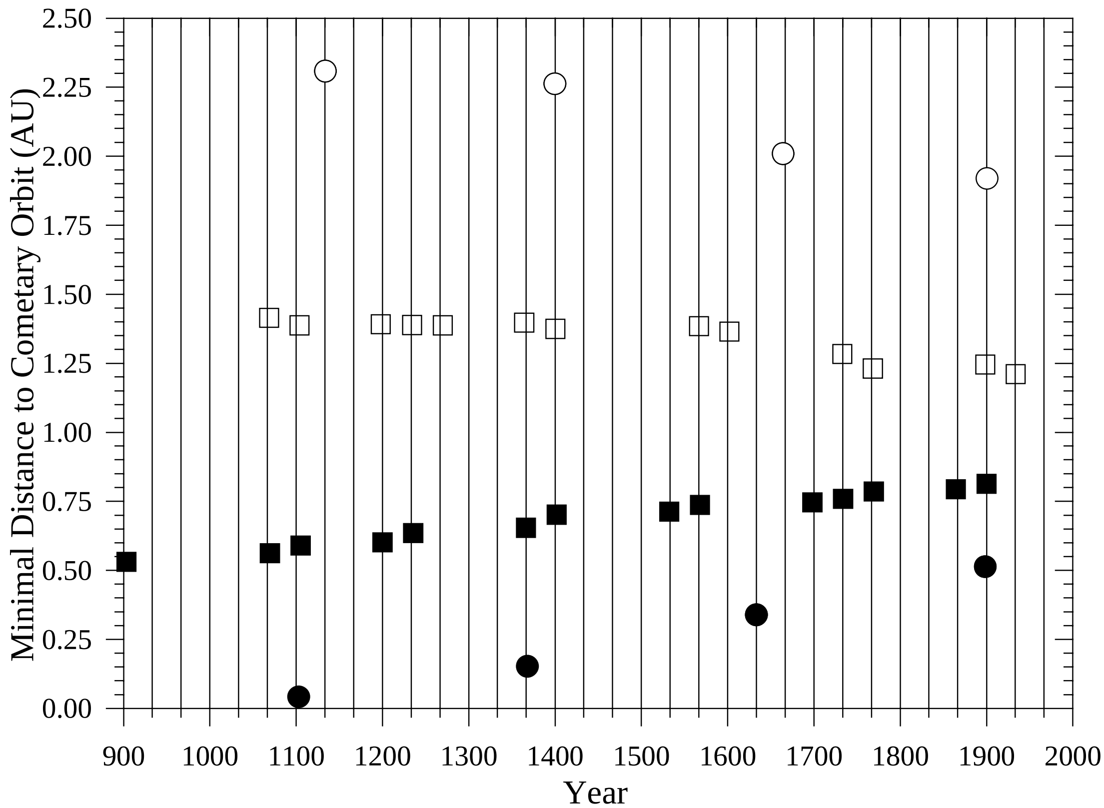

Fig 6.32: Actual close approaches of Jupiter (squares) and Saturn (circle) to 55P/Tempel-Tuttle at the epoch of its (nearest) perihelion passages to these encounters. Only approaches to the orbit of Tempel-Tuttle that are within 20° of the mean anomaly of the comet are shown. The solid symbols are for inbound (pre-perihelion) perturbations on the stream and the open symbols are for outbound (post-perihelion) encounters with the Leonids. The symbols are placed at the instant when the maximally perturbed portion of the stream reaches the descending node.

Our approach to investigating the effects of perturbations on the stream numerically is to remove each planet in turn and note the effects on the stream's development as a whole as opposed to attempting any analytic treatment for such a complex system.

To first order, the pre-perihelion effects of Jupiter and Saturn may be expected to dominate as they have the closest planetary encounters of major planets with the stream. We recall that the stream is a nearly continuous ribbon of material and that some Leonid meteoroids will always experience the maximum perturbations due to close approaches by the planets.

However, as the parent comet orbit varies with time, so too will the encounter conditions of the stream over the last 1000 years. In Figs 6.30 and 6.31 we show the varying minimum approach distance between Tempel-Tuttle and Jupiter and Saturn respectively.

From Fig 6.30 it is clear that the pre-perihelion Jovian perturbations have become significantly lessened over the last thousand years while the post-perihelion effects have increased slightly. Fig 6.31 paints a more interesting picture. While the post-perihelion distance between the comet's orbit and Tempel-Tuttle has increased slightly, the pre-perihelion effects have become much smaller, though the encounter distance is still less than is the case for Jupiter. Intriguingly, the minimum approach distance between Saturn and the stream reached a broad minimum for the pre-perihelion encounter between 900-1200 AD when the distance averaged ~0.05 A.U. The extreme minimum distance reached in 1070 AD was of order 0.02 A.U., which is inside the Saturnian satellite system. This suggests that Leonid showers were visible on Saturn (and Titan) some 900 years ago. It is unlikely that Leonid storms comparable to those seen on Earth occurred at Saturn, as the stream is significantly wider at Saturn's distance and the encounter velocities lower. Indeed, the only time Saturn reached its minimum distance to the Leonid orbit and passed within 10° of mean anomaly of Tempel-Tuttle during this time period was in mid-1099 when the two bodies were separated by approximately 0.6 A.U. (Yeomans *et al.*, 1996) (though Saturn passed less than 0.05 A.U. from Tempel-Tuttle's orbit a few months later).

Fig 6.32 shows the years (referenced to the time the affected material passed through the descending node) in which encounters with either Jupiter or Saturn occurred along the stream orbit within ±20° of the mean anomaly of the parent comet. It is these encounters that have the largest effect on the storm producing segment of the stream and that would be expected a priori to cause a significant change in the densest portion of the stream (without necessarily affecting the parent comet as greatly).

The encounter pattern with Jupiter is such that every five orbits of Tempel-Tuttle, two successive close approaches to the stream are made by the planet on both the inbound and outbound leg of the stream orbit. These tend to have their maximum perturbations in front of and behind the comet in opposite pairs (i.e. the inbound perturbation maximizes behind the comet and then on the next orbit of Tempel-Tuttle the outbound perturbations maximizes behind the comet and vice-versa for perturbations in front of the comet).

The impulsive perturbation cycle with Saturn is such that every eight to nine revolutions of the comet, a similar pattern occurs with a perturbation (typically) first on the inbound leg of the stream and then on the next orbit of the comet on the outbound leg. The encounters after perihelion tend to move the nodal points of the affected meteoroids away from the sun, while the pre-perihelion passages tend to move meteoroid nodal points inward. Thus, depending on the geometry between the comet and the Earth, these perturbations (in the short-term) may serve to move the material to intersect the Earth (as was the case with the 1899 material perturbed in 1901 and again in 1932 moving the nodal point out far enough to be encountered in November, 1966) or to not intersect it (as was the case for material released in the previous eight revolutions prior to 1899 which was already largely interior to Earth's orbit at the node and was perturbed further inward due to pre-perihelion perturbations from both Saturn in 1895 and Jupiter in 1898).

These encounters also serve to disrupt and diffuse the dense cometary trail of material developed over the previous five passages of the comet. When strong perturbations occur they serve to move some material away from the comet and may be the limiting factor in the development of the dense Leonid storm producing segments of the trail. Kresak (1992; 1993) was among the first to recognize that encounters between Jupiter and the Leonids could disrupt the dense trail behind Tempel-Tuttle. In the present work, it is clear that the stream decreases in density quickly (Sect 6.5) and such disruptions (or more gradual perturbations) can easily move the trail away from the comet, but the material may still intersect the Earth and cause a storm (as occurred in 1966). It is the magnitude of the disruption (compared to gradual perturbations) and what its effect on the trail relative to the comet-Earth geometry which affects the appearance or not of a storm as seen at Earth.

To investigate the effects from each of the planets on stream development as a whole, we plot the dispersion in mean anomaly, nodal radius and ascending nodal longitude as a function of time for each planet removed in turn over the last 500 years for model 22 meteoroids in Figs. 6.33, 6.34 and 6.35 respectively (compare to Figs 6.22, 6.23 and 6.24).

From Fig 6.33 it is apparent that while the abrupt changes in dispersion in mean anomaly are due to planetary perturbations (mainly Jupiter), the overall effects are small and the dispersion is not controlled primarily by planetary perturbations, but rather by radiation pressure effects and ejection velocities. Note the complete lack of observable effect due to removal of Uranus.

Fig 6.34 clearly demonstrates that Jupiter is the primary mechanism in the diffusion of the nodal radius, with increasingly lesser effects from Saturn and Uranus. Perturbations perpendicular to the orbital plane, which directly affect the nodal longitude, are completely dominated by Jupiter (an observation previously made also by Kresak (1992)). Fig 6.35 shows that there is nearly an order of magnitude difference in nodal longitude dispersion with Jupiter present as with it removed; far lesser effects are due to Saturn and there are almost no measurable effects from Uranus.

In terms of the final activity profiles visible at Earth, the net effect of the removal of each of the planets on the number of particles visible as a function of time at Earth follows the same pattern, with the largest changes involving removal of Jupiter or Saturn and much smaller effects from the removal of Uranus.

The clear trend (as might be expected a priori) is for the planetary perturbations to be dominated by Jupiter with small effects from Saturn (with the possible exception of close approaches to the stream orbit some 900 years ago) and lesser still from Uranus.

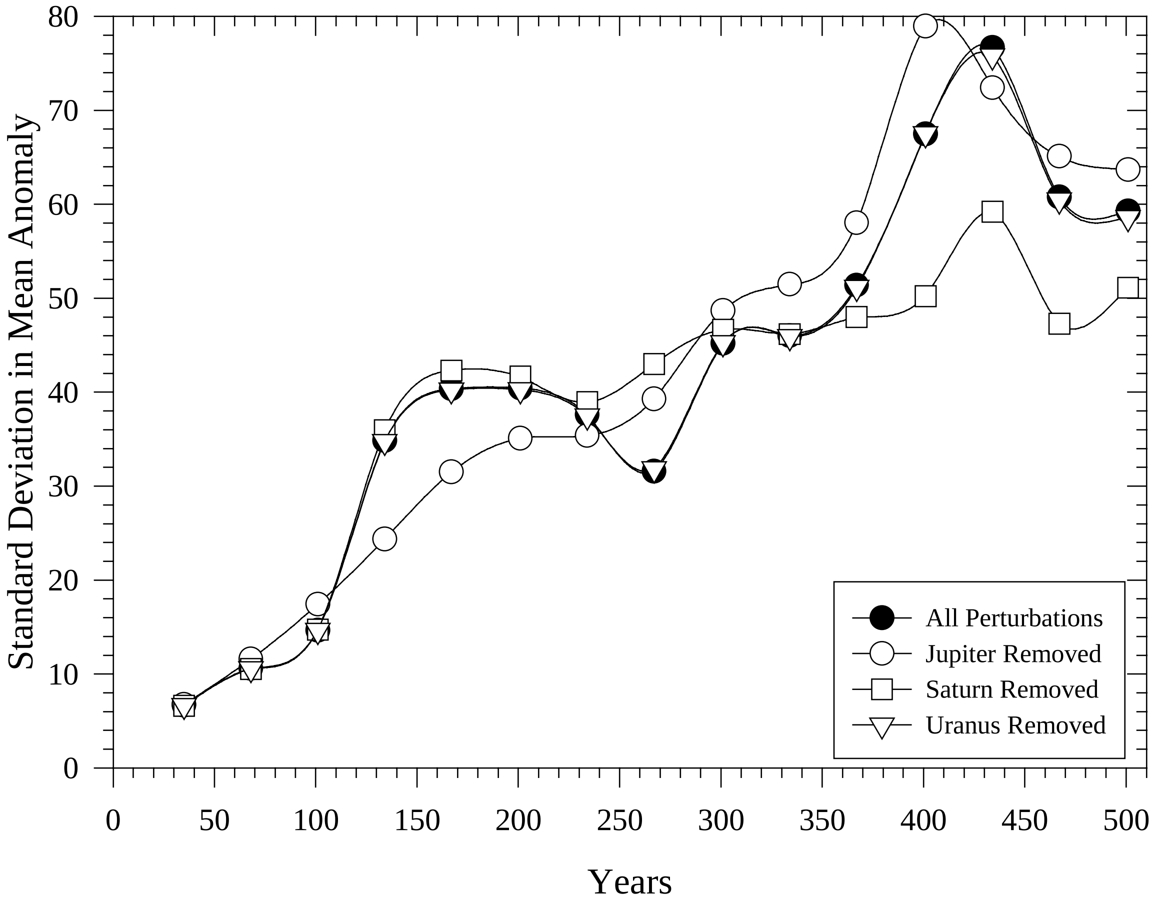

Fig 6.33: The standard deviation in the mean anomaly for all visual-class Leonid meteoroids ejected using model 22 over the last 500 years (solid circles). Also shown are the same initial conditions with the direct perturbations from Jupiter, Saturn and Uranus removed (see legend).

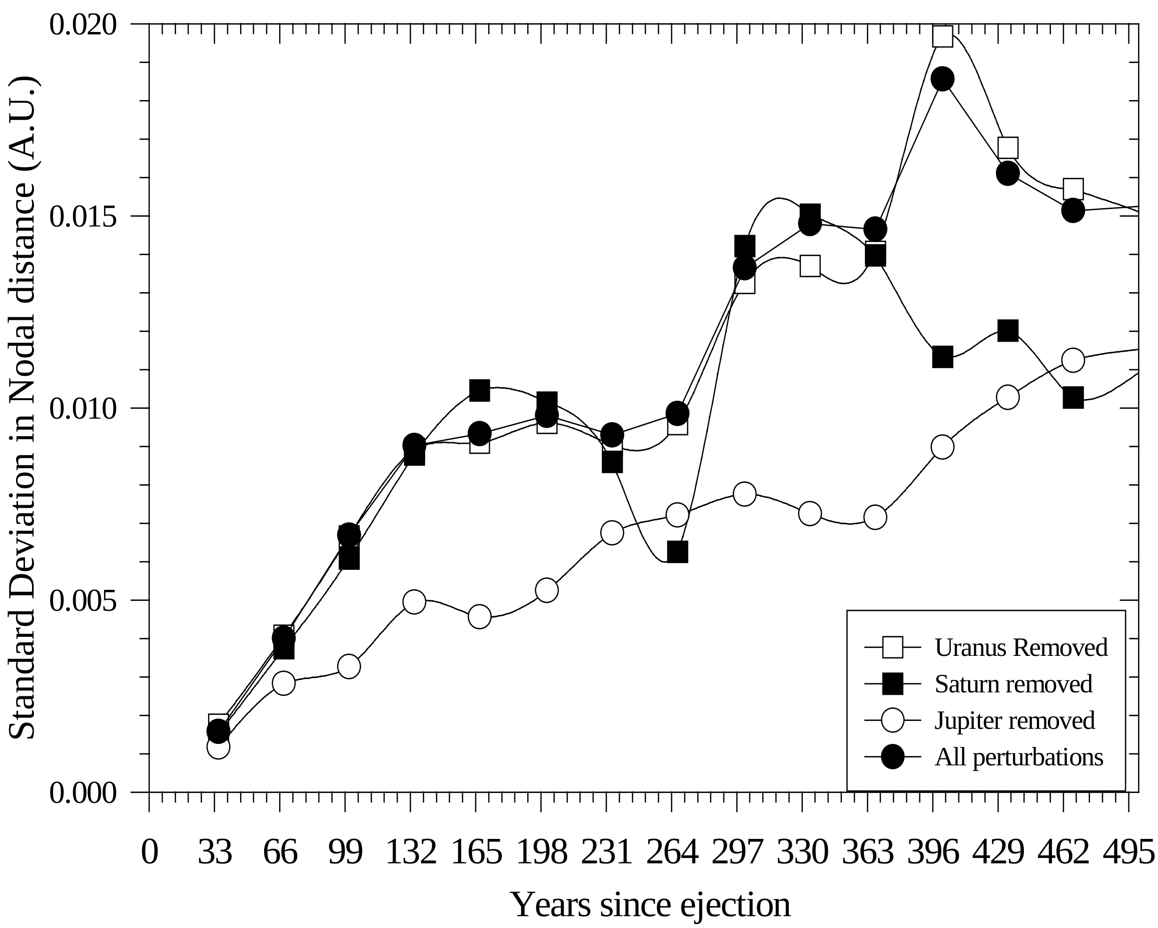

Fig 6.34: The standard deviation in the nodal radius for each ejection over the last 500 years using model 22 visual-sized meteoroids (solid circles). This is compared to the standard deviation in the nodal radius with Jupiter removed (open circles), Saturn removed (solid squares) and Uranus removed (open squares). Note the large effect of removing Jupiter.

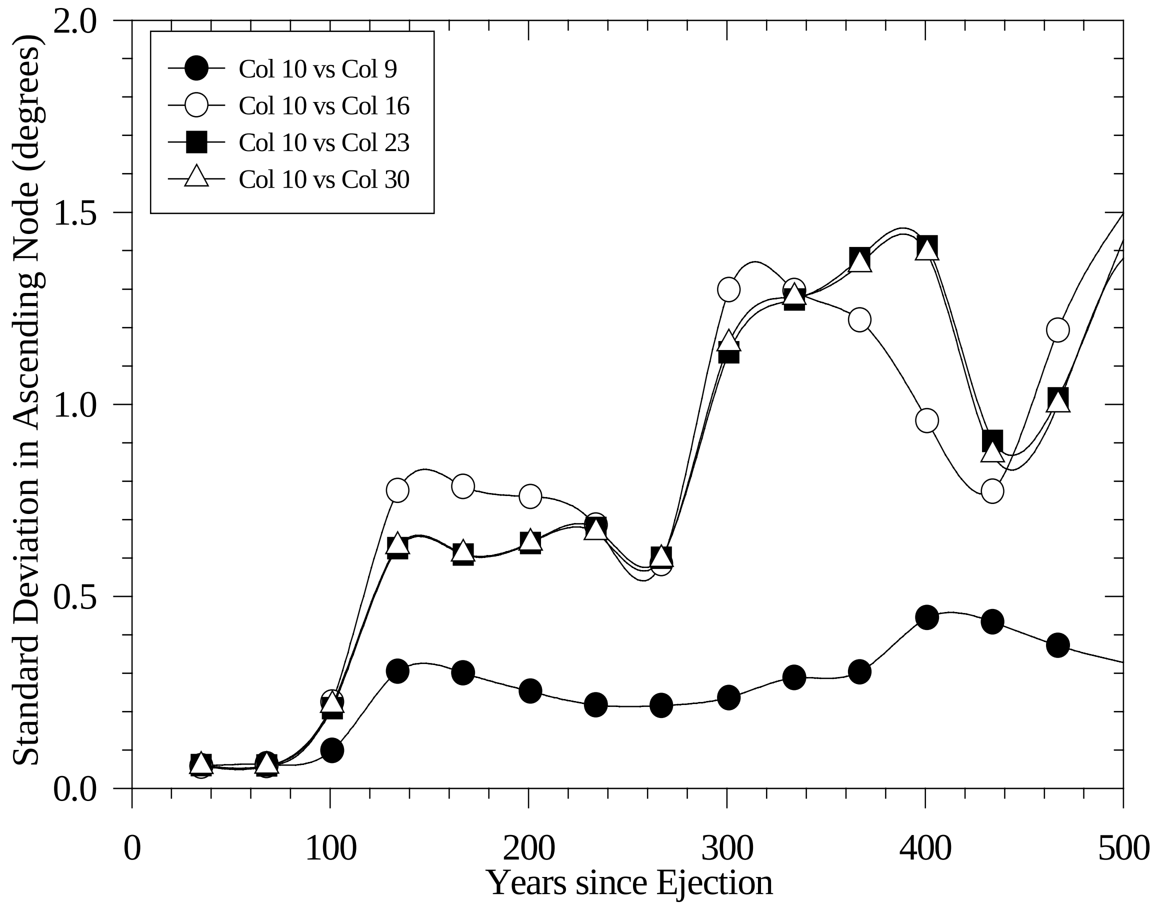

Fig 6.35: The standard deviation in the ascending nodal longitude for model 22 visual-class meteoroids ejected over the last 500 years at the present epoch with all perturbations included (solid squares), with Jupiter removed (solid circles), Saturn removed (open circles) and Uranus removed (open triangles) for comparison. Note the dominant effect of Jupiter and the negligible effect of Uranus.

Perturbations from Uranus appear to have greatest effect upon the delivery of meteoroids near the time of the nodal passage of Tempel-Tuttle, a result not in contradiction with the concept of the 5:2 near-resonance “protecting” meteoroids nearest the comet from perturbations (Williams, 1997). Without Uranus far fewer meteoroids reach Earth in the one to five years after the comet’s passage as shown in Fig 6.36. Note, however, that Uranus increases the number of meteoroids for years well away from the comet’s passage, in contradiction to the role for the planet proposed by Williams (1997).

6.6.2 The Role of Resonances

That the major outer planets dominate the evolution of the stream after time intervals >100 years with radiation pressure and ejection velocities playing significant roles in the first few revolutions was established in the previous section. The precise mechanism of the interaction, however, is still to be defined.

Stoney and Downing (1898) were the first to note the near commensurabilities in the period of the stream with Jupiter (5:14), Saturn (8:9) and Uranus (5:2). Emel’yanenko (1984) noted the possible role the 5:14 resonance with Jupiter might have on the density of material in the stream and Williams (1997) has suggested a major role for the 5:2 resonance with Uranus in removing meteoroids from Earth-intersection.

We expect a resonance to be manifested in an oscillation in the value of the semi-major axis. Fig 6.37 shows this value for Tempel-Tuttle over the last 2000 years. The value does oscillate with a period near 166 years (five revolutions of the comet). This suggests either Jupiter or Uranus may play a role in the evolution of the parent comet (and by implication much of the youngest portions of the Leonid stream). However, the amplitude of the oscillation is not constant, nor does the period hold strictly over this full 2000 year interval and the location of the resonance (the mean value of semi-major axis) does not remain fixed.

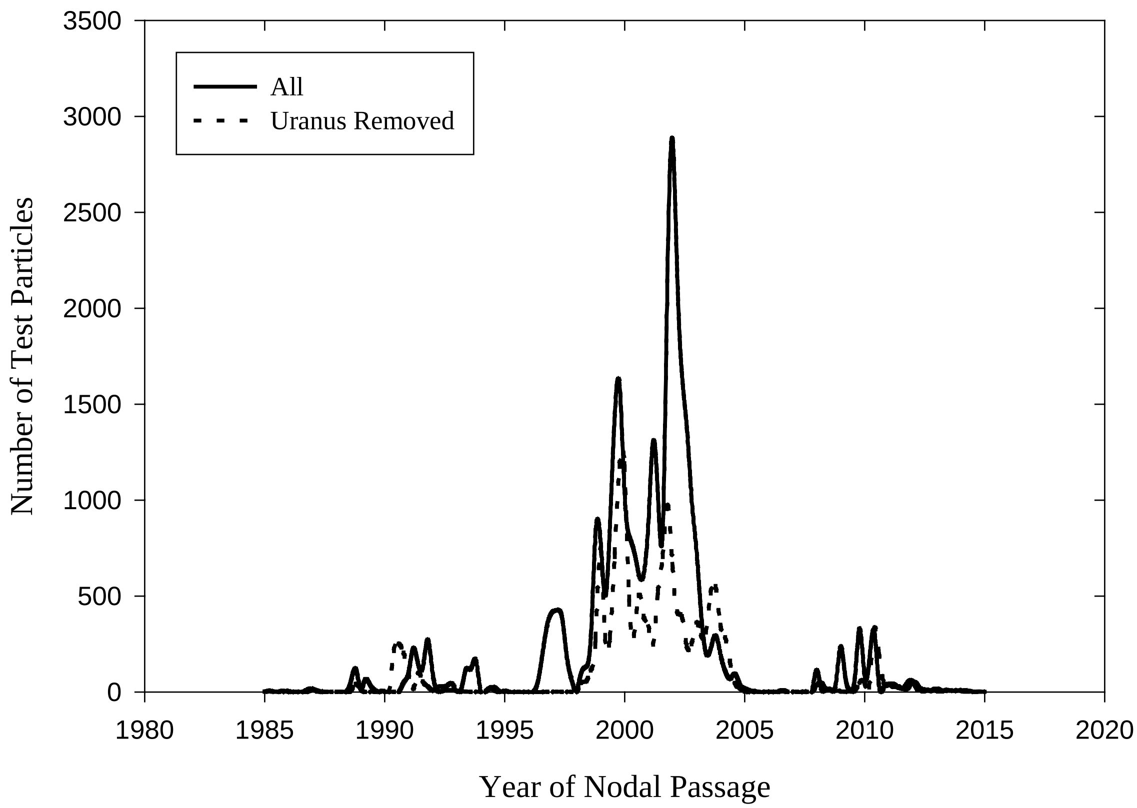

Fig 6.36: The effect of Uranus on delivery of Leonid test particles to Earth. The solid curve represents visual-sized Leonid meteoroids which have nodal points within 0.001 A.U. of Earth (binned in units of 0.2 years) from all ejections over the last 500 years using model 22 for initial ejection velocity conditions. The dotted line shows the same, but with the direct perturbations of Uranus removed. Much larger changes in the numbers of Earth-intersecting Leonids are found by removal of Jupiter and/or Saturn.

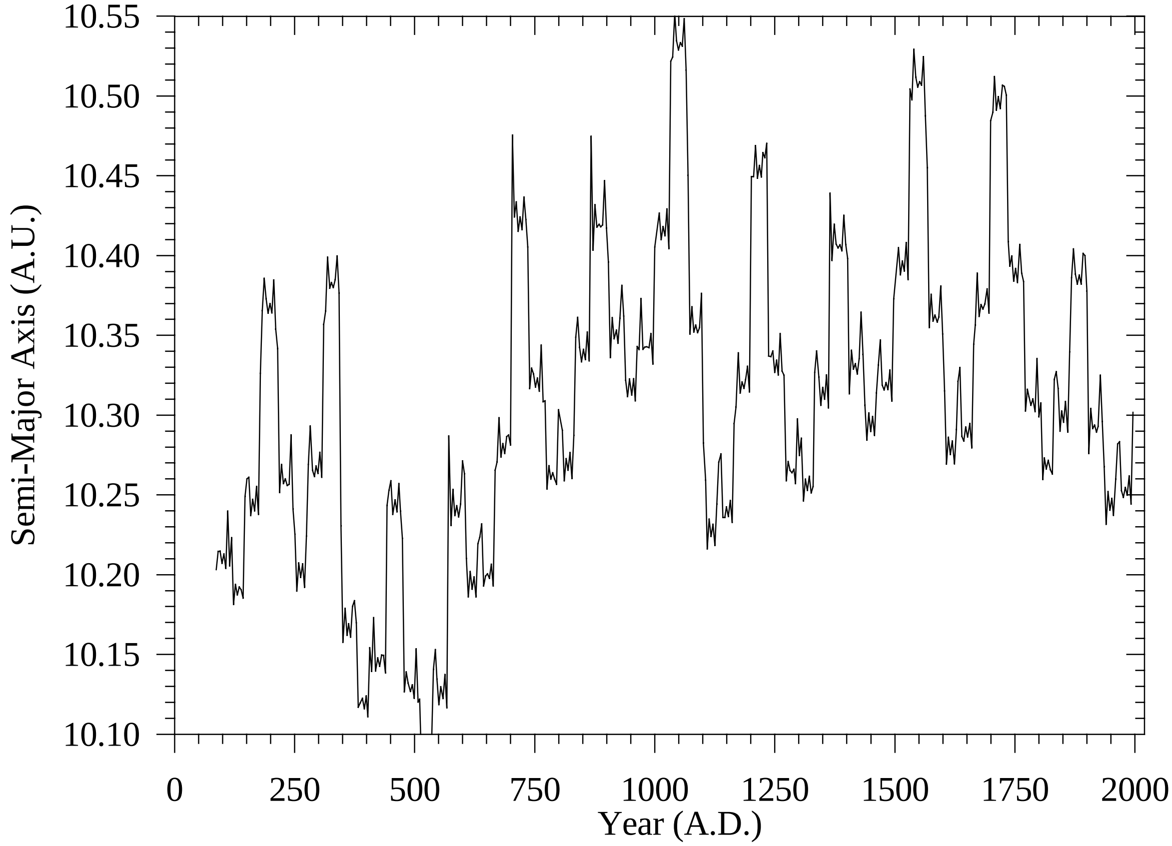

Fig 6.37: The semi-major axis of 55P/Tempel-Tuttle over the last 2000 years.

This result implies that any resonance which affects Tempel-Tuttle is unstable and that the comet may be continually slipping into and out of resonances (possibly with both Jupiter and Saturn which have resonances centred at 10.33 A.U. and 10.31 A.U. respectively).

To determine if any of these mean motion commensurabilites are the actual sites of resonances with Tempel-Tuttle, we examine the critical resonance argument (σ) which is of the form (Schubart, 1968; Chambers, 1995):

$$\sigma = i\lambda_p - j\lambda + (j - i)\varpi \tag{6.4}$$

where λ_p is the mean longitude of the major body (planet) involved, λ is the mean longitude of the minor body and ϖ is the longitude of perihelion of the minor body for a resonance of the form *i:j* where *i* is the integer period of the minor body and *j* the integer period of the major body. This critical argument will show regular librations about a fixed value of σ over time if the bodies are in a stable *i:j* resonance.

Fig 6.38a, b, and c show the value for the critical argument for Jupiter (5:14), Saturn (8:9) and Uranus (5:2). From Fig 6.38c it is clear that Tempel-Tuttle has not been in the 5:2 resonance with Uranus at any period over the last 2000 years. From Fig 6.38a there does appear to be some aperiodic librations in the 5:14 critical argument beginning ~600 AD. These are not the regular oscillations indicative of a stable libration for a Halley-type comet (cf. Chambers, 1995), but suggest more complex behaviour such as a continuous movement into and out of the resonance over this period, chaotic motion or the simultaneous effect of more than one resonance. Unfortunately, the period of the oscillations is of order 400 - 500 years and shows only a few periods of this oscillation for the time interval in which we have an accurate ephemeris for Tempel-Tuttle. Indeed, it is possible that the sudden shift completely out of the resonance at 600 AD may be the simple result of the larger errors in computing Tempel-Tuttle's elements back this far (Yeomans, 1998, pers comm).

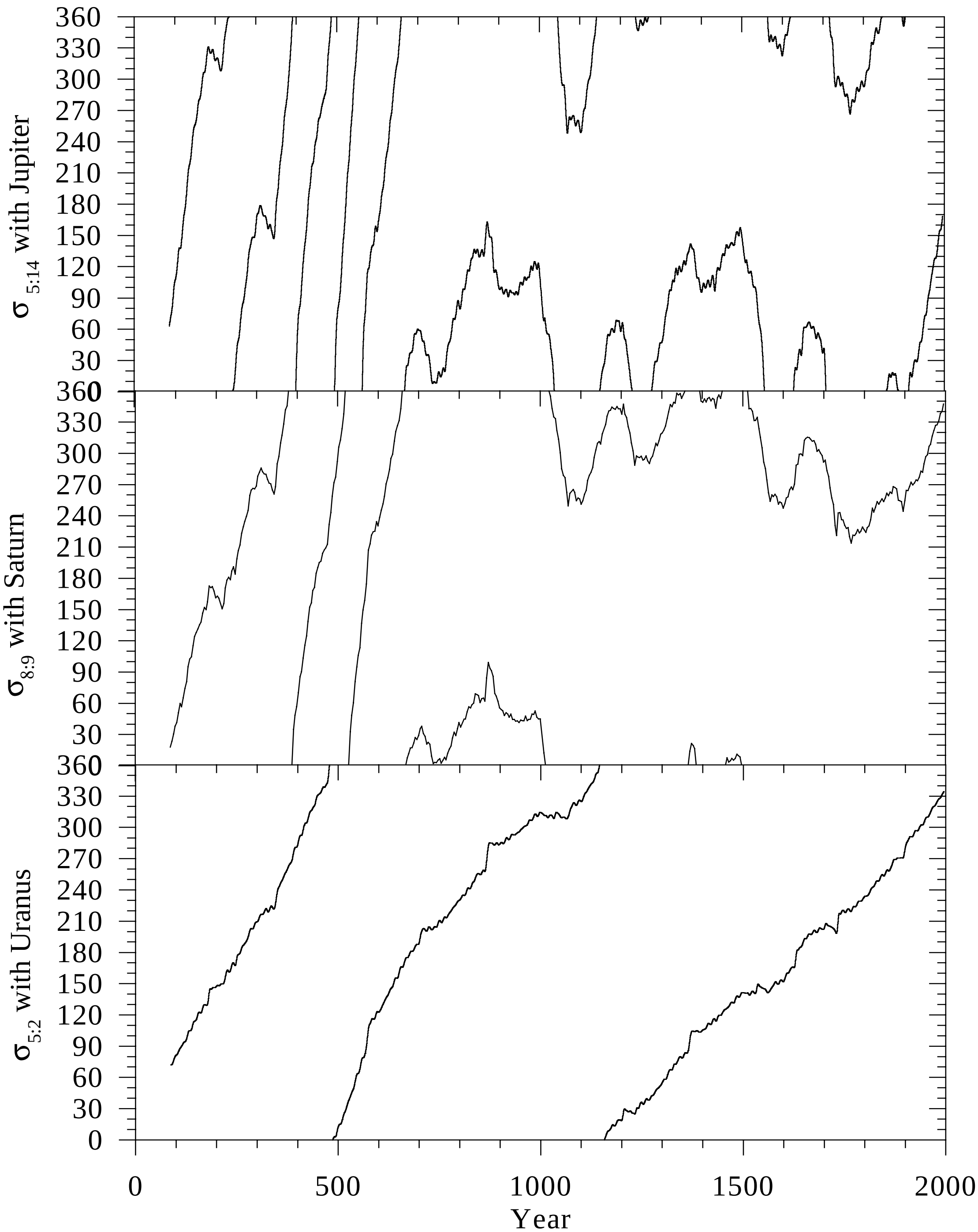

Fig 6.38: Evolution of the critical argument for Tempel-Tuttle with respect to the 5:14 resonance with Jupiter (a – top); the 8:9 resonance with Saturn (b – middle); and the 5:2 resonance with Uranus (c – bottom).

The librations are about the comet's perihelion (centred for convenience at 180° in Fig 6.38a). Fig 6.38b shows the 8:9 critical argument with Saturn which displays similar coherent behaviour. However, the librations in Fig 6.38b are not fixed about one value for σ and drift significantly over just a single period (~600 years). In fact, this may be entirely due to the near commensurability between the periods of Jupiter and Saturn (which are nearly in the ratio of 5:2), as the closeness in the semi-major axis of the 8:9 with Saturn (at 10.31 A.U.) and the 5:14 with Jupiter (at 10.33 A.U.) implies that a drift in mean anomalies between the two planets at conjunction is approximately 1° per decade, entirely accounting for the ~60° shift over 600 years for similar features in the aperiodic oscillation in Fig 6.38b. Alternatively, this may reflect a more complex three-body resonance (eg. Murray *et al.*, 1999). It therefore appears most probable that the primary resonance, which influences Tempel-Tuttle and the Leonids, is the 5:14 with Jupiter.

Interestingly, the low semi-major axis values prior to 600 AD may be associated with the 4:11 resonance with Jupiter, the critical argument of which shows librations similar to the 5:14 from 0-600 AD (though over only one cycle and therefore not entirely convincing).

The apparent lack of a stable resonance at these high resonance orders is not wholly unexpected; indeed for high eccentricity orbits the strongest (first-order) resonances are of the type *1:k* (Chambers, 1995), where *k* is an integer. Thus we expect the resonances discussed here to be weak. As a result, even if Tempel-Tuttle enters one of these high order resonances, slight changes in orbital energy from planetary perturbations may easily exceed the energy in a high-order resonance and quickly shift the body out of the resonance regime once again, as was noted by Carusi et al (1987). The resonance behaviour in 6.38a may best be described as chaotic, based on its alteration from rotation to oscillation as defined by Murray *et al.* (1999).

Carusi *et al.* (1987) also showed that many Halley-family comets (those with Tisserand<2, as is the case for Tempel-Tuttle where T=-0.6) show regular librations about integer multiples of Jupiter's revolution period. They found that typical cycles were of order five to six cometary revolution periods for this behaviour, very similar to what we find here for the 5:14 with Jupiter for Tempel-Tuttle. Carusi *et al.* (1987) have also shown that most Halley-family comets are under the influence of Jupiter (essentially what is found in the present investigation for Tempel-Tuttle).

Despite the weak nature of many of the Jovian resonances, Jupiter's influence on the distribution of semi-major axis of Leonid meteoroids in our simulations is significant. Examining the distribution of test particle semi-major axis as a function of time with Jupiter present and with it absent (Fig 6.39a,b) demonstrates that one of the primary effects of Jupiter is to increase/decrease the concentration of particle semi-major axes near several resonances. Of particular note is the role Jupiter plays in accelerating the movement of Leonid meteoroids to large semi-major axis values and concentrations close to 10.8 A.U., which is near the location of the 1:3 resonance with Jupiter, previously noted as important for the Leonids (Brown and Jones, 1993). This might be a partial reason for strong showers in the two to three years after the parent comet. An example is the cluster of meteoroids ejected in 1866 near 10.9 A.U. (most likely shepherded by the 1:3) which might, for example, encounter Earth in November, 2000.

While it is clear that resonances do have a major effect on the stream, the magnitude of the role for any one resonance depends to a great degree on the spreading in the semi-major axis due to radiation pressure forces and initial ejection velocities. The most probable resonances affecting the stream, based on these examined distributions are the 5:14, 4:11 and 1:3 resonances with Jupiter and the 8:9 with Saturn.

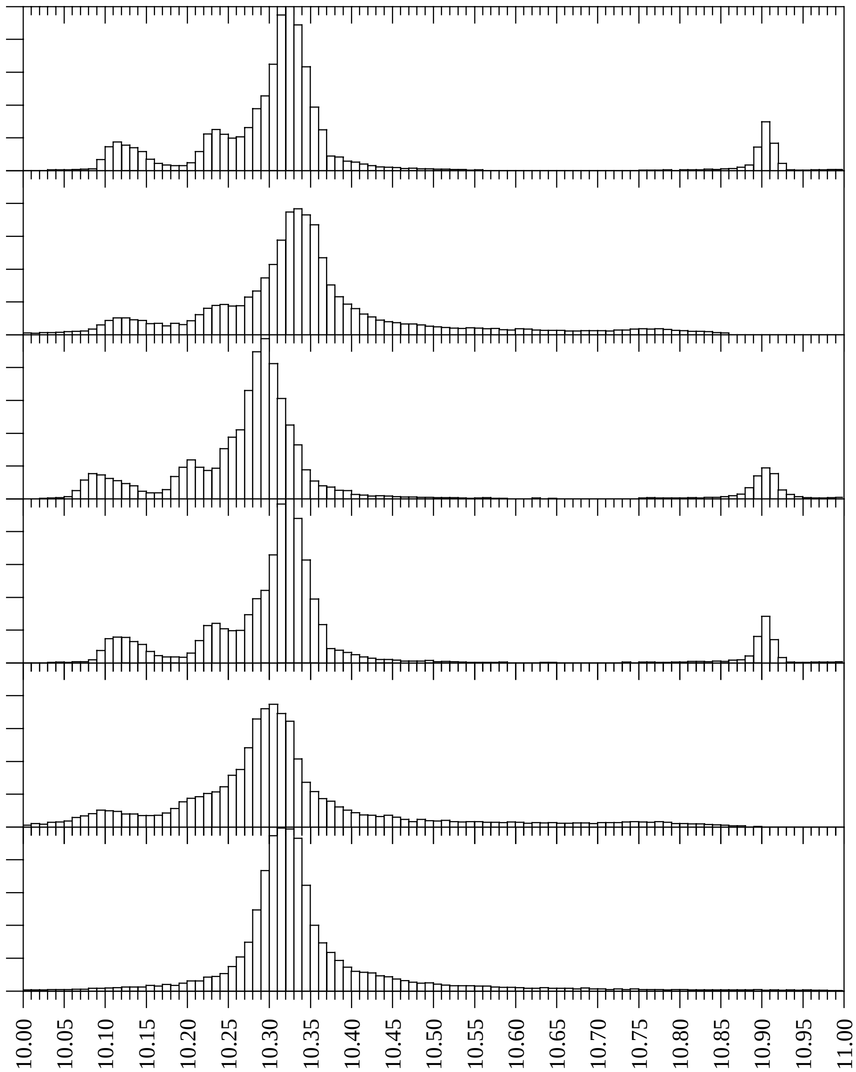

Fig 6.39a: The distribution of model 22 visual-class Leonid test particle semi-major axis ejected in 1899 using model 22 and followed to the present epoch. First (top) plot shows the distribution with all planets and forces included. Second plot shows distribution with Jupiter removed, third with Saturn removed and the fourth with Uranus removed; the fifth plot is with all planets removed; the last is with all planets and radiation pressure removed. Ordinate is the number of test particles per 0.01 A.U. bin in semi-major axis (abscissa), each major tick being 1000 test particles.

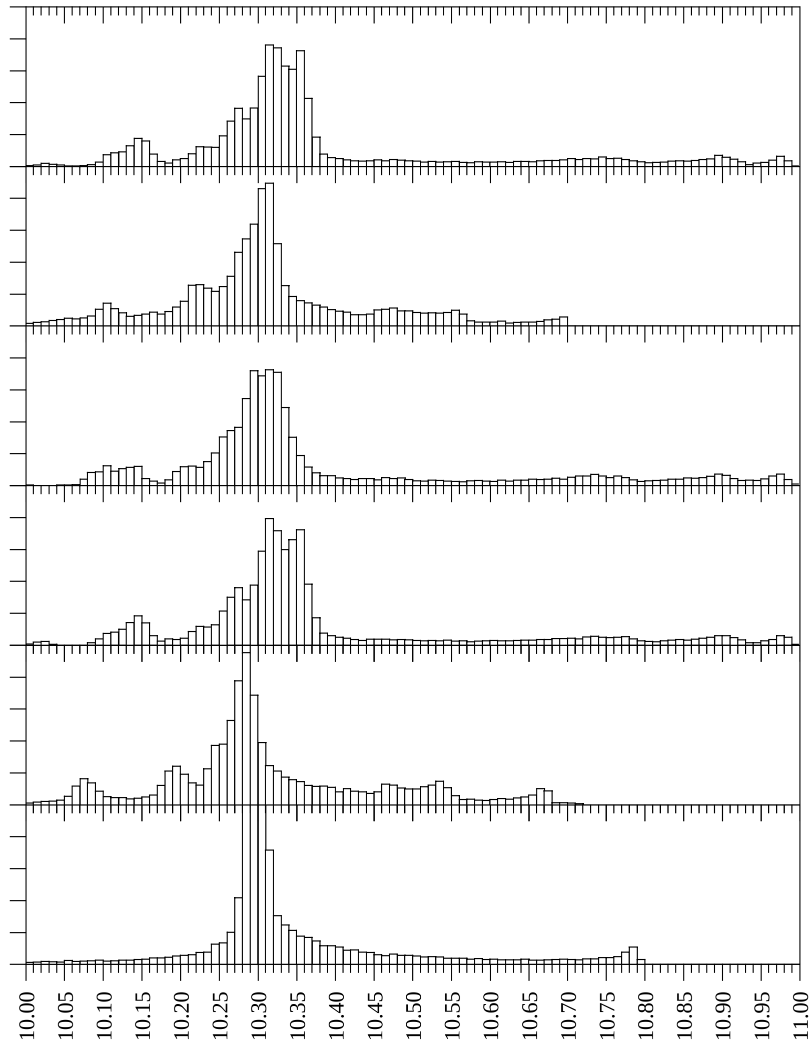

Fig 6.39b: The distribution of visual-class Leonid test particle semi-major axes ejected in 1799 using model 22 and followed to the present epoch. First (top) plot shows the distribution with all planets and forces included. Second plot shows distribution with Jupiter removed; third with Saturn removed; and the fourth with Uranus removed. The fifth plot is the distribution with all planets removed and the last is with all planets and radiation pressure removed. Ordinate is the number of test particles per 0.01 A.U. bin in semi-major axis (abscissa), each major tick being 1000 test particles.

6.7 Current Leonid Cycle (1998 Epoch)

6.7.1 Model Comparison and Interpretation of Leonid showers 1994-1998

Of all the recent Leonid epochs, the current one has been the most studied and has the most precise activity curves available.

Fig 6.9 shows the number of particles with nodal passages as a function of time for several models with our adopted binning. The peak circa 2002 is due to very old material and while many test particles are involved, they are very spread out in solar longitude and unlikely to be associated with storms.

For each year with sufficient test particles, Table 6.7 lists the breakdown in terms of the most significant ejections summed over all solar longitudes. As the table reveals, only a few of the years nearest the passage of the comet have significant amounts of recent ejecta; all other years are from much older passages of the comet.

To investigate more fully the change in age composition for the oldest material of the stream from year-to-year, beginning with the first observed activity in 1994, we make use of the integrations carried out in Sect 6.5 for model 22. Fig 6.40 shows the number of test particles per perihelion passage accepted in the given year to a sieve distance of 0.001 A.U.

Activity in 1994 is primarily from ejections 600-700 years old, while the 1995 return is a century older still. Observations of these returns (see Chapter 5) were characterized by broad activity with an abundance of larger meteoroids, which would be expected given the large amount of time available for planetary perturbations to cause significant spreads in the nodal longitudes and for the increased loss of smaller particles (both trends are directly confirmed through these integrations whereby the largest particles in these years have the highest transfer efficiencies).

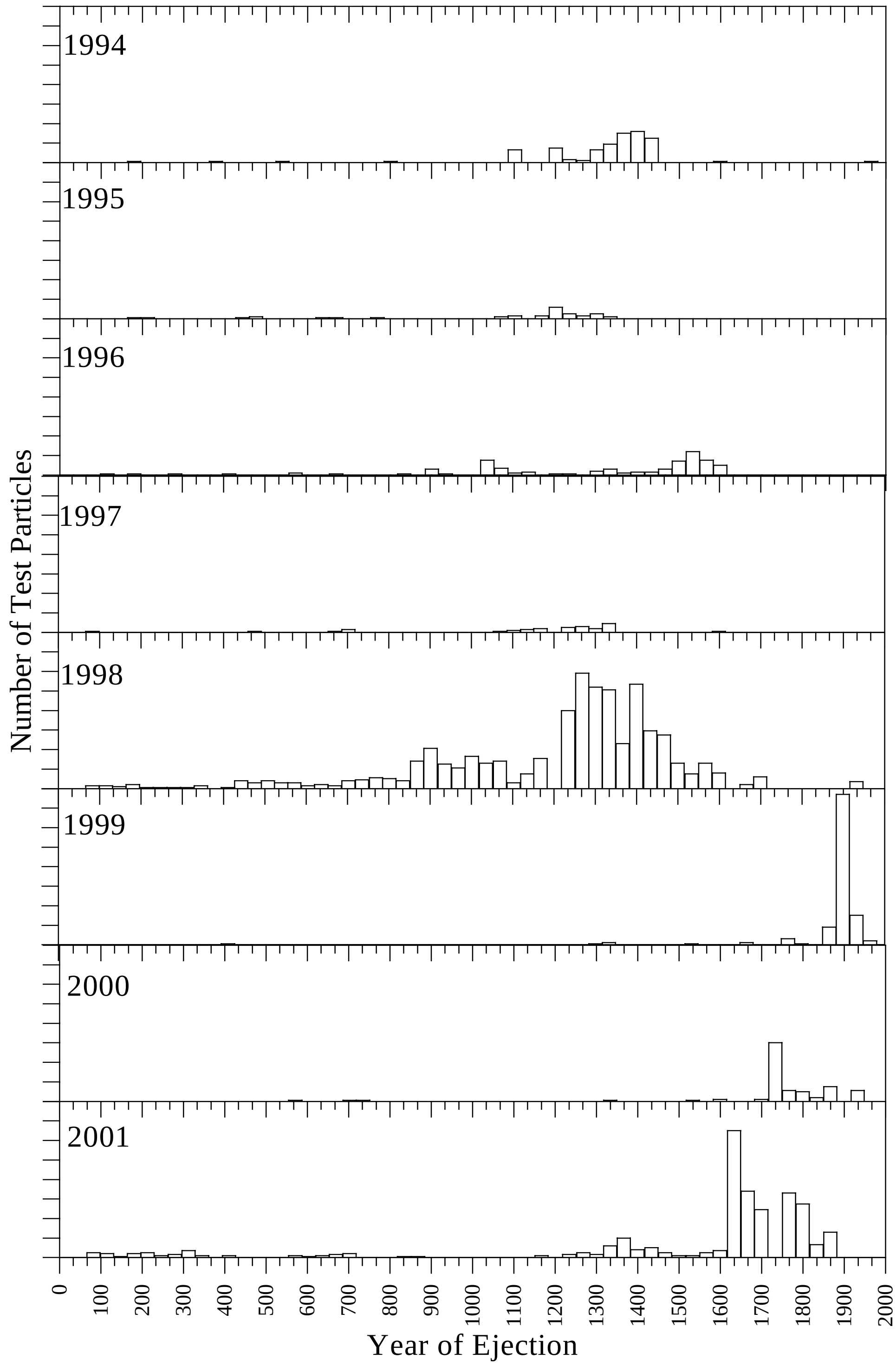

Fig 6.40: The total number of Earth-intersecting meteoroids from model 22 from all ejections over the last 2000 years for Leonid returns from 1994-2001. The ordinate is the same for all plots and runs from 0 to 170.

The 1996 return is the first that shows significant contributions less than 500 years old (and hence is the first year listed in Table 6.8). All models suggest that the activity in this year was primarily from one or a combination of meteoroids ejected during the passages from 1533-1599. Observations from 1996 (Langbroeck, 1999; Brown *et al.*, 1998) show clear evidence of a narrow enhancement of activity near 235.17° in addition to a broad background component similar to that observed in 1994 and 1995. Using the long-term model 22 integrations, the material accepted in the solar longitude range 235.1°-235.2° is composed mainly of material from 1499, but with smaller additional contributions for 100 years on either side of this epoch. It is not possible to narrow the likely ejection era further, but based on these results we can say that a more recent origin for this structure is unlikely. Examination of broader acceptance sieves, both spatial and temporal, failed to yield any material less than 400 years in age in these solar longitude ranges from any models. The location of this peak is unsurprising in light of the results shown in Sect 6.5 (Figs 6.27 and 6.28); material 400-500 years old has peak activity locations in solar longitude in the region from 235°-235.2°, very similar, coincidentally, to peak locations from recent ejections.

The narrow width of this feature (approximately two to three hours full width), however, is more consistent with dispersions in ascending nodes for ejections of order three to four revolutions at most (see Eq. 6.1) and not 10-15 revolutions old as suggested by the previous considerations alone. One possibility is that the material is much younger than the modelling suggests; in this case the material may represent particles outside the range of β and ejection velocities studied. Alternatively, the population may be as old as suggested here but have extremely small β and have experienced very similar planetary perturbations (a “clump”). As the narrow filament was rich in smaller meteoroids, a final possibility is a combination of the two; namely very young material with very small β ($<10^{-5}$) which falls outside our range of adopted β and corresponding ejection velocities. For this material to precede the comet by 1.5 years suggests that small β‘s are likely and leads to the probable hypothesis that the material associated with this narrow structure was of higher bulk density than the average in the stream.

Modelling for 1997 suggests a return to older meteoroids, namely 600 - 800 years in age. Observations in 1997 (Arlt and Brown, 1998) were hampered by a full moon but confirm a broad background, rich in bright meteors, as expected for such old material. A narrower faint component may have been recorded somewhat later than 1996, but its presence is uncertain. The fainter population of Leonids shows no evidence of significant fragmentation (Hawkes *et al*, 1998), a further indication of an older population as the modelling suggests.

The modelling results for 1998 are dominated by large meteoroids occurring significantly before the nodal passage of the comet. From Fig 6.40, the age of material composing the 1998 return is primarily between 500 - 800 years, but significant amounts of even older material are also present. Notable is a possible small contribution only of more recent material (from 1932) and little else younger than 1700, a result consistent across all models (see Table 6.7). Fig 6.41 shows the distribution in mass of accepted test particles and a significant component of larger meteoroids.

Fig 6.41 (bottom): The distribution in Log mass as a function of solar longitude in 1998 for model 22 Earth-intersecting Leonids summed for all ejections from 89-1965 A.D.

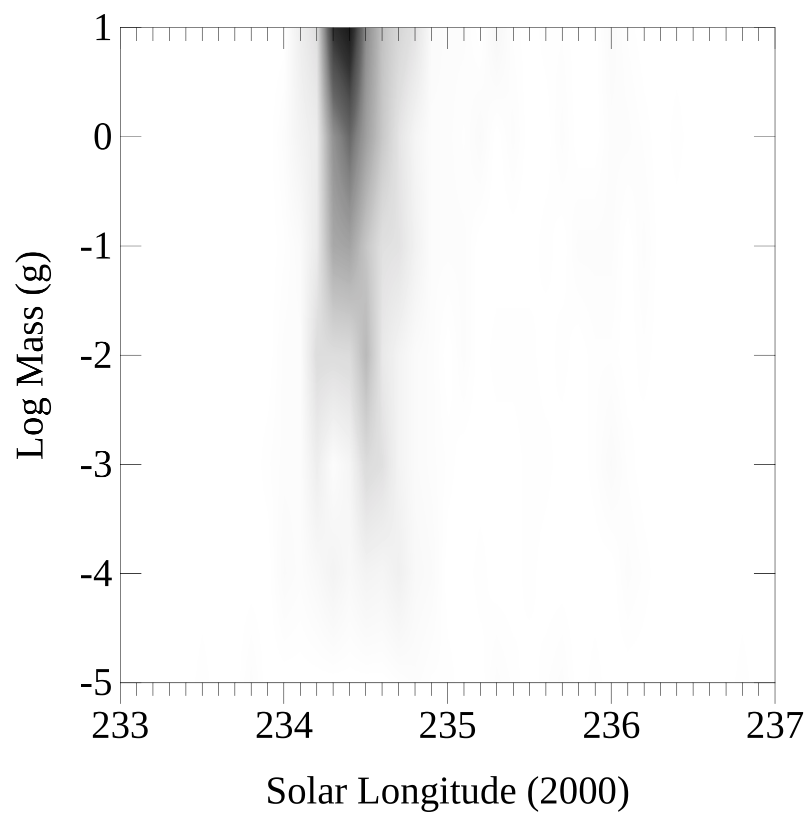

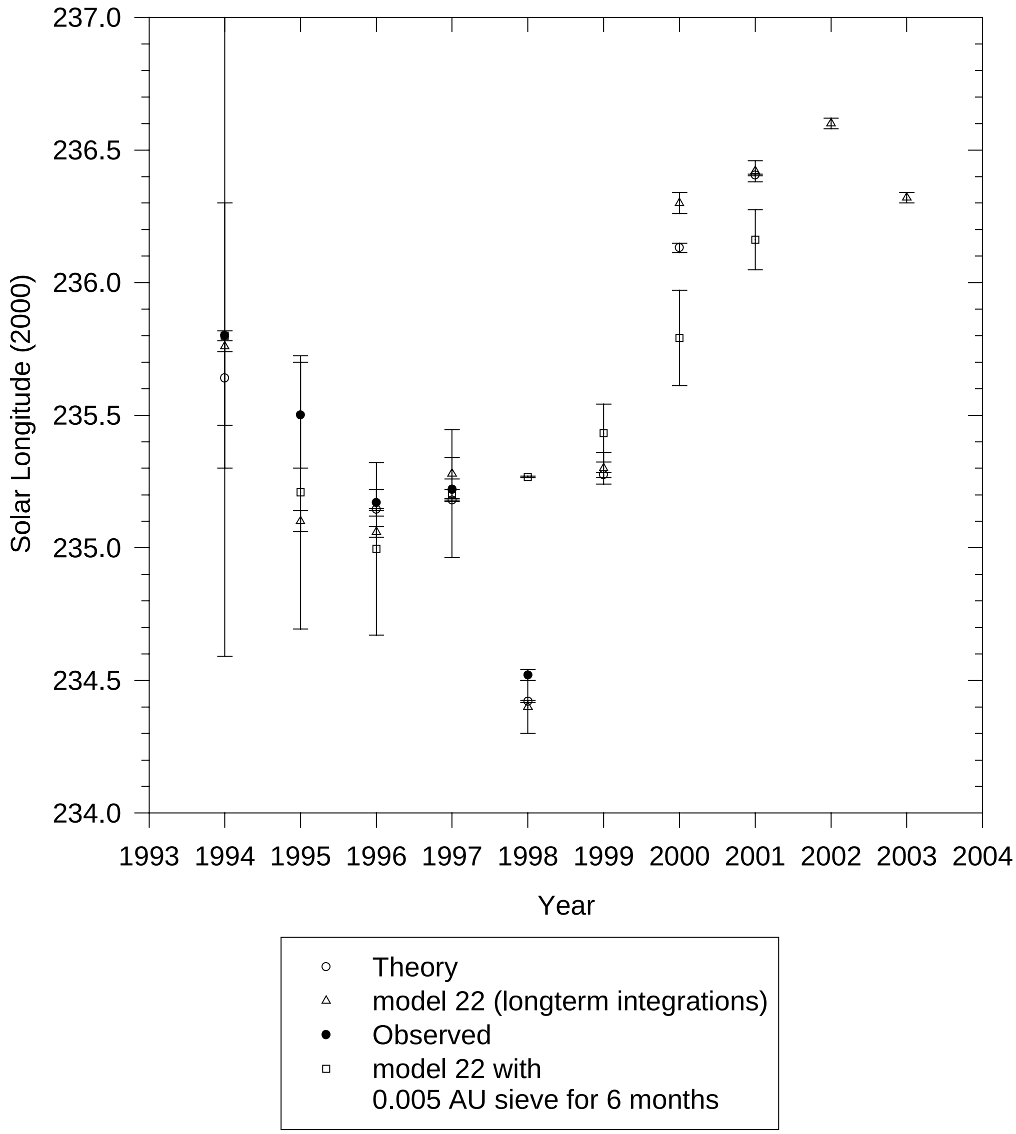

Fig 6.42: Locations of peak ZHR's for the 1998 Leonid epoch. The observed locations (for 1998 and earlier) as well as several model predictions are given as shown in the legend.

6.7.2. Leonid returns 1999-2002 : Predictions based on the modelling

Based on all results to this point, using the best combinations of acceptable models, sieve sizes and temporal nodal acceptance widths we may estimate the expected behaviour of the shower over the next four years.

Fig 6.42 shows the measured position of the peak ZHR for the Leonids from 1994-1998. Also shown in the figure are the theoretical locations based on a weighted average of all models using a 0.001 A.U. sieve with two week nodal time bins. For comparison the peak locations which are derived with a 0.005 A.U. bin and six month nodal time bins are also shown. For completeness, we have also noted the locations of maxima based on the long-term model 22 integrations, the only reliable measure of peak locations for those years with significant material older than 500 years.

The agreement between observations and the modelling is encouraging. A major discrepancy occurs in 1998 when the wide binning (0.005 A.U.) places the maximum near the node, while the true ZHR maximum (and the maximum chosen with narrower acceptance criteria) is nearly 20 hours earlier. In 1998, this was the result of inclusion of large quantities of material which were still significantly inside the Earth's orbit but which we believe are more likely to be visible at Earth in 1999. The distance to the most recent trails in 1998 is shown in Fig 6.43.

Also shown in Fig 6.43 is the trail distribution in 1999. In 1999 we expect (using all methods) the peak to be near the node of the comet, while later returns are anticipated significantly later. This trend is a direct result of slightly older material dominating the influx from 2000 onwards, with these ejections having maximum locations nearer 236° (see Figs. 6.27 and 6.28).

A similar trend has been observed (and predicted - see Chapter 4) for the Perseid shower for similar reasons. As Table 6.7 and Fig 6.43 indicate, in 1999 we will intersect the youngest material during the current cycle, namely ejecta from 1899.

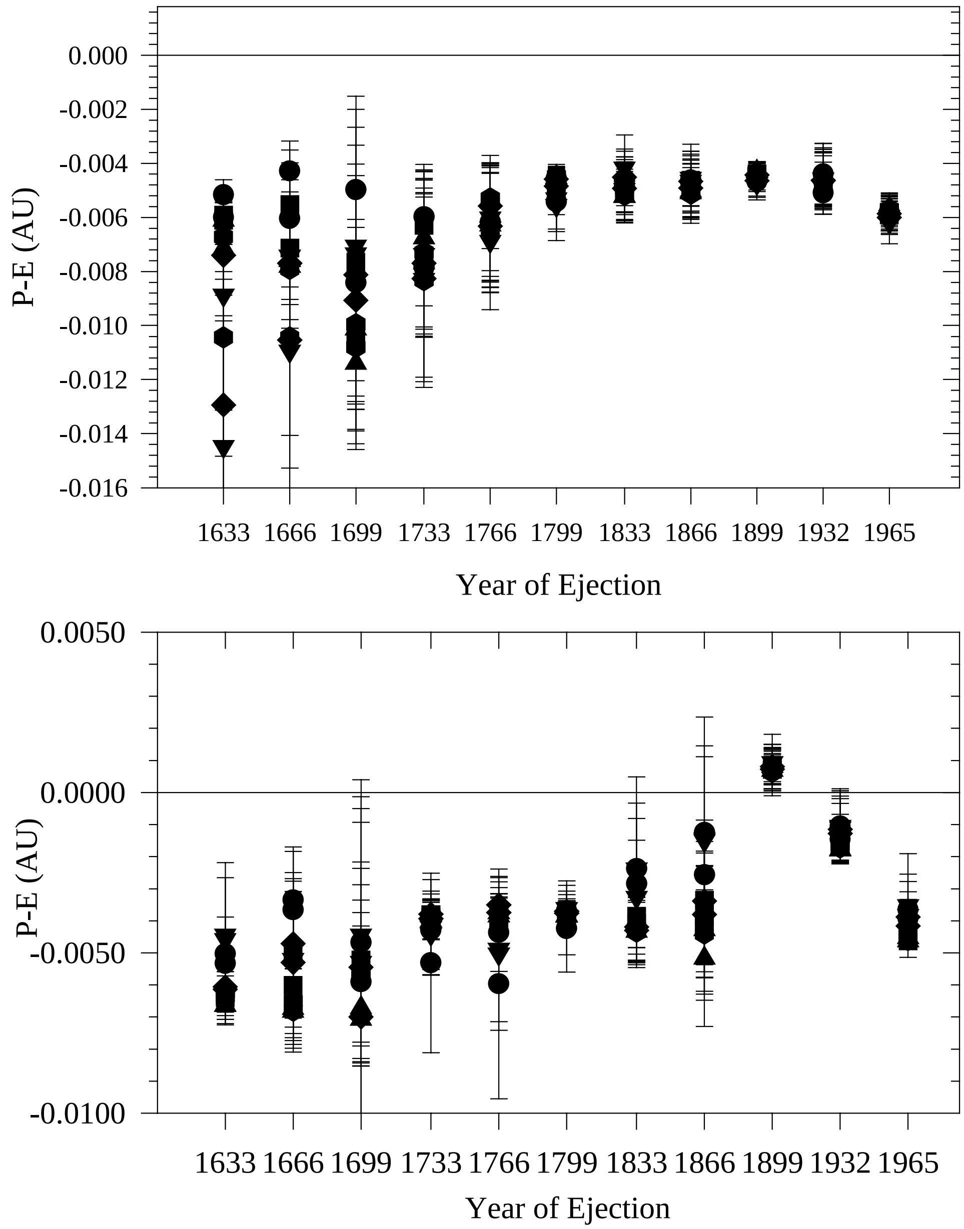

Fig 6.43: The distance from the Earth of various “trails” ejected by Tempel-Tuttle in the years listed on the abscissa. The symbols correspond to the same models as Fig 6.6. Top plot shows trail distances to Earth for test particles within 1 week of the time of the shower in 1998. The bottom plot shows the same for 1999.

This same cometary trail most probably caused the 1966 storm (see Sect 6.4.1). Fig 6.43 shows the distance between the center of each of the last eleven cometary trails and the Earth's orbit at the time of the 1999 return. Note the spread in mean distances and the large region covered by the error margins (which represent the standard deviation of the nodal radii for the particular model). While 1899 is closest to the Earth's orbit (the models having means from 6-8$\times 10^{-4}$ A.U. from Earth's orbit), the 1932 ejection is likewise close and might be expected to contribute also to any storm. Both 1866 and 1833 overlap with Earth's orbit within the limits of their error margins, but the spreads in their nodal radii are large both between models and for any individual model. This is a direct consequence of the planetary perturbations these meteoroids experienced circa 1899-1901. As a result, should a storm occur, it is most likely to be produced by material from 1899 or (less likely) from 1932. Both trails are still compact based on our modelling, have not suffered severe planetary perturbations and pass reasonably close to the Earth. While the numbers are small, the modelling does suggest we may just skirt the outer portions of either (or both) of these trails producing quite possibly a very strong shower or small storm at Earth.

Comparison with 1966 and the same trail shows that we are approximately three times further away from the 1899 trail than in 1966; thus a 1966 class storm is unlikely. Using the modelled decrease in density for the stream as a function of time from Sect 6.5, we expect diffusion to have decreased the trail spatial density by approximately 5-10 times since 1966. Additionally, as we pass three times further from the trail center than in 1966, and assuming a r^{-2} drop-off in density from the centre of the trail, we may tentatively estimate any storm occurring in 1999 to be ~two orders of magnitude lower in flux than in 1966. Assuming a similar mass index holds in 1999 as was observed for the 1966 storm, we tentatively estimate a peak ZHR value of order 1000 - 2000 with a peak slightly after the nodal longitude of Tempel-Tuttle in 1999. From the modelling, the 1999 display is likely to display a broader particle population and to be richer in small meteoroids relative to 1998, with the modelling suggestive of a peak in the neighborhood of β=0.001.

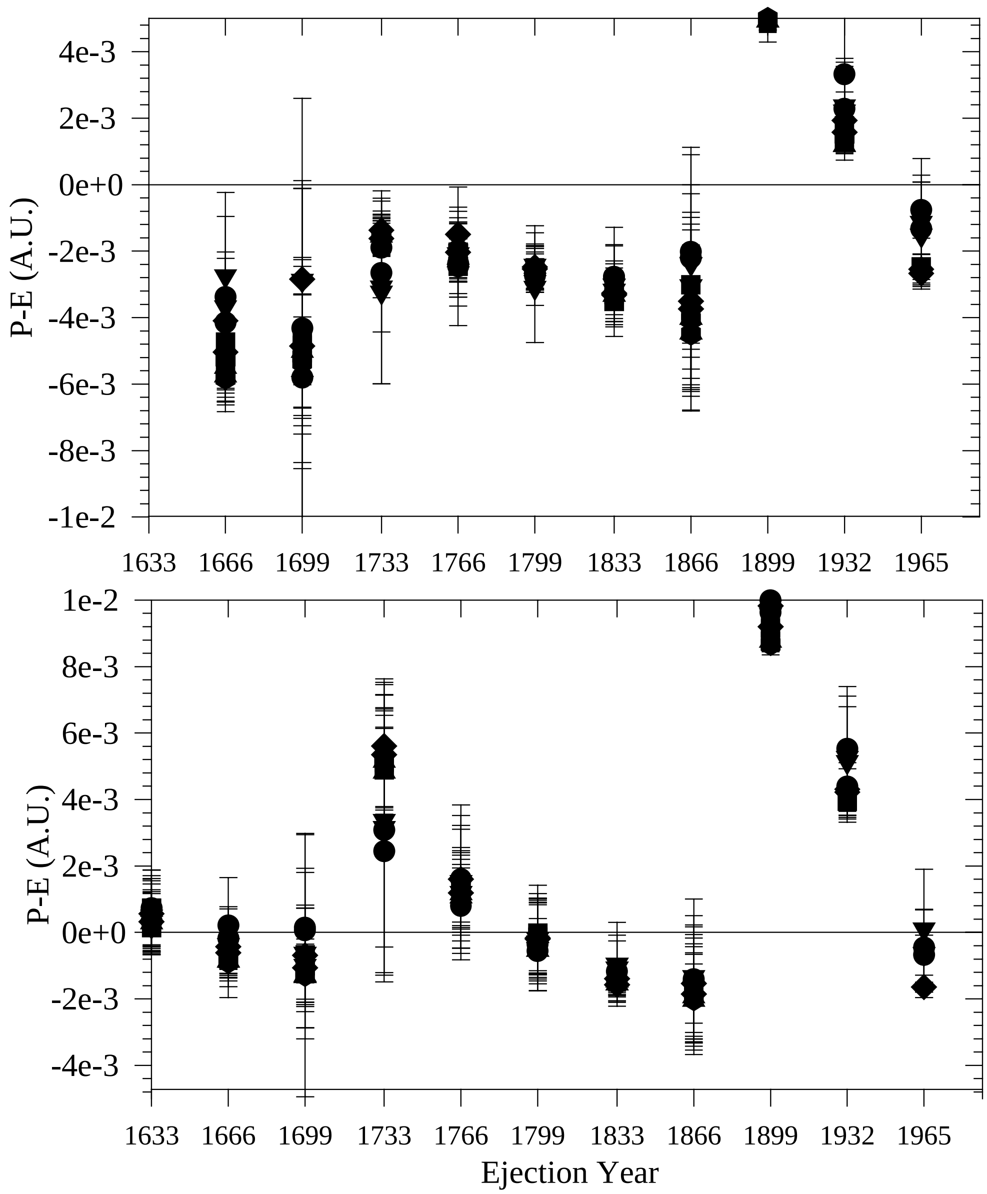

Fig 6.44: The distance from the Earth of various “trails” ejected by Tempel-Tuttle in the years listed on the abscissa. The symbols correspond to the same models as Fig 6.6. Top plot shows trail distances to Earth for test particles within 1 week of the time of the shower in 2000. The bottom plot shows the same for 2001.

Table 6.7. Age of Leonid showers for a given year as a function of modelling. The first number in each box is the total number of test particles with nodal radaii within 0.001 A.U. of Earth and times of nodal passage within 1 week of the Earth's passage through the stream. The following numbers give the primary year contributing to the integrated activity from the model and (in brackets) the fraction of all particles in a particular test year from this ejection. This summation is for all particles at all solar longitudes in the given year.

Model/Year	1996	1998	1999	2000	2001
11	0	32 **1600(.94)** 1533(.03)	191 **1899(.59)** 1932(.15)	198 **1733(.65)** 1965(.10)	613 **1699(.24)** 1633(.23)
12	2 **1533(.50)**	134 **1499(.49)** 1599(.20)	197 **1899(.70)** 1932(.14)	103 **1733(.52)** 1866(.19)	991 **1666(.35)** 1633(.34)
13	57 **1533(.47)** 1566(.21)	273 **1499(.48)** 1599(.21)	71 **1899(.80)** 1932(.08)	99 **1733(.76)** 1866(.06)	910 **1666(.39)** 1633(.34)
21	35 **1533(.43)** 1566(.29)	77 **1499(.22)** 1599(.17)	224 **1899(.58)** 1932(.23)	109 **1932(.28)** 1965(.19)	286 **1633(.21)** 1766(.20)
22	63 **1533(.38)** 1566(.24)	106 **1499(.25)** 1599(.15)	216 **1899(.71)** 1932(.14)	116 **1733(.52)** 1866(.13)	423 **1633(.31)** 1666(.16)
23	120 **1533(.33)** 1566(.25)	169 **1533(.28)** 1566(.24)	167 **1899(.77)** 1932(.11)	100 **1733(.64)** 1766(.18)	597 **1633(.34)** 1666(.25)
31	39 **1533(.31)** 1599(.26)	115 **1566(.25)** 1599(.22)	241 **1899(.58)** 1932(.22)	95 **1932(.22)** 1733(.19)	297 **1633(.28)** 1766(.20)
32	73 **1533(.30)** 1599(.27)	207 **1499(.24)** 1599(.23)	232 **1899(.75)** 1932(.18)	87 **1733(.54)** 1866(.14)	468 **1633(.29)** 1666(.20)
33	90 **1599(.28)** 1566(.27)	303 **1566(.26)** 1599(.25)	110 **1899(.89)** 1866(.05)	107 **1733(.70)** 1766(.08)	695 **1633(.34)** 1666(.33)
41	29 **1533(.45)** 1566(.17)	100 **1499(.26)** 1699(.23)	240 **1899(.60)** 1932(.19)	116 **1733(.31)** 1932(.14)	343 **1633(.27)** 1766(.16)
42	55 **1566(.29)** 1533(.25)	189 **1499(.28)** 1566(.23)	186 **1899(.76)** 1932(.15)	96 **1733(.42)** 1866(.18)	583 **1633(.34)** 1666(.26)
43	85 **1533(.41)** 1599(.21)	273 **1499(.29)** 1599(.27)	107 **1899(.84)** 1932(.08)	77 **1733(.68)** 1866(.14)	733 **1633(.35)** 1666(.33)

Fig 6.44 shows the proximity of the recent trails to the Earth at the time of the 2000 Leonid shower. Both the 1965 and 1932 trails may be modestly close to the Earth depending on the physical properties of the particles; however, in both cases it is probable that the centre of these recent trails will be much more than 10^{-3} A.U. from Earth, a likely requirement for the production of storms. Indeed, the bulk of the particles encountered from the modelling in 2000 is largely from the 1733 ejection (the same trail which produced the 1866 Leonid storm) and possibly the 1866/1932/1965. It is probable that a strong shower, and possibly a small storm, may occur in 2000, but it would likely be smaller than the 1999 shower. Peak ZHRs in this year are more likely in the range of a few hundred and if the older material from 1733 dominates it is probable the maximum will occur near 236.3° (while a dominant population of newer material would peak shortly after the nodal longitude of the comet).

The 2001 modelled shower marks a return to older material, and is proportionately richer in larger meteoroids than the 2000 modelled display (though showing a wider range in accepted masses than 1998). In terms of dense recent trails, Fig 6.43 shows that only the 1965 or the 1866 (or older) trails might be significant. All the material from 1965 that is accessible in 2001 has very high β ($\sim 5\times10^{-3}$), reminiscent of the 1969 shower geometry. Peak ZHRs are likely in the range of a few hundred, and a short-lived shower similar to 1901/1903 peaking at 236.4° is suggested by the modelling, assuming that older material dominates. This older material (from 1633-1699) shows a peak transfer efficiency near $\beta\sim10^{-4}$.

The 2002 shower shows potential for material from several trails to interact with Earth. The Earth's proximity to each of these trails in 2002 suggests that if significant numbers of relatively small β particles are present a strong shower (comparable to the 1969 Leonid outburst) might occur. Of course the main concentrations in these trails passed through the descending node several years earlier and thus only modest particle numbers would be expected (relative to storm years). Notable is the confinement of this outburst to a narrow range of β from 5×10^{-4} - 10^{-3}.

6.8 Summary and Conclusions

Based on the foregoing numerical modelling of the Leonid stream we may directly summarize the most probable answers to the questions posed in Sect 6.1.

1. The age and origin of the ejecta which constitute the primary Leonid storms (outlined in Chapter 5) all have recent (less than two or at most three passages old) ejection origins. The only possible exception is the return in 1832 that may consist of meteoroids released ~150 years earlier, but the actual character of the 1832 display (whether a storm or a long enduring shower consisting of bright meteors) is in doubt. All storms in these years were caused by cometary trails averaging (summed over all models and visual masses) $(8\pm6)\times10^{-4}$ A.U. from Earth's orbit at the time of the storms. The trails associated with the strongest storms were less than 7×10^{-4} A.U. in width and one to three times (on average) this amount in radial spread for our chosen range of βs. The trails may best be described as "thick" sheets or elongated tubes. The dense trails are moved to Earth-intersection through perturbations by Jupiter and Saturn, in the above cases in particular by distant, primarily post-perihelion perturbations which move the trails outward as a function of nodal return time and thus allow trails to reach Earth.

That storms occur outside Tempel-Tuttle's orbit and after its nodal passage has been previously noted (cf. Yeomans 1981). However, the mechanism most identified as causing this behaviour has been the direct effects of radiation pressure (Yeomans 1981; Wu and Williams 1991). From Fig 2.6 and Figs 6.3, 6.14 we see that radiation pressure changes to the nodal radii for the majority of Leonid meteoroids (released near perihelion) are negligible in comparison to the effects of planetary perturbations for meteoroids of the sizes considered here, a conclusion also reached by Sekanina (1974). Radiation pressure does cause meteoroids to lag the comet as demonstrated extensively in our simulations, but this alone is not a sufficient condition for causing storms. The distant perturbations from Jupiter affect a significant portion of the stream on most passages of Tempel-Tuttle; it is the effect of these on the future nodal distances of Leonid meteoroids that allows material which progressively lags the comet to move outward from the sun at the node and intersect the Earth.

2. The most complete information concerning the initial ejection velocities comes from comparison of the activity curves for the 1866, 1867, 1966 and 1969 storms/showers with the modelled results. Comparing the observed profiles of these showers with the final activity widths from test particles released during the perihelion passage causing the storms and the relating these back to the normal components of the ejection velocities, we find that a range of probable ejection velocities has been established. In particular, the best fits to the observed profile were found for meteoroids with total ejection velocities of ~5 m/s for the 1866 storm, 15-20 m/s for 1867, 3-4 m/s for the 1966 storm and 10-15 m/s for the 1969 outburst. These values represent the average expected ejection velocities for material encountering the Earth at the time of these storms and do not necessarily represent the actual distribution of ejection velocities at the comet. These results simply suggest that significant numbers of meteoroids must be ejected from Tempel-Tuttle with velocities <20 m/s. Meteoroid populations ejected at higher velocities and which can be detected at Earth have final activity widths inconsistent with the observed widths. Note that the best fit velocities vary from storm to storm due to differences in the favorability of Earth-intersection based on initial ejection geometry, subsequent perturbations etc. and do not reflect changes in the mean ejection velocities between perihelion passages (which are the same in our modelling).

3. and 4. The comet-Earth distance for past ejections plays a minor role only in determining the future (~centuries) delivery of Leonid meteoroids to Earth. This results directly from the fact that the magnitude of the change in nodal distance due to planetary perturbations is much larger than the average comet-Earth distance over the last millenium. Strong perturbations from Jupiter, for example, may move the nodal points of Leonid meteoroids en masse by up to 0.01 A.U. every ~150 years, with the average comet-Earth separation being smaller than this value. Meteoroids with smaller β arrive in Earth-intersecting orbits more frequently after 300 years, independent of initial ejection conditions, possibly due to lesser overall differential planetary perturbations (and thus diffusion) compared to higher-β populations.

5. Numerical computation of the average relative change in stream density, as measured at the descending node, shows that the average flux within the stream for the models and masses studied decreases by between two and three orders of magnitude 100-150 years after ejection, with different models showing similar behaviour. Fig 6.25 summarizes the typical model results for the average relative changes in density.

6. Jupiter dominates the evolution of the Leonid stream. It is the main perturbing force on the Leonids, and its perturbations “peak” every five revolutions of 55P/Tempel-Tuttle. Mean motion resonances, particularly the 5:14, 4:11 and 1:3, affect the development of the stream by removing and/or concentrating Leonid meteoroids in semi-major axis intervals determined by these resonances. Saturn affects the stream to a smaller degree, but acts in concert with Jupiter to affect noticeably the delivery of Leonids to Earth, potentially through the 8:9 mean motion resonance. Uranus has a much lesser effect on the stream and its 5:2 mean motion resonance shows no effects on the semi-major axis distribution of Leonids, nor has Tempel-Tuttle been located in this resonance over the last 2000 years. Uranus does appear to modify the delivery to Earth of some Leonid meteoroids shortly after nodal passage of Tempel-Tuttle, in partial agreement with the conclusions of Williams (1997). That Uranus dominates many of the evolutionary aspects of the stream, however, as suggested by Williams (1997) is not confirmed by our work.

7. From Fig. 6.26, the combined effects of initial ejection velocity and radiation pressure limit the flux of the stream over intervals <100 years. Over longer time intervals, the flux is limited by planetary perturbations, primarily from Jupiter. For the lower ejection velocities suggested from **2** (which are several times lower than utilized in Fig 6.26), the effects of radiation pressure may be expected to dominate the first century of density decrease in the stream for smaller meteoroids.

8. From **1** the most representative models would appear to be those with the lowest ejection velocities, namely Crifo’s extended production model 1. Of the three densities chosen for model 1, the lowest density (corresponding to the largest cross-sectional areas for a given mass) also has the lowest ejection velocities. To confirm this, we have computed the residuals between the observed activity profiles of the four Leonid returns for which we have the greatest confidence in ejection origin and sufficient observations (1866, 1867, 1966 and 1969) and the complete model profile. These normalized residuals are given in Table 6.9. As expected, model 11 is the best fit overall. That the ejection velocities from Tempel-Tuttle are low has been repeatedly emphasized in previous work (see Sect 1.1), with values very similar to those we find most probable. Whipple-sized ejection velocities appear to be too high by a factor of several for Tempel-Tuttle. Given the various uncertainties in the physical properties of the meteoroids and the great simplifications of the Whipple approach (compared to modern coma-dust models such as Crifo and Rodinov 1999), it is hardly surprising that the model is not a precise analog to reality for every comet.

The disagreement between the predicted Whipple ejection velocities and our most probable velocities is not outrageous. Use of smaller average cross-sections or the existence of specific active areas producing jets with more sunward average velocity components (and hence smaller normal velocities) than our uniform hemispherical production could all account for the discrepancies within the uncertainties. Indeed, Wu and Williams (1996) have proposed ejection velocities up to an order of magnitude higher than those predicted by the Whipple formalism, underlining the range of inherent uncertainty.

Table 6.8: Normalized residuals of fit between the total scaled model activity profiles and gaussian fits to ZHR curves in each of the given years. For each model distribution, the largest peak number of test particles per 0.005° solar longitude bins was scaled to match peak ZHRs in the solar longitude interval about the observed storm peak and other model bins were then scaled by this factor. The resulting theoretical ZHR profiles for all models were subtracted from the observed gaussian fits over the same number of bins and the sum of the squares of these differences computed. These final residual values were then scaled such that the smallest residual was given the value of unity. As a consequence of the large differences in absolute numbers, the values of the normalized residuals between years has little meaning – only the relative values of fit within a given year are meaningful. Model residuals omitted for a given year are due to no test particles being accepted near the observed ZHR maximum.

Model\Year	1969	1966	1867	1866
11	1	1	2.975	1
12	-	15.845	3.087	1.561
13	-	8.799	-	1.512
21	1.213	4.299	1	1.087
22	-	22.293	1.624	1.309
23	-	4.041	-	1.264
31	1.25	9.468	1.986	1.098
32	-	5.23	1.564	1.196
33	-	2.897	-	1.685
41	2.662	13.396	1.429	1.115
42	-	4.595	2.288	1.668
43	-	8.579	1.824	1.563

9. The sudden large increases in Leonid flux near the time of comet's passage and the equally sudden decrease three to four years after its perihelion passage are a natural consequence of the rapid diffusion of older material within the stream and Earth's sampling farther from the maximum density within the stream (which is typically <20° mean anomaly after the comet). From Fig 6.40, for example, Leonid returns only one to two years after perihelion passage of the comet are the only years which have significant populations of meteoroids with ejection ages of less than a century (see also a similar trend in Tables 6.3-6.7). Based on **1**, these are also the only returns where material is dense enough to cause a storm or strong shower. In years when material even a few revolutions older is encountered, the flux has fallen greatly. This is in part a consequence of diffusion of older material (Fig 6.25) and of the Earth's sampling temporally further from the densest portions of the trail(s) within the stream. The age of the annual component of the Leonids is of order ~1000 years based on the results of Sect 6.5, with ejections older than this contributing little at the present time to the stream fluence. This age is consistent with the first recorded observations of the Leonid storms in 902 A.D. and with the ~10 day total duration of the shower (from Chapter 5), producing an age estimate of <2000 years using the results of Fig 6.22. A contributing factor limiting the lifetime of the broader, annual component of the stream, may be the closer inbound encounter distances to Jupiter and Saturn 900 – 1000 years ago (see Figs 6.30 and 6.31). This may also account for the drop in the number of test meteoroids in the present epoch at Earth from ejections prior to 1100 A.D.

References

Adams, J.C. 1867. On the Orbit of the November meteors, *Mon. Not. R. Astron. Soc.,* **27**, 247-252.

Arlt, R. and P. Brown. 1998. Bulletin 12 of the International Leonid Watch: Final results of the 1997 Leonids and prospects for 1998. *WGN J. Int. Met. Org*. **26(4)**, 161-165.

Asher, D.J. 1999. On the Leonid Storms of 1833 and 1966, *MNRAS,* in press.

Berberich, A. 1898. On the orbit-perturbations of the Leonid meteor-stream since 1890. *Astron. Nachr*. **147**, 359.

Brown, P. 1999. The Leonid Meteor Shower: Historical Visual Observations, *Icarus*, in press.

Brown, P. and J. Jones. 1993. Evolution of the Leonid meteor stream. In *Meteoroids and Their Parent Bodies* (J. Stohan and I. P. Williams, Eds.) pp. 57-61. Astronomical Inst. Slovak Acad. Sci., Bratislava.

Brown, P. and J. Jones. 1998. Simulation of the formation and evolution of the Perseid meteoroid stream. *Icarus* **133**, 36-68.

Brown, P., M. Simek, and J. Jones. 1997. Radar Observations of the Leonids: 1964-1995, *A&A*, **322**, 687-695.

Carusi, A., L. Kresak, E. Perozzi and G. B. Valsecchi. 1987. High-order librations of Halley-type comets. *Astron. Astrophys*. **187**, 899.

Chambers, J. E. 1995. The long term dynamical evolution of comet Swift-Tuttle. *Icarus* **114**, 372-386.

Crifo, J. F. 1995. A general physicochemical model of the inner coma of active comets. I-Implications of spatially distributed gas and dust production. *Astrophys. J.* **445**, 470-488.

Crifo, J.F. and A.V. Rodionov 1999. Modelling the Surface Activity of Cometary Nuclei, IAU Symposium 168, in press.

Emel'yanenko, V. V. 1984. Meteor-stream density evolution by planetary perturbations. *Sov. Astron. Letters* **10**, 131.

Fulle, M. 1996. Dust environment and nucleus spin axis of comet P/Tempel 2 from models of the infrared dust tail observed by IRAS. *Astron. Astrophys*. **311**, 333-339.

Greenberg, R. 1977. Orbit-orbit resonances in the solar system - Varieties and similarities. *Vistas Astron*. **21(3)**, 209-239.

Hainaut, O.R., K.J. Meech, H. Boehnhardt and R.M. West, 1998. Early Recovery of Comet 55P/Tempel-Tuttle, *A&A*, 333, 746-752.

Hasegawa, I. 1993. Historical records of meteor showers. In *Meteoroids and Their Parent Bodies* (J. Stohl and I. P. Williams, Eds.), pp.209-227. Astronomical Inst. Slovak Acad. Sci., Bratislava.

Hawkes, R. L., M. Campbell, D. Babcock and P. Brown. 1998. The physical structure of Leonid meteoroids: evidence from optical observations. In *Proceedings of the Leonid Meteoroid Storm and Satellite Threat Conference, Manhattan Beach, California, April 27-28, 1998* (D. Lynch, Ed.). American Institute of Aeronautics and Astronautics, Los Angeles.

Herrick, E. C. 1841. Contributions towards a history of the star-showers of former times. *Amer. J. Sci. Arts*. **40**, 349.

Jones, J. 1985. The structure of the Geminid meteor stream. I – The effect of planetary perturbations. *Mon. Not. R. Astron. Soc*. **217**, 523-532.

Jones, J. 1995. The ejection of meteoroids from comets. *Mon. Not. R. Astron. Soc*. **275**, 773-780.

Kazimirchak-Polonskaja, E.I., Belijaev, N.A., Astapovic, I.S., and A.K. Terentjeva. 1968. Investigation of the perturbed motion of the Leonid meteor stream. In *Physics and Dynamics of Meteors Proceedings of IAU Symp No. 33*, (L. Kresak, and P.M. Millman, Eds.),pp. 449-475, D. Reidel, Dordrecht-Holland.

Kondrat'eva, E. D. and E. A. Reznikov. 1985. Comet Tempel-Tuttle and the Leonid meteor swarm. *Astron. Vest*. **19**, 96.

Kresak, L. 1992. On the ejection and dispersion velocities of meteor particles. *Contr. Skalnate. Pleso* **22**, 123-130.

Kresak, L. 1993. Cometary dust trails and meteor storms. *Astron. Astrophys*. **279**, 646-660.

Langbroek, M. 1999. Leonid outburst activity 1996: A broad structure and a first occurrence of a narrow peak in fainter meteors, *MAPS*, **34**, 137-147.

Le Verrier, U-J-J. 1867. Sur les Etoiles filantes de 13 Novembre et du 10 Aout, *Comptes Rendus*, **64**, 94-99.

Littman, M. 1998. *The Heavens on Fire*. Cambridge University Press, Cambridge.

Mason, J. W. 1995. The Leonid meteors and comet 55P/Tempel-Tuttle. *J. Brit. Astron. Assoc.* **105 (5)**, 219-235.

McDonnell, J. A. M., and 9 colleagues. 1987. The dust distribution within the inner coma of comet P/Halley 1982i—Encounter by Giotto's impact detectors. *Astron. Astrophys.* **187**, 719-741.

McIntosh, B. A. 1973. Origin and evolution of recent Leonid meteor shower. In *Evolutionary and Physical Properties of Meteoroids (NASA SP-319)* (C. G. Hemenway, P. M. Millman, and A. F. Cook, Eds.), pp. 193-199. NASA, Washington, DC.

Murakami, T. 1959. On the structure of the Leonid stream. *Pub. Astron. Soc. Japan.* **11**, 171.

Murakami. T. 1961. On the structure of the Leonid stream, II. Magnitude-distribution of meteoric particles in the Leonid stream. *Pub. Astron. Soc. Japan*. **13**, 51.

Murakami, T. 1961. On the structure of the Leonid stream, III. The formation and development of the Leonid stream. *Pub. Astron. Soc. Japan*. **13**, 212.

Murray, N. Holman, M. and M. Potter, 1999. On the origin of chaos in the asteroid belt, *AJ*, **116**, 2583-2589.

Newton, H. A. 1863. Evidence of the cosmical origin of shooting stars derived from the dates of early star-showers. *Amer. J. Sci. Arts (2nd Series)*. **37**, 145.

Olbers, H. W. M. 1837. Die Sternschnuppen. In *Schumacher's Jahrbuch fur 1837*, pp. 36.

Olmsted, D. 1834. Observations of the meteors of November 13, 1833. *Am. J. Sci*. **25**, 354-411; 26, 132-174.

Schiaparelli, G. V. 1867. Sur les Etoiles Filantes, et specialement sur l'identification des

Orbites des Essaims d'Aout et de Novembre avec celles des Cometes de 1862 et de 1866. *Comptes Rendus* **64**, 598-599.

Schubart, J. 1968. Long-period effects in the motion of Hilda-type planets. *Astron. J.* **73**, 99-103

Sekanina, Z. 1974. Meteoric storms and the formation of meteor streams. In *Asteroids, Comets and Meteoric Matter* (C. Cristescu, W. J. Klepczynski, and B. Milet, Eds.), pp. 239-267. Scholium Int., New York.

Stoney, G.J. and A. M. Downing. 1899. Perturbations of the Leonids. *Proc. Roy. Soc. London.* **64**, 403.

Whipple, F. L. 1951. A comet model II. Physical relations for comets and meteors. *Ap. J.* **113**, 464.

Williams, I. P. 1997. The Leonid meteor shower - Why are there storms but no regular annual activity? *Mon. Not. R. Astron. Soc.* **292**, L37-L40.

Williams, I. P., C. Johnson, and K. Fox. 1986. Meteor storms. In *Asteroids, Comets, Meteors II;Proceedings of the International Meeting, Uppsala, Sweden, June 3-6, 1985* (C.-I. Lagerkvist, B. A. Lindblad, H. Lundstadt, and H. Rickman, Eds.) pp. 559-563. Astronomiska Observatoriet, Uppsala, Sweden.

Wu, Z. and I. P. Williams. 1991. Formation of the Leonid meteor stream and storm. In *Asteroids, comets, meteors 1991; Proceedings of the International Conference, Flagstaff, Arizona, June 24-28, 1991* (A. W. Harris and E. Bowell, Eds.) pp. 661-665. The Lunar and Planetary Institute, Houston, Texas.

Wu, Z. and I. P. Williams. 1996. Leonid meteor storms. *Mon. Not. R. Astron. Soc.* **280**, 1210-1218.

Yeomans, D. 1981. Comet Tempel-Tuttle and the Leonid meteors. *Icarus* **47**, 492-499.

Yeomans, D., K. K. Yau and P. R. Weissman. 1996. The impending appearance of comet Tempel-Tuttle and the Leonid meteors. *Icarus* **124**, 407-413.